Peripheral Sensory Neuropathy in Nile Grass Rat Model of Type-2 Diabetes

by

Jyoti Singh

A thesis submitted in partial fulfillment of the requirements for the degree of

Doctor of Philosophy

Department of Physiology

University of Alberta

ABSTRACT

Peripheral sensory neuropathy (PSN) is a chronic neurological disease affecting over half of type-2 diabetes (T2D) patients worldwide. It presents with multiple devastating, often progressive symptoms such as numbness, altered sensitivity to temperature, tactile allodynia, hyperalgesia, and paresthesia. PSN typically affects the feet first and gradually progresses to hands in a 'stocking-glove' pattern. These symptoms manifest primarily due to dysfunction of distal peripheral sensory nerves; however, pathologic alterations may also occur at their dorsal root ganglion (DRG) neuron (DRGN) somata. Although animal models have been used to elucidate mechanisms underlying T2D-PSN pathogenesis, none of these models displays the full spectrum of the human T2D complications suggesting the requirement of a new model. Male African Nile grass rats (NGRs) serve as a potential T2D model as they show human-like T2D progression when fed with a high calorie, low fiber ('chow') diet. It has been published that chow-fed NGRs develop insulin-resistance, hyperinsulinemia, increased body weight and pancreatic β-cell dysfunction among other human T2D outcomes. Therefore, I hypothesized that T2D NGRs also develop PSN. To address this, I initially demonstrated in 12-24 months-old T2D NGRs that these animals display hallmark PSN pathophysiological features. First, I demonstrated with immunohistochemistry retraction of the sensory nerve fibers in the epidermal skin of T2D NGR hind foot. Next, using Von Frey filaments and a Hargreaves apparatus, I found in behavioral tests that the plantar hind paw has decreased sensitivity to mechanical and heat stimuli. Using further immunohistochemical approaches, I demonstrated that the diverse DRGN subpopulations are still viable in T2D while their mRNA and protein levels are upregulated for the voltage-gated sodium channel (Nav) variants Nav 1.7 and Nav 1.9, but not Nav1.8. Also, a significant portion of satellite glial 'helper' cells that

surround DRGNs are activated and DRGs were infiltrated with macrophages, both processes indicating trauma and inflammation.

In a further set of experiments, I established the 'skin-nerve' preparation that has so far been used only for other rat and mouse species, for studying neurophysiological properties of sensory saphenous nerve fibers innervating the NGR dorsal foot skin. I first demonstrated the viability of this '*ex-vivo*' preparation by manually probing the dermis side of the isolated skin patch via mechanical stimulation with a rod to evoke single-fiber action potentials (SFAPs) from different receptive field (RF) points and determine their adaptation behavior. With subsequent electrical stimulation, I determined the threshold and latency of activation of the SFAP and identified it as either a Aδ- or C-fiber based on nerve conduction velocity. Next, SFAPs evoked by both rod and electrical stimulation at one RF point were compared with those evoked with Von Frey filament stimulation whose mechanical excitation thresholds were determined. It turned out that SFAP responses evoked with Von Frey filaments were from different fibers and therefore they were grouped as 'mechanosensitive fibers'. In T2D NGRs, the amplitude and threshold of electrically-evoked SFAPs were decreased for both Aδ- and C-fibers and mechanosensitive fibers also had a lower mechanical threshold. In summary, the above human-like PSN pathological features established NGRs as a novel model to study T2D-PSN.

NGRs serve as a potential model that, unlike any other existing model, has a unique advantage to investigate the onset and early progression of T2D-PSN and therefore provides an opportunity to develop novel approaches for effective therapeutic interventions.

PREFACE

The thesis is an original work by Jyoti Singh. The research project, of which this thesis is a part, received research ethics approval from the University of Alberta Research Ethics Board, Project name "Nile rats and type-2 diabetes", AUP00000328, January 2016.

Portions of Chapter-1, 2, 3 and 4 of this thesis have been published as "*Jyoti Singh*, Muhammad Saad Yousuf, Kelvin E. Jones, Paige T.M. Shelemey, Twinkle Joy, Haecy Macandili, Bradley J. Kerr, Douglas W. Zochodne, Yves Sauvé, Klaus Ballanyi, Christine A. Webber. "Characterization of the Nile Grass rat as a unique model for type 2 diabetic polyneuropathy". Journal of Neuropathology & Experimental Neurology, Volume 77, Issue 6, 1 June 2018, Pages 469–478".

This paper represents a collaborative work between all the authors. I was responsible for data collection, analysis, preparation and manuscript composition. Drs. Klaus Ballanyi and Christine A. Webber were the supervisory authors and were involved with concept formation and manuscript composition. Dr. Sauvé provided the animals for all the experiments and contributed to manuscript edits. Dr. Bradley J. Kerr and his student Muhammad Saad Yousuf helped with mRNA experiments and their analysis, Drs. Jones and Webber performed the motor nerve conduction study. Dr. Zochodne provided resources to perform immunohistochemistry, advised on experimental design and helped editing the manuscript. The summer student Paige T.M. Shelemey and the technicians Twinkle Joy and Haecy Macandili in Dr. Webber's laboratory provided the technical support and data collection for immunohistochemistry.

All the work was supported by Natural Sciences and Engineering Research Council, Canadian Institute of Health and Research, the University of Alberta Hospital Foundation and the Department of Physiology.

DEDICATION

This thesis is dedicated to the memory of my beloved late mother, Mrs. Prem, who passed away last summer. She remained my ideal, my life-coach and it would not have been possible where I am today without her constant motivation, her belief in my ability and support.

ACKNOWLEDGEMENTS

First and foremost, I am indebted to my wonderful supervisors Drs. Klaus Ballanyi and Christine A. Webber who has provided me an opportunity to work in their lab and helped me improving personally and scientifically. Your constant support and tireless efforts have kept me on the right track and allowed me to come this far. Your critical feedback and time investment have been invaluable to elevate the quality of this thesis. You provided me a productive cheerful environment and allowed me to take initiatives and be independent to hone my scientific skills. Thank you very much.

I would also like to thank my committee members Drs. Yves Sauvé and Kelvin E. Jones for their brilliant suggestions and helped me to critically think and expand my depth of knowledge. Thank you for teaching me the basics and enhanced my interest in the area of diabetes and electrophysiology. Your constant motivation, feedback, and support helped me to face the challenges in the scientific world. I am very thankful for your invaluable time. I would also like to extend my thanks to Drs. Peter Smith and Simon Gosgnach for helping me broaden scientific knowledge.

I would like to thank my graduate coordinator and chair Dr. Gregory D. Funk and chair Dr. James Young for endless help throughout the program as well as all the Department of Physiology and Department of Surgery staff for always providing a friendly environment and help me throughout the program.

I would like to thank members of Dr. Sauvé laboratory- Sharee Kuny, Ted Han and Hui Huang for their help and cooperation during experiments.

I would also like to thank my wonderful colleagues and friends in Drs. Ballanyi and Webber laboratory to make this journey more memorable and enthusiastic.

I am grateful to Natural Sciences and Engineering Research Council, Canadian Institute of Health and Research, the University Hospital Foundation and the Department of Physiology for providing financial support throughout my PhD.

Finally, I would like to thank my father, brother, sister and brother-in-law who remain the pillars of my life and provide consistent support, encouragement and motivation in all aspects of my life.

TABLE OF CONTENTS

LIST OF TABLES

LIST OF FIGURES

CHAPTER-1 INTRODUCTION

CHAPTER- MATERIALS AND METHODS

CHAPTER-3 RESULTS

LIST OF ABBREVIATIONS

AP(s)	Action potential(s)
AGEs	Advanced glycation end-products
ATP	Adenosine triphosphate
au	arbitrary unit
BMI	Body mass index
Ca^{2+}	Calcium ion
CGRP	Calcitonin gene-related peptide
CMAP	Compound muscle action potential
DRG(s)	Dorsal root ganglion(s)
DRGN(s)	Dorsal root ganglion neuron(s)
EDTA	Dipotassium ethylenediaminetetraacetic acid
FBG	Fasting blood glucose levels
FRAP	fluoride-resistant acid phosphatase
GDNF	Glial-derived neurotrophic factor
GFAP	Glial-fibrillary acid protein
HbA1c	Haemoglobin A1c
Hfib	High-fiber diet
Iba1	Ionized calcium-binding adapter molecule
IB4	Isolectin B4
IDF	International diabetes federation
IENFs	Intraepidermal nerve fibers

IFG	Impaired fasting glucose
IGT	Impaired glucose tolerance
IL	Interleukin
K^+	Potassium ion
LTMRs	Low-threshold mechanoreceptors
NA	No activity
Na^+	Sodium ion
NADPH	Nicotinamide dinucleotide phosphate
Nav	Voltage-gated sodium channels
NCV	Nerve conduction Velocity
NF200	Neurofilament 200
NGF	Nerve growth factor
NGR(s)	Nile grass rat(s)
PBS	Phosphate buffer saline
pE_2	Prostaglandin E_2
PGP9.5	Protein gene product 9.5
PKC	Protein kinase-C
PSN	Peripheral sensory neuropathy
qRT-PCR	Quantitative real-time PCR
RA	Rapidly-adapting
RF	Receptive field
RNA	Ribonucleic acid
ROS	Reactive oxygen species

SA	Slowly-adapting
SEM (or sem)	Standard error of the mean
SFAP(s)	Single-fiber action potential(s)
SNAP	Sensory nerve action potential
T1D	Type-1 diabetes
T2D	Type-2 diabetes
TNFα	Tumor necrosis factor α
TrKA	Tyrosine kinase receptor A
TRP	Transient receptor potential
TRPA1	Transient receptor potential ankyrin-1
TRPC1	Transient receptor potential canonical 1
TRPM8	Transient receptor potential melastatin-8
TRPV1	Transient receptor potential vanilloid 1
TTX	Tetrodotoxin
TTXr	Tetrodotoxin-resistant
TTXs	Tetradotoxin-sensitive
WHO	World health Organization

CHAPTER-1

INTRODUCTION

1.1 Dorsal root ganglion neurons as targets to analyze peripheral sensory neuropathy

This thesis is devoted to answering the question of whether Nile grass rats (NGRs) are a powerful novel animal model to study mechanisms of peripheral sensory neuropathy (PSN) related to type-2 diabetes (T2D). Analysis of this type of neuropathy, involving neuropathic ('chronic') pain, can occur at different anatomical levels. PSN originates within the peripheral nervous system, but the extent of its sensation is modified within the central nervous system by neural networks forming the afferent pathway between the pain information entry site in to the spinal cord and the final projection sites in the somatosensory cortex (Waxman et al., 1995; Purves et al., 2001; Hudspeth et al., 2013; McMahon, 2013). This thesis deals exclusively with findings on dorsal root ganglion (DRG) neurons (DRGNs) comprising the somatosensory division of the peripheral nervous system. DRGNs relay mechanical, thermal or pain stimuli with specific receptors in their peripheral nerve endings located in skin, muscle, bones, joints, and parietal membranes, and then transfer this information to neurons in the dorsal horn of the spinal cord (Waxman et al., 1995; Honma et al., 2010; Dubin et al., 2010; Abraira et al., 2013; McMahon, 2013). Sensory stimuli at the distal nerve endings of DRGNs cause a local receptor potential. If the stimulus amplitude is large enough to bring the receptor potential to the action potential (AP) threshold, a 'train' of these electrical communication signals propagates along the peripheral (distal) axon. The APs propagate to the neuronal cell body (soma) within the DRG, then along the central axon of the DRGN and finally reach the presynaptic terminals in the spinal cord to trigger release of the excitatory neurotransmitter glutamate (Purves et al., 2001; Sasaki et al., 2011; Hudspeth et al., 2013; Hübel et al., 2017). Most findings in this thesis refer to PSN-related anatomical and functional changes in DRGN axons comprising different groups. In this thesis, the term 'axon' will be used for specific

properties of DRGN axons while the term ‘fiber’ will be used to compare different DRGN axon groups.

1.1.1 Peripheral nerve constituents and function

The PNS contains the somatosensory, the autonomic and the somatomotor divisions (Fig. 1-1). The somatomotor component of the PNS comprises efferent axons of motor neurons extending from their somata in the spinal cord or brainstem to skeletal muscles. The autonomic nervous system of the somatic body wall consists of pre- and postganglionic neurons of the sympathetic nervous system, which innervate smooth muscles (of the viscera, arteries and arrector pili muscles of the skin), the cardiac muscle and glands (gastric, sweat, sebaceous) (Zochodne, 2008; Gibbons and Freeman, 2012; Jenkins and Lumpkin, 2017). The cell body of the somatomotor and preganglionic sympathetic neurons are located in the ventral horn, and interomediolateral cell column of the spinal cord, respectively, and their axons exit the spinal cord via the ventral spinal nerve roots.

The DRGNs are located within the intervertebral foramen of the vertebral column. These ‘pseudounipolar’ neurons project their central axon branch via the dorsal root into the dorsal horn of the spinal cord while a second axonal (anatomically dendritic) branch extends into the periphery. After unification (also called fasciculation or bundling) of the dorsal and ventral roots, the axon bundles of all these neurons form for a short distance a mixed spinal nerve which divides them into a dorsal and ventral ramus each branching out towards the peripheral target tissues.

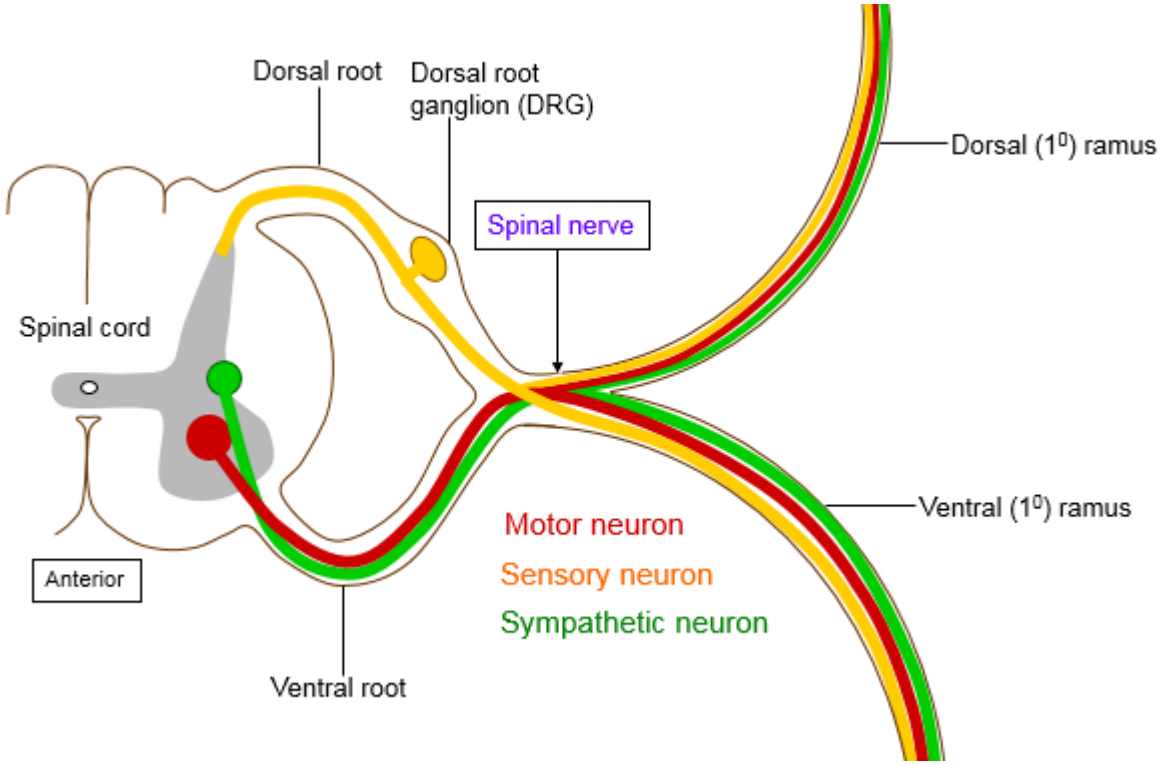

Fig. 1-1: Spinal nerve. The spinal nerve is formed by ventral and dorsal root axons (nerve fibers) which bundle (fasciculate) for a variable distance at the spinal nerve before branching into a respective dorsal and ventral ramus. Dorsal root axons are primarily somatosensory and the dorsal root ganglion (DRG) contains the cell bodies ('somata') of these DRG neurons (DRGNs). Ventral root axon somata are located either in the ventral horn (somatic motor neurons) or interomediolateral cell column (preganglionic sympathetic neurons) of the spinal cord. (Schema used with kind permission from CA. Webber.)

A typical peripheral nerve trunk contains mixed large myelinated α-motor and sensory Aα-fibers, smaller myelinated sensory Aβ- and Aδ-fibers and unmyelinated C-fibers. The fundamental properties and functions of nerve fiber groups are discussed below (1.1.2). Both, myelinated and unmyelinated nerve fibers are surrounded by a loose connective tissue layer, the endoneurium. Several nerve fibers form fascicles surrounded by a further connective tissue layer, the perineurium. Bundles of fascicles are ensheathed by a collagen-containing outer connective tissue layer, the epineurium, which surrounds the nerve and protects it from compression or stretch injury (King, 2013; Ilfeld et al., 2016). Peripheral nerves contain small veins and arteries that run into the epineurium and branch out in the perineurium to provide metabolic support. Nerves also contain lymphatic vessels that run adjacent to the blood vessels in the epineurium (Fig. 1-2).

Essential for normal axonal functions, peripheral nerves also contain two types of glial cells, specifically Schwann cells and satellite glial cells. There are two main types of Schwann cells, i.e. myelinating and non-myelinating ('ensheathing') ones. Schwann cells myelinate axon segments by thinning out their cytoplasm and layering their myelin lipid-containing plasma membrane 60- to 300-fold around the axon to form lamellae (Waxman et al., 1995) (Figs. 1-2, 1-3). Large myelinated peripheral axons have more myelin lamellae, hence a thicker myelin sheath compared to smaller axons (Waxman et al., 1995). All motor axons, most sensory axons and preganglionic sympathetic axons are myelinated. A non-myelinating Schwann cell surrounds, and thus isolates, several small diameter axons to form a Remak bundle of unmyelinated axons. All sensory C-fibers and postganglionic sympathetic axons are unmyelinated. Schwann cells contain various proteins that regulate their proliferation, survival, and myelin integrity. Major myelin-forming proteins, found primarily in myelinating Schwann cells, are myelin basic protein, myelin-associated glycoprotein,

P_0 glycoprotein, and peripheral myelin protein 22. The membrane proteins associated with non-myelinating Schwann cells include growth-associated protein-43, glial-fibrillary acid protein (GFAP), and the low-affinity nerve growth factor (NGF) p75 receptor (Waxman et al., 1995; Zochodne, 2008).

The myelin insulates the axon to prevent an 'ephaptic' AP spread between axons through the interstitial space and also accelerates AP propagation along myelinated axons. A myelinated axon segment is called 'internode' while the neighboring small areas of unmyelinated axonal plasma membrane are termed 'Nodes of Ranvier'. As discussed in detail below (1.3.3), Nodes of Ranvier contain a high density of voltage-gated sodium channels (Nav) that mediate AP generation and propagation (Fig. 1-4). When these Nav are activated, there is a depolarizing sodium ion Na^+ influx at the node whereas the internodal segments serve as a high-resistance/low-capacitance electrically-insulating region and thus prevent leakage of depolarizing current from the axon. As a result, the AP 'jumps' instantaneously in the low millimeter spatial domain from node to node, a process called 'saltatory conduction' that ultimately results in a high AP propagation speed (1-120 m/s). Nav are sparsely and uniformly distributed along unmyelinated axons resulting in progressive depolarization of neighboring membrane regions in the submicrometer spatial domain. As activation of each Nav takes ~1 ms, this accounts for the slower, continuous AP propagation.

A

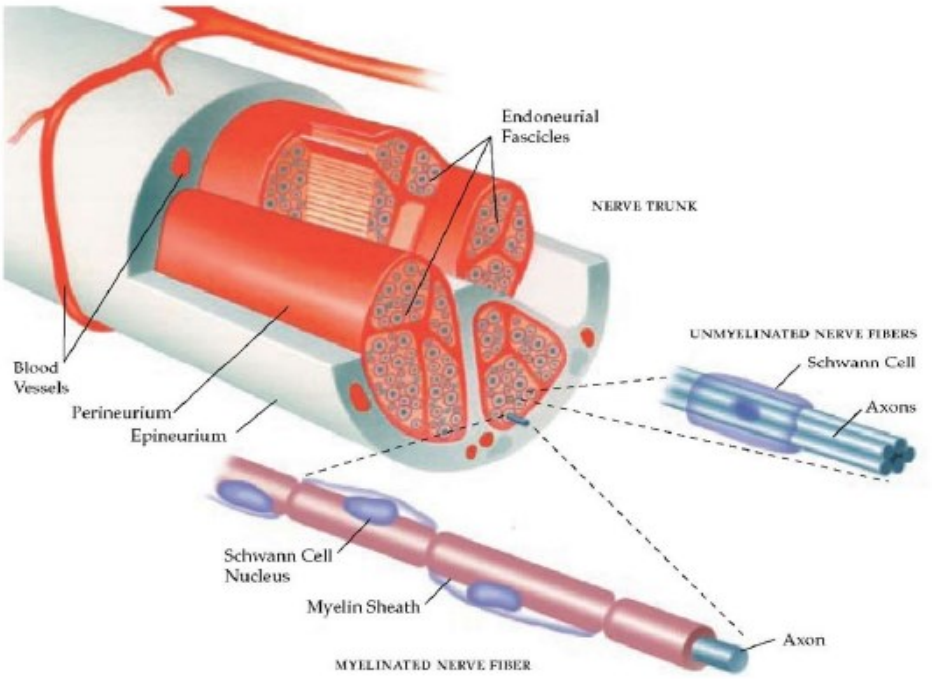
Endoneurial
Fascicles
NERVE TRUNK
UNMYELINATED NERVE FIBERS
Schwann Cell
Axons
Blood
Vessels
Perineurium
Epineurium
Schwann Cell
Nucleus
Myelin Sheath
Axon
MYELINATED NERVE FIBER

B

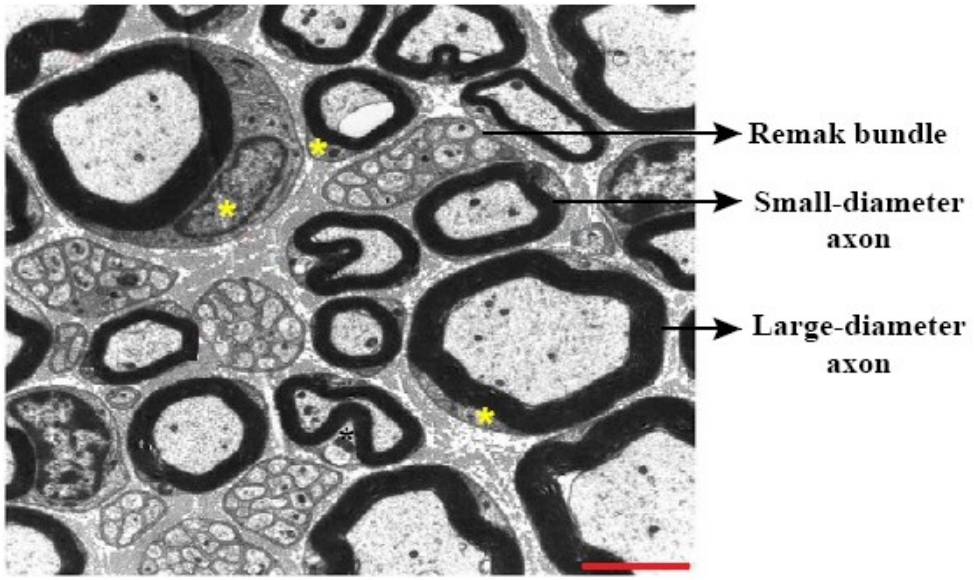
Remak bundle
Small-diameter
axon
Large-diameter
axon

Fig. 1-2: Peripheral nerve anatomy. A, Schema illustrates structure of a peripheral nerve ensheathed by an epineurium layer. The individual nerve fibers within the nerve trunk are surrounded by an endoneurium layer and bundled together by a perineurium sheath into fascicles and are supplied by blood vessels. The epineurium is the outermost layer surrounding the peripheral nerve. Individual large myelinated nerve fibers are mechanically and electrically insulated by a myelin sheath formed by Schwann cells. Unmyelinated axons are surrounded by non-myelinating Schwann cells to form Remak bundles. B, Cross-section of a peripheral nerve consisting of large- and small-diameter myelinated axons. The myelinating Schwann cell nuclei are seen next to some axons (see yellow asterisks). The unmyelinated axons are grouped together to form Remak bundles (scale bar is 50 μm). (reproduced with kind permission from http://what- when- how.com/ acp-medicine/ diseases- of-the- peripheral- nervous- system-part-1 [A]; Themistocleous et al., 2014 [B].)

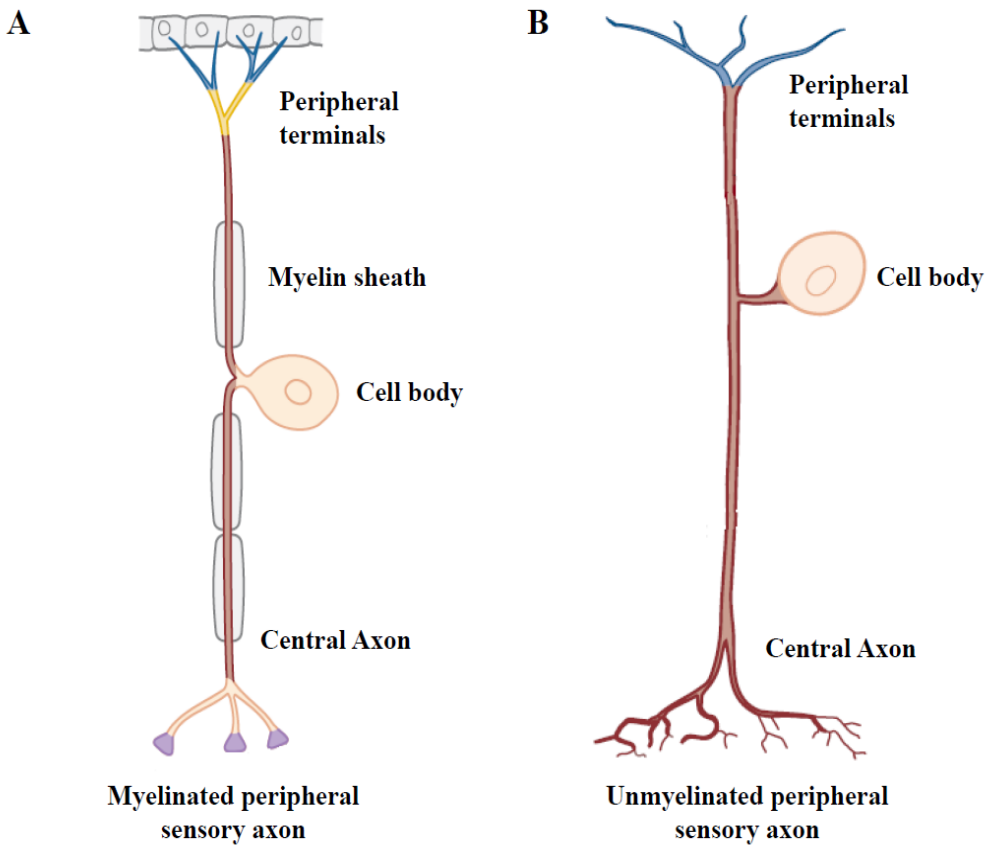

Fig. 1-3: Myelinated and unmyelinated DRGN axons. All DRGNs are pseudounipolar with a peripheral (distal) branch projecting towards the skin or muscle, while the central (proximal) branch extends to the spinal cord. These sensory axons have their somata located in the DRG in the peripheral nervous system. A, Myelinated DRGNs have their central and peripheral axons enwrapped by a myelin sheath produced by Schwann cells. B, Unmyelinated peripheral sensory axons are not enwrapped by these Schwann cells. Instead, non-myelinating Schwann cells enwrap the unmyelinated axons (to form Remak bundles, not shown here). (Reproduced with kind permission from Hudspeth et al., 2013.)

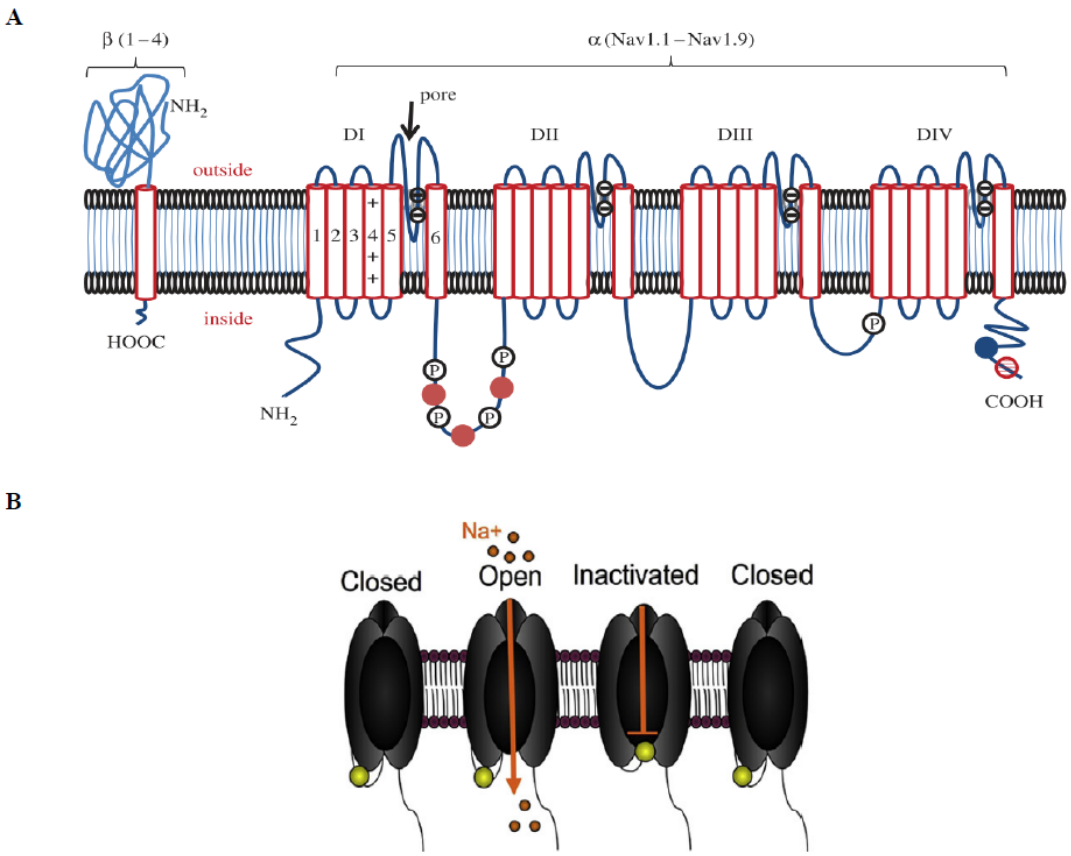

Fig. 1-4: Voltage-gated Na^+ channels (Nav). A, Nav comprise an α-subunit with 4 homologous domains (DI-DIV) each containing transmembrane segments (1-6) with segment 5 and 6 forming the ion-selective pore and S4 acting as a voltage sensor. The β-subunit (1-4) regulates voltage-dependence and gating properties as well as Nav localization. B, At resting membrane potential (~70 mV), Nav are closed (but activatable) and thus non-permeable to Na^+ ions. Nav open (activate) in response to depolarization and allow an influx of Na^+ to generate an action potential (AP). Activation is followed by Nav inactivation that changes later to the closed state. (Reproduced with permission from Fraser et al., 2014 [A]; B, Barbosa et al., 2016 [B].)

Contrary to Schwann cells, 1-3 satellite glial cells enwrap DRGN somata depending on their size. These gap junction-coupled glial cells are separated from the DRGNs by a small (~20 nm) extracellular space where neuron-glia signaling occurs (Hanani, 2005). These glial cells can be identified by expression of molecular markers such as glutamine synthase and GFAP. Under physiological conditions, GFAP is expressed under the detection limit; however following stress such as a peripheral nerve injury or inflammation, its expression is upregulated (Nascimento et al., 2014; Hanani et al., 2014; Costa and Neto, 2015). Satellite glial cells also undergo other changes after nerve injury or inflammation such as release of cytokines and have thus been linked to chronic pain states (Warwick and Hanani, 2013; Hanani et al., 2014).

1.1.2 Groups of peripheral nerve fibers

Peripheral nerve fibers are classified into three groups (A, B and C) based on the degree of myelination, nerve conduction velocity (NCV), soma size, axon diameter, and function. Group A fibers are myelinated and comprise the largest group with four subtypes (α, β, γ, and δ). Group B fibers are myelinated preganglionic autonomic fibers. Autonomic postganglionic and (primary nociceptive) sensory group C fibers are unmyelinated. More specifically, large diameter (12-22 μm) Aα-fibers (or somatomotor fibers) are thickly myelinated and have the fastest NCV ranging from 70-120 m/s. These fibers innervate the extrafusal fibers of muscle spindle and are activated in response to muscle contractions.

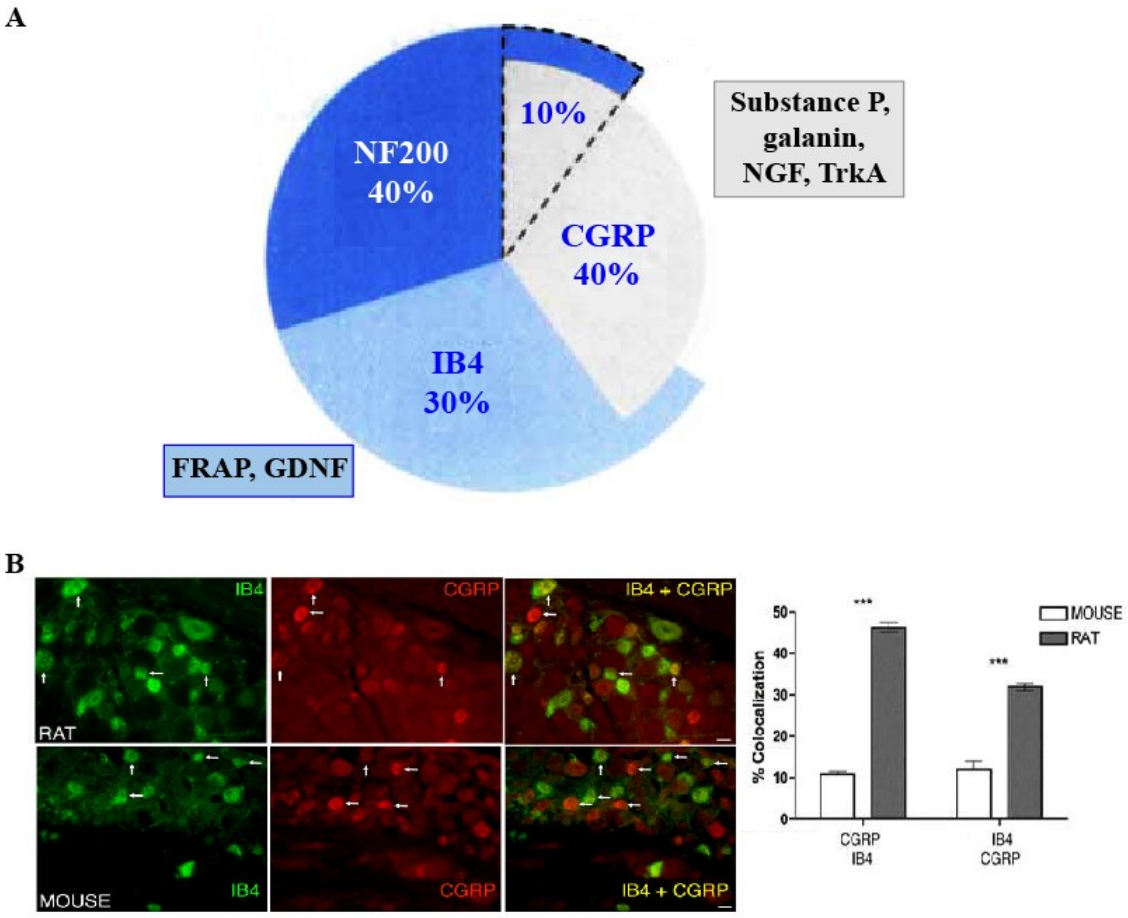

Fig. 1-5: DRGN subgroups expressing different markers. A, Pie chart showing the distribution of immunomarkers in the DRGNs; 40 % express only neurofilament 200 (NF200), 10 % co-express calcitonin gene-related peptide (CGRP) and NF200 while 40 % express only CGRP. Peptidergic DRGNs co-express substance P, galanin, nerve growth factor (NGF) and tyrosine kinase receptor A (TrkA) receptor. Non-peptidergic DRGNs (30 %) are immunoreactive to isolectin B4 (IB4) and express both fluoride-resistant acid phosphatase (FRAP) and glial-derived neurotrophic factor (GDNF). Note DRGNs also contain other markers. B, immunofluorescent images showing colocalization of CGRP and IB4 in the rat (~40 %) and mouse (~10 %) DRGNs. (Reproduced with kind permission from Meyer et al., 2006 [A]; Price and Flores, 2007 [B].)

Aβ-fibers have a smaller diameter (5-12 μm), an intermediate NCV (30-70 m/s) and include low-threshold cutaneous mechanoreceptors responding to light touch, vibration and hair movement (Zochodne, 2008; Manzano et al., 2008; Purves et al., 2012). Aγ-fibers (or fusimotor fibers) (2-8 μm) are medium-sized, thinly myelinated fibers that innervate intrafusal fibers of muscle spindles and their NCV ranges from 15-30 m/s. These fibers are activated in response to the muscle lengthening. Aδ-fibers are thinly myelinated with a 1-5 μm diameter and slow NCV (5-30 m/s) (Zochodne, 2008; Dubin and Patapoutian, 2010). These fibers process information on nociception (sharp pain), pressure, temperature (hot/cold) and crude touch. Unmyelinated C-fibers have the smallest diameter (0.5-1 μm), correspondingly slowest NCV (0.4-2 m/s) and are primarily nociceptive (slow and long-lasting dull pain) (Basbaum et al., 2009; Dubin and Patapoutian, 2010). Most Aδ- and C-fibers are pain-sensing nociceptors. The small-diameter DRGNs corresponding to C-fibers have soma size of <30 μm; the size of medium-diameter DRGN somata of Aδ-fibers range from 30-40 μm, while the soma size of large-diameter Aβ-fibers is >0 μm (Price, 1985; Ho and O'Leary, 2011; Black et al., 2012; Dib-Hajj et al., 2015).

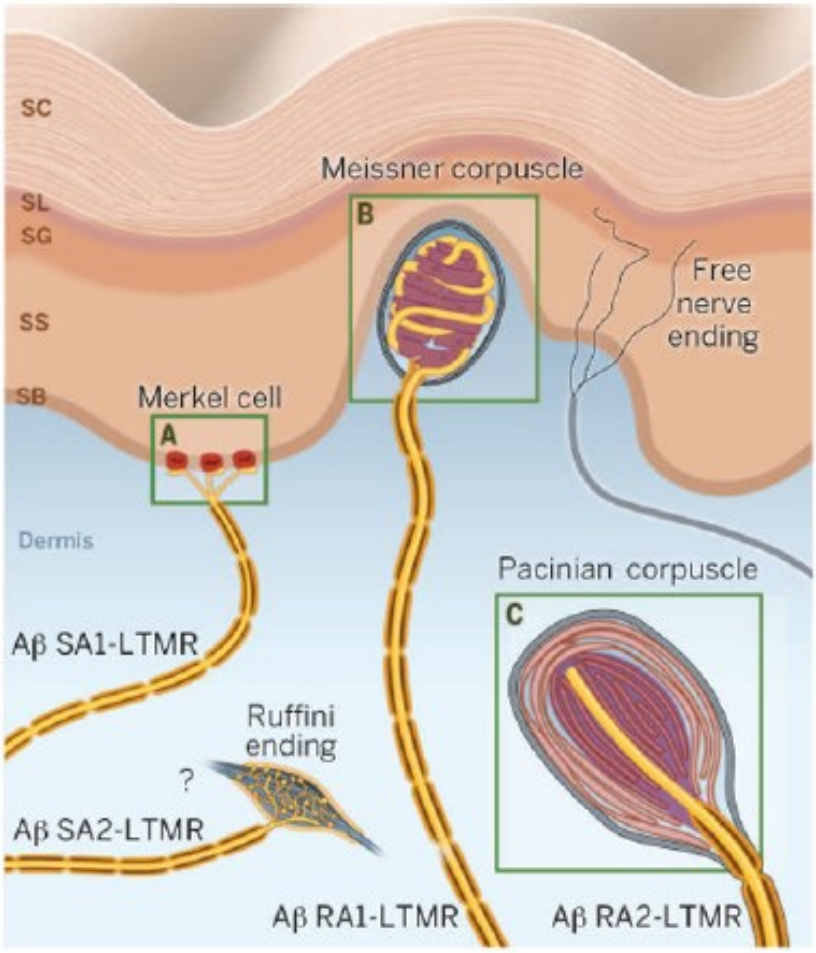

Fig. 1-6: Somatosensory receptors in the glabrous skin. Aβ-fiber low-threshold mechanoreceptors (LTMRs) of slowly-adapting 1 (SA1) types are part of Merkel cells; slowly-adapting 2 (SA2) types Aβ-fiber LTMRs are present presumably in Ruffini endings; rapidly-adapting 1 (RA1) and rapidly-adapting 2 (RA2) type Aβ-fiber LTMRs are contained in Meissner corpuscles and Pacinian corpuscles, respectively. Free nerve endings branch into the epidermis. Abbreviations: SB, *stratum basale*, SS, *stratum spinosum*, SG, *stratum granulosum*, SL, *stratum lucidum*, SC, *stratum corneum*. (Reproduced with kind permission from Zimmerman et al., 2014.)

DRGNs can also be classified based on their specific neuropeptide, neurotrophin receptor or ion channel expression. Immunohistochemically, large and medium-diameter DRGNs express neurofilament 200 (NF200) whereas small diameter DRGNs are classified as peptidergic if they express calcitonin gene-related peptide (CGRP), galanin, substance P and the NGF tropomyosin-related kinase/ receptor tyrosine kinase (TrkA). Contrary, non-peptidergic small diameter DRGNs are preferentially labeled with the plant isolectin B4 (IB4) from Griffonia simplicifolia (Gold and Gebhart, 2010). These non-peptidergic DRGN subtypes contain fluoride-resistant acid phosphatase (FRAP) and express glial-derived neurotrophic factor (GDNF) receptor (Coutaux et al., 2005) (Fig. 1-5A). In rats, 40 % of DRGNs are peptidergic; of these, 40 % form C-fibers and 20 % are Aδ-fibers (Meyer et al., 2006; McMahon, 2013). Expression of these markers also varies between mammalian species, for instance, immunohistochemical labeling of rat DRGs unravels nearly 40 % of colocalization of CGRP and IB4 in rats compared to only 10% in mice (Price and Flores, 2007; Tucker and Mearow, 2008) (Fig. 1-5B). It is common practice to use CGRP and IB4 as immunological markers to classify peptidergic versus non-peptidergic DRGNs in both rats and mice. However, substance P colocalization with CGRP and IB4 is also more common to discriminate nociceptive from non-nociceptive DRGNs in rats compared to mice (Belanger et al., 2002; Price and Flores, 2007). Although the above immunohistochemical markers are not specific enough to distinguish DRGN subtypes, the combination of electrophysiological, immunohistochemical and molecular techniques is quite well suited for this.

1.1.3 Sensory skin receptors

Primary cutaneous sensory fibers relay information via stimulation of their nerve terminals in the epidermal or the dermal layers of the skin. The epidermis consists of five cell layers, which are,

from superficial to deep, the: *stratum corneum* (15-20 rows of dead keratinocytes), *stratum lucidum* (primarily found in glabrous skin of the palms of the hand and soles of the feet), *stratum granulosum* (3-5 rows of flattened keratinocytes)*, stratum spinosum* (8-10 rows of keratinocytes) and a single-row stem cell layer, the *stratum basale* (derived stem cells that differentiate into keratinocytes) (Zimmerman et al., 2014; Jenkins and Lumpkin, 2017). The dermis is the deeper layer of the skin that is rich in collagen and elastin secreting fibroblast cells (papillary and reticular layer), blood vessels, sweat and sebaceous glands, hair follicles (in the hairy skin) and peripheral sensory nerve and sympathetic nerve terminals (Fig. 1-6). Glabrous skin is found in hairless, highly innervated regions of the body surface such as the lips, palm of the hands, fingertips, and the plantar surface of the foot. These areas can detect a wide range of stimuli such as light touch via low-threshold mechanoreceptors (LTMRs) and high-threshold mechanoreceptors, stretch, pressure, vibration, itch, warm, hot or cold temperature (thermoreceptors), hair deflection and nociception (Abraira and Ginty, 2013; Zimmerman et al., 2014). The nerve terminals of most somatosensory receptors are encapsulated to optimize the response to particular types of mechanical stimuli. Contrary, the free nerve endings of Aδ- and C-fibers extend past the dermal-epidermal junction to innervate the *stratum spinosum* layer of the epidermis. Thus, temperature and pain fibers are the most superficial nerve endings. The glabrous skin consists of four types of encapsulated mechanosensory receptors: Pacinian corpuscles, Ruffini endings, Meissner corpuscles, and Merkel discs.

Mechanoreceptors can be classified based on their ability to adapt to (changes in) stimulus intensity into slowly-adapting (tonic, SAI or SAII) or rapidly-adapting (phasic, RAI or RAII) types and their receptive fields (RFs) (Lawson, 2002; Abraira and Ginty, 2013):

a. Meissner corpuscles: are large myelinated Aβ-fiber RAI LTMRs in the dermal papillae of the glabrous skin and are surrounded by capsule-like horizontally arranged flattened lamellar cells. They are activated at low frequency (2-40 Hz) vibration and have smaller RF in the skin.
b. Pacinian corpuscles: are RAII-type encapsulated LTMRs located deep in the dermis and respond to very high frequency vibrations (40-500 Hz) and skin stretch. The encapsulated structure is composed of onion-like lamellae cells lined by flattened Schwann cells and surrounding Aβ-fiber terminals. They are highly sensitive and have a large RF in the skin, and also in joints to detect foot movement.
c. Merkel discs: are located below the epidermal *stratum basale* layer of both hairy and glabrous skin. They are SAI-type sensitive to pressure in the skin with a small RF and are innervated by Aβ-fibers LTMRs.
d. Ruffini endings: are SAII-type LTMRs that are encapsulated by structures in the deep dermal layer of the skin as well as in joints and ligaments innervated by Aβ-fibers. These receptors have a small RF to sense sustained pressure on skin stretch, changes to joint positioning and temperature change.

Thermoreceptors, located in the dermis, are activated by low-threshold, innocuous warm (15-45 ºC) and cold temperatures (5-20 ºC). Thermoreceptors also include a type of nociceptive C- and Aδ-fibers that responds to high-threshold, noxious hot (>45 ºC) or cold temperatures (<5 ºC) that cause remarkable damage to the tissue.

Free nerve endings are nociceptors and typically correspond to C- and Aδ-fibers in the epidermis. At the dermal-epidermal junction, the Remak bundles and Aδ-fibers lose their Schwann cell cover and extend into the epidermis towards *stratum corneum* layer as free nerve endings. C-fibers are 'polymodal' nociceptors as they respond to mechanical, heat/cold or chemical stimuli (Woolf and Ma, 2007; Dubin and Patapoutian, 2010; Gold and Gebhart, 2010). A subgroup of C-fiber nociceptors, defined as 'silent', is only activated by inflammatory mediators released following tissue injury and inflammation. The nociceptors express distinct types of receptors that are activated at noxious temperatures. Transient receptor potential (TRP) vanilloid 1 (TRPV1) receptor is a polymodal receptor activated by noxious heat (>45 ºC), capsaicin (an ingredient of hot chili peppers), and acidic pH (Woolf and Ma, 2007; Basbaum et al., 2009; Dubin and Patapoutian, 2010). TRP melastatin-8 (TRPM8) is a menthol-activated receptor that gets activated at innocuous low temperatures (10-15 ºC); however noxious cold (<5 ºC) activates TRP ankyrin-1 (TRPA1) receptors promoting a notable calcium ion (Ca^{2+}) influx in nociceptors (Basbaum et al., 2009).

1.1.4 Ex-vivo approach to study DRGN axon properties

Basic electrophysiological properties of somatosensory fibers such as NCV or ion channel conductances were already determined in the early 1960s in humans and nonhuman species using *in-vivo* microneurography (Binnie et al., 1995; Mallik and Weir, 2005; Vallbo et al., 2004). However, the correlation between anatomical, neurochemical and biophysical properties of cutaneous peripheral sensory fibers in diseases is poorly understood (Reeh, 1986; Abraira and Ginty, 2013). This is partly because complete control over environmental factors cannot be achieved with microneurography to study the effect of pharmacological compounds. Progress was made in this regard since the 1980's by the development of a mammalian dorsal foot skin

saphenous -nerve preparation (abbreviated in this thesis as 'skin-nerve' preparation). This '*ex-vivo*' model was first applied to rats and guinea pigs and later adapted to mice (Reeh, 1986, 1988; Zimmermann et al., 2009) (Fig. 1-7 A, B). It allows identification and characterization of individual cutaneous sensory nerve fibers by direct stimulation of RFs using mechanical, cold, heat and chemical stimuli (Fig. 1-7 C, D, and E). The results from such *ex-vivo* studies were similar to those from *in-vivo* studies (Reeh, 1988). Since then, the preparation is widely used for pharmacological analysis of sensory receptors and their responsiveness in neuropathic pain and hyperalgesia. For example, excitatory effects of low pH (<5.4) due to local acidosis during disease and tissue injury were studied on nociceptors (Steen et al., 1992). In addition, sensitization and excitation of rat and mouse cutaneous nociceptors was seen when their RFs were stimulated with an inflammatory cocktail containing bradykinin, serotonin, histamine, prostaglandin E2 (pE_2) and substance P, all of which play crucial roles in pain and hyperalgesia in neurogenic inflammation (Kessler et al., 1991; Steen et al.,1995) (Fig. 1-7 F).

The *ex-vivo* model was further applied to study properties of somatosensory fibers innervating hairy mouse skin and embryonic chick skin (Koltzenburg et al., 1997; Koltzenburg and Lewin, 1997). The contribution of TRP channels (TRPA1, TRPV1 and TRPM8) to inflammatory mechanical hyperalgesia and neuropathic pain in cutaneous sensory afferents was also determined using the skin-nerve preparation (Lawson et al., 2008; Garrison et al., 2012; Smith et al., 2013; Lehto et al., 2016). As discussed in section 1.1.3, Nav are fundamental in generating APs and thus regulating neuronal excitability. Various isoforms of Nav (discussed in 1.3.3) are abundantly expressed in DRGNs, The upregulation (or gain-of-function) or downregulation (loss-of-function) either results in increased hyperexcitability or loss of neuropathic pain-related symptoms,

respectively (Craner et al., 2002; Dib-Hajj et al., 2009) The properties of these channels have been studied in cutaneous sensory receptors using skin-nerve preparation in combination with other electrophysiological techniques such as 'threshold tracking'. For instance, it has been demonstrated that in C-fiber nociceptors, Nav1.8 is crucial for heat and cold nociception (Zimmermann et al., 2007; Touska et al., 2018) (Fig. 1-7 G). Similarly, Nav1.9 is important for heat and cold sensation under physiological conditions but is also involved in acute inflammatory hyperalgesia and allodynia (Hoffmann et al., 2017), and cold allodynia (Lolignier et al., 2015). Nav1.9 knock-out mice demonstrate impaired/alleviated mechanical, cold and thermal responses as well as reduced electrical excitability (Lolignier et al., 2015; Hoffmann et al., 2017). Further, the loss-of-function mutation in Nav1.7 resulted in impaired responsiveness of mechanosensitive C-fibers to heat stimulation (Hoffmann et al., 2018). The skin-nerve preparation also revealed a reduction in large-diameter Aβ-fibers proportions in a T2D mouse model (Lennertz et al., 2010). Similarly, it was used in a streptozotocin T2D rat model to investigate the electrophysiological properties of C-fiber nociceptors during hyperglycemia, hypoxia acidosis (Fuchs et al., 2010).

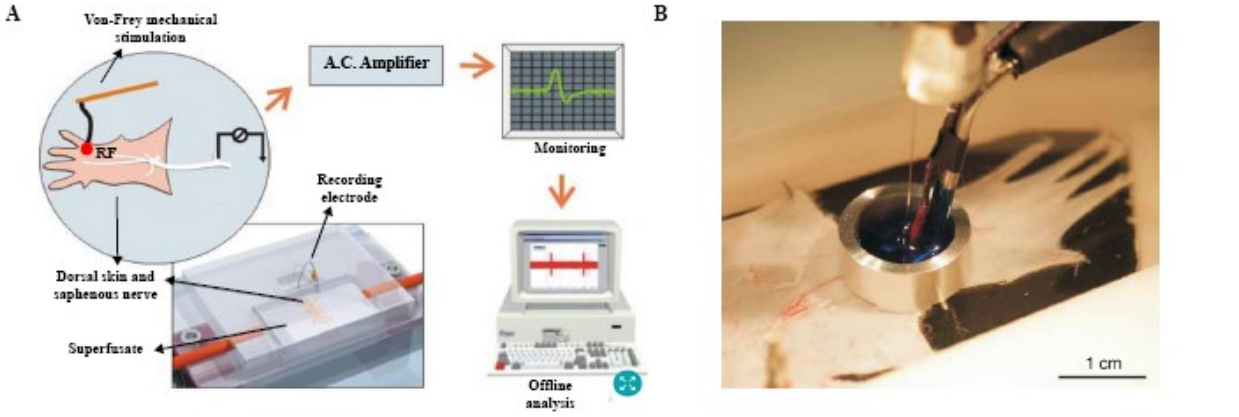
A
Von-Frey mechanical stimulation
A.C. Amplifier
Monitoring
RF
Recording electrode
Dorsal skin and saphenous nerve
Superfusate
Offline analysis
B
1 cm

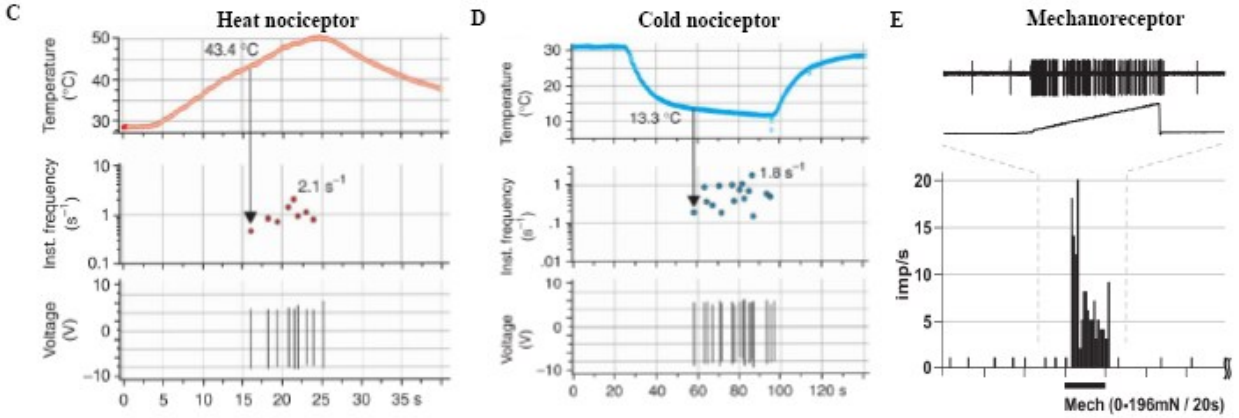
C
Heat nociceptor
Temperature (°C)
43.4 °C
Inst. frequency (s⁻¹)
2.1 s⁻¹
Voltage (V)
D
Cold nociceptor
13.3 °C
1.8 s⁻¹
E
Mechanoreceptor
imp/s
Mech (0·196mN / 20s)

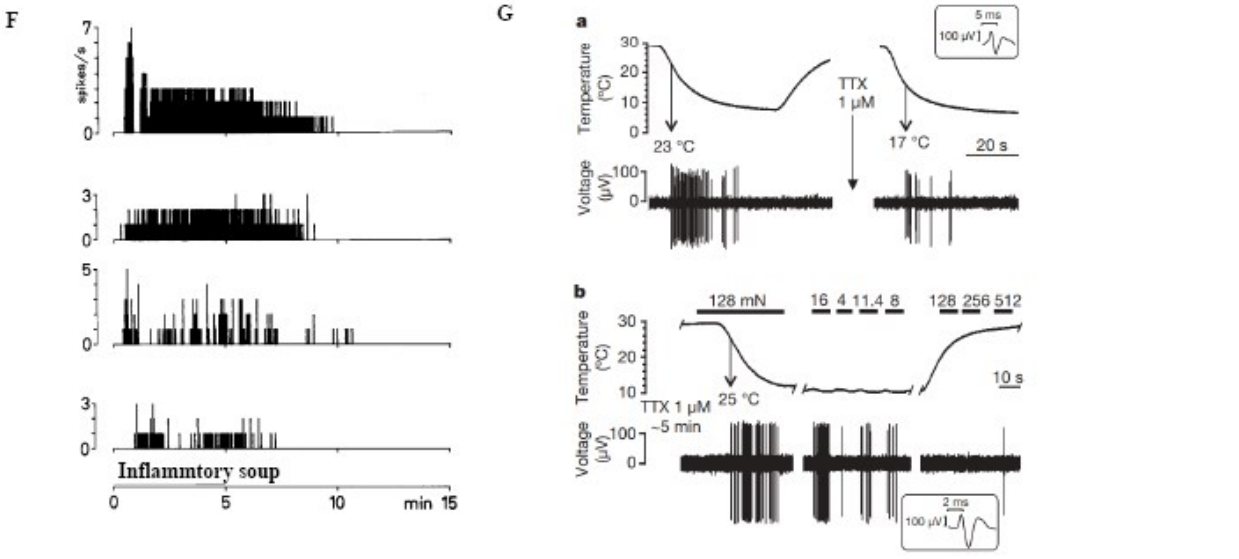
F
spikes/s
Inflammtory soup
min
G
a
Temperature (°C)
23 °C
TTX 1 µM
17 °C
20 s
Voltage (µV)
b
128 mN
16 4 11.4 8
128 256 512
10 s
25 °C
TTX 1 µM
~5 min

Fig. 1-7: Examples of discoveries made with the mammalian dorsal foot skin-saphenous nerve preparation. A, Schema of the experimental 'skin-nerve' preparation setup. B, Dorsal skin-nerve flap mounted dermal side up with the isolated receptive field (RF) within hollow steel ring. C, D, E, Nociceptor responses to sustained heat (43.4 ºC, C), cold (13.3 ºC, D) and mechanical stimulation (0-196 mN, E) F, Types of tonic AP discharge when stimulated with 'soup' containing inflammatory mediators. G, Role of tetrodotoxin-resistant (TTXr) Nav1.8 in cutaneous nociceptor at cooling; nociceptor response was blocked by TTX at 30 ºC, and further mechanical response could not be evoked (a); however, at low temperature, nociceptors were excitable to mechanical stimulation (b). (Reproduced with kind permission from Dr. Paul Heppenstall [A]; Zimmerman et al., 2009 [B-D]; Taguchi et al., 2010 [E]; Kessler et al., 1992 [F]; Zimmerman et al., 2007 [G].)

A major part of this thesis will focus on the skin-nerve preparation that has been adapted here for NGRs to study electrical and mechanical properties of mechanosensitive Aδ- and C-fibers and their changed excitability in T2D-PSN.

1.2 T2D

1.2.1 Epidemiology and complications of T2D

T2D or 'insulin-resistant' is a chronic metabolic syndrome and the most common form of diabetes. According to the International Diabetes Federation (IDF) and the World Health Organization (WHO), the T2D accounts for 90% of the 425 million diabetic patients worldwide. Over 50 million cases were reported in North America and the Caribbean (IDF, 2017) (Fig. 1-8A). The total number of diabetic patients is expected to rise to nearly 629 million by 2045 and has already become an epidemic and global health burden to the healthcare providers (IDF, 2017; Sminkey, 2017). T2D is a progressive chronic disorder primarily affecting 20-79 years old adults, with a higher prevalence in men (Fig. 1-8B) and is more common in urban areas. Moreover, the incidence of T2D has increased in children and adolescents over the past two decades (Ogden et al., 2002; Rosenbloom, 2002; IDF, 2017). Nearly 4 million people older than 65 have been reported to die of T2D globally in 2017 (IDF, 2017).

At early stages of T2D (‘the first several years’), over one-third of the cases remain undiagnosed due to the absence of symptoms. Undiagnosed or untreated T2D results in chronic hyperglycemia and ultimately T2D-associated macrovascular and microvascular complications. Macrovascular complications can evoke cardiovascular diseases due to increased blood cholesterol levels resulting in blood coagulation, increased blood pressure, angina, heart failure, stroke, myocardial infarction and peripheral vascular diseases (Forbes and Cooper, 2013; IDF, 2017). As examples for microvascular complications, hyperglycemia can directly affect the eyes resulting in blindness due to abnormal retinal vascularization and other complications such as cataract and retinopathy (Zochodne, 2007; Shin et al., 2014). Renal complications initiate with increased albumin excretion (microalbuminuria) and progressive nephropathy, ultimately resulting in kidney failure (Tesfaye et al., 2010). Moreover, hyperglycemia can lead to a spectrum of neurological outcomes including PSN resulting in impaired sensory, motor and autonomic functions (Bansal, 2006). This will be further discussed in detail in 1.3. Progressive numbness is also a most common presentation of PSN and can lead to foot ulceration and amputations (Boulton, 2014; Malik, 2014).

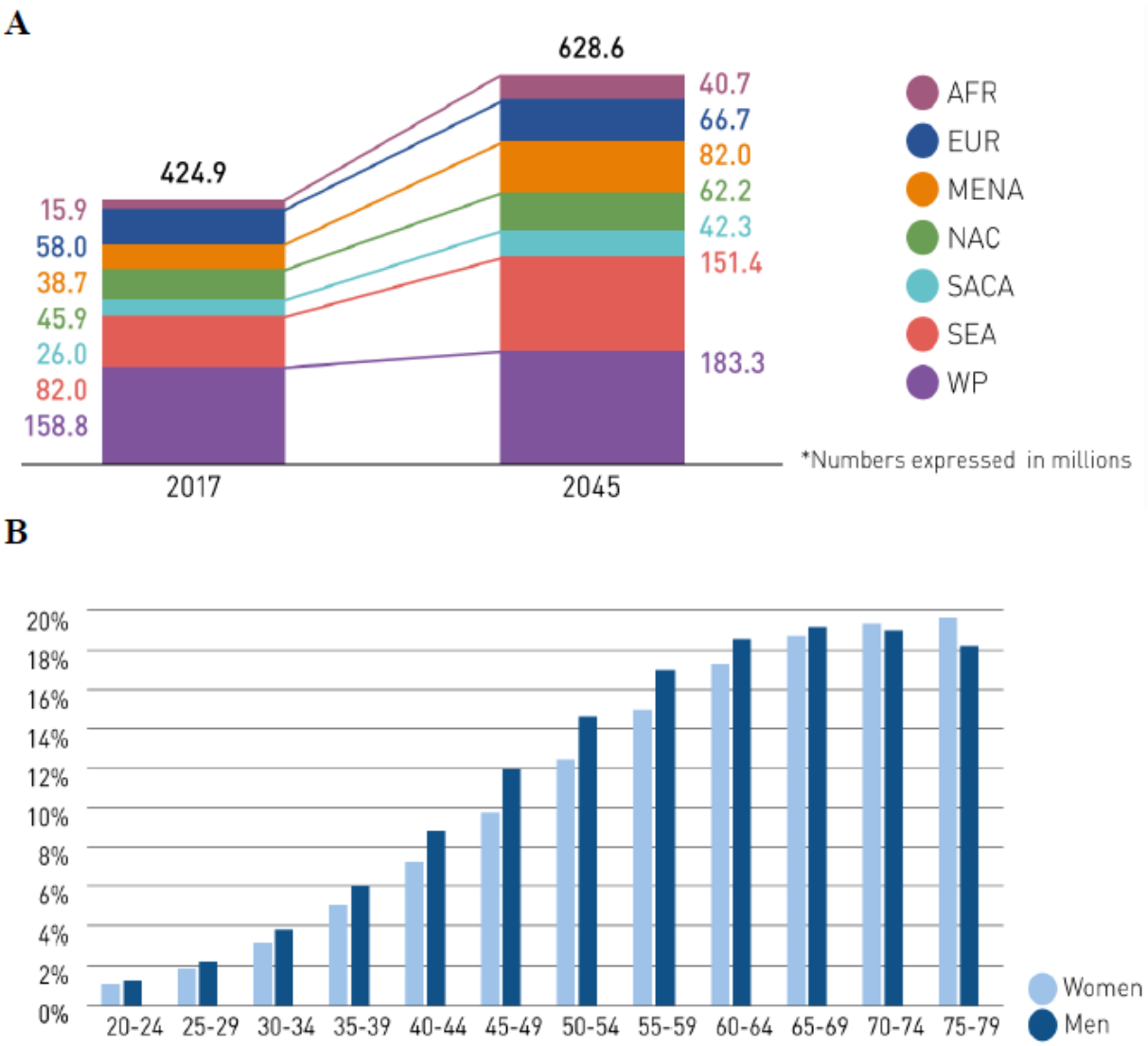

Fig. 1-8: Global distribution of diabetes. A, Prevalence of diabetes in 2017 and its expected increase for 2045. AFR, Africa; EUR, Europe; MENA, Middle East and North Africa; NAC, North America and Caribbean; SACA, South and Central America; SEA, South East Asia; WP, Western Pacific. B, Global prevalence (%) of diabetes related to sex and age (in years) in 2017. (Reproduced with kind permission from International Diabetes Federation, 2017.)

The hallmark of T2D is chronic hyperglycemia which results either from impaired insulin secretion by pancreatic β-cells or the body's ineffective use of insulin to maintain normoglycemia (Alam et al., 2014; Sminkey, 2017). The lack of insulin secretion or the lack of response to secreted insulin results in hyperglycemia. In healthy subjects, food consumption triggers insulin release from the β-cells into the blood to reestablish resting glucose levels and inhibit the activity of glucagon (secreted by pancreatic α-cells) that elevates endogenous blood glucose levels. The balance between insulin and glucagon in the blood is referred to as 'glucose homeostasis' (Hædersdal et al., 2018). During fasting, sleep, or the time interval between meals, low blood plasma glucose levels are elevated by glucagon which stimulates the liver to release glucose into the blood to restore normal blood glucose levels (Fig. 1-9). Disturbed glucose homeostasis may lead to metabolic disorder such as T2D. Chronically elevated blood glucose levels can result in hyperinsulinemia (insulin-resistance) due to the increased release of hepatic glucose into the blood to maintain normal glucose levels and ultimately leading to β-cell death and substantial hyperglycemia. Chronic hyperglycemia causes dysregulation of carbohydrate, protein and lipid metabolism resulting in potentially life-threatening complications.

Prediabetes is a clinical condition in which fasting blood glucose levels (FBG) elevate above normal levels (>6.1 mM), but not high enough to be diagnosed as T2D (>7 mM). Not all subjects with prediabetes develop T2D, but it predisposes them to the disease. Prediabetes can be diagnosed by the impaired glucose tolerance (IGT) and impaired fasting glucose (IFG) tests. The IGT is positive if a patient has FBG of 7.8-11.0 mM 2 h following oral consumption of 75 g glucose. IFG is determined when FBG are between 6.1-6.9 mM and become >7 and <7.8 mM following 2 h of oral 75 g glucose consumption. If oral glucose consumption elevates FBG to >11.0 mM, T2D is

confirmed (Ziegler et al., 2014; Sminkey L., 2016; IDF, 2017). T2D can also be confirmed by the presence of glycated hemoglobin A1c levels, HbA1c >48 mM (>6.5%) which are usually <36 mM (<5.7%) in nondiabetic patients (Olokoba et al., 2012; DeFronzo et al., 2015). The onset of T2D in prediabetic patients can be delayed or prevented by choosing a healthier lifestyle, quitting smoking and maintaining the normal FBG. If these measures are inadequate to manage blood sugar levels, oral antidiabetic medications such as metformin are prescribed as a standard initial treatment (Bergman, 2013; DeFronzo et al., 2015; IDF, 2017; Sminkey, 2017). These medications enhance the body tissue sensitivity to insulin or increase insulin secretion to control for elevated FBG.

The risk of developing T2D is not clearly known; however, obesity due to poor dietary habits and a sedentary lifestyle may put the individual at higher risk. Other factors involved are ethnicity, genetic predisposition, family history, smoking, as well as the occurrence of gestational diabetes (occurrence of diabetes during pregnancy). Therefore, regular checkups and adaptation of a healthy lifestyle with proper nutrition and physical exercise are important to prevent the risk of developing T2D and associated complications.

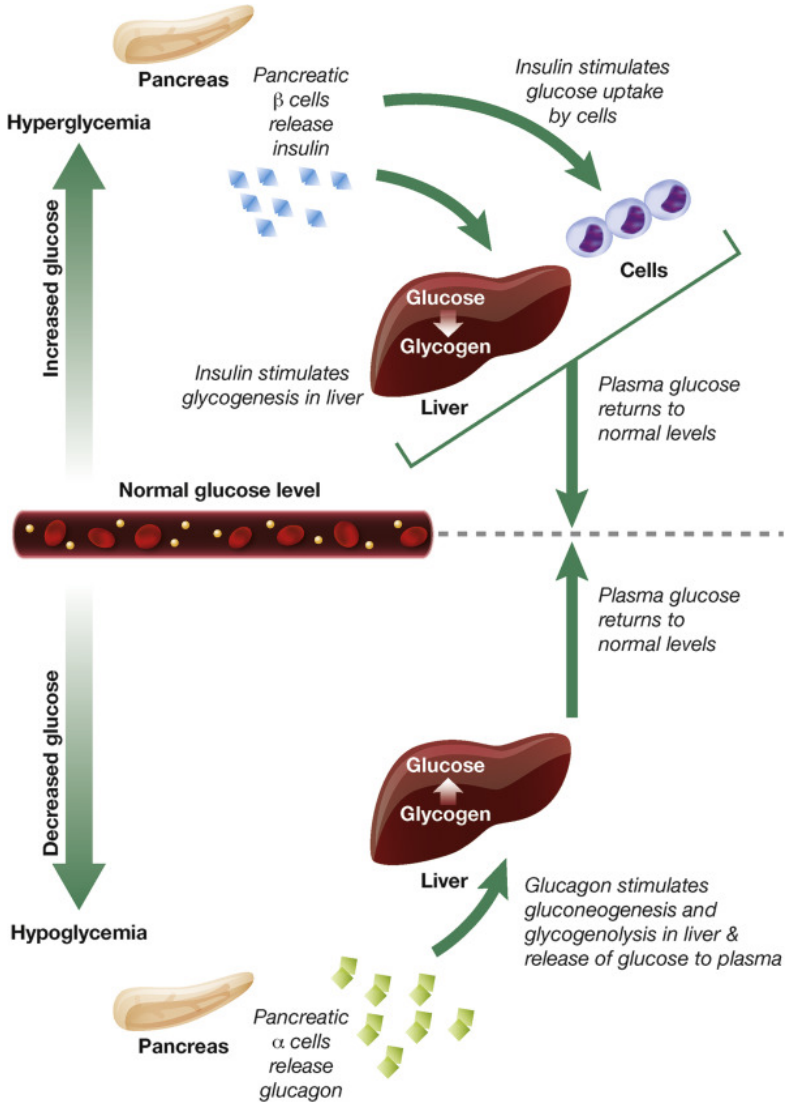

Fig. 1-9: Glucose homeostasis. At low blood glucose levels (hypoglycemia) during fasting or a long gap between two meals, the hormone glucagon is secreted by pancreatic α-cells which bring the blood glucose levels to normal via the processes of gluconeogenesis and glycogenolysis in the liver. At hyperglycemia (high blood glucose levels) insulin is released by pancreatic β-cells which facilitates uptake of glucose in the cells to maintain normal blood glucose levels. (Reproduced with kind permission from Hædersdal et al., 2018.)

1.2.2 T2D Progression

The progression of T2D has 5 stages (Weir and Bonner-Weir, 2004) (Fig. 1-10):

Stage-1 (Compensation): is marked by either normal or raised plasma insulin levels without a change in β-cell mass. The raised plasma insulin levels indicate compensation for high demands of glucose uptake into the cells to maintain normal FBG (<6.1 mM).

Stage-2 (Stable adaptation/borderline): allows for the stable adaptation of β-cells a slight increase in FBG to 6.1-6.8 mM. At the upper limit of this range, IGT develops with progression towards T2D. This stage can be stable in individuals for several years with proper management of diet and exercise. Nonetheless, a rise in plasma glucose levels at this stage indicates changes in β-cell phenotype marked by changes in gene and protein expression.

Stage-3 (Early decompensation/unstable): is the progression to T2D with a rapid increase in FBG (>11.0 mM) as a result of the decline in insulin production following severe β-cell differentiation and reduction in β-cell mass. This stage is unstable and transient with immediate transitioning to stage-4 as a result of severe glucotoxicity. Patients in this stage can return to stage-2 if they improve their diet and exercise regimes.

Stage-4 (Stable decompensation): represents apoptosis of β-cells (up to 50% loss) which results in insulin deficiency. Patients commonly present with glycosuria and polyuria. This stage is stable up to several years or last for a lifetime and does not immediately transit to stage-5.

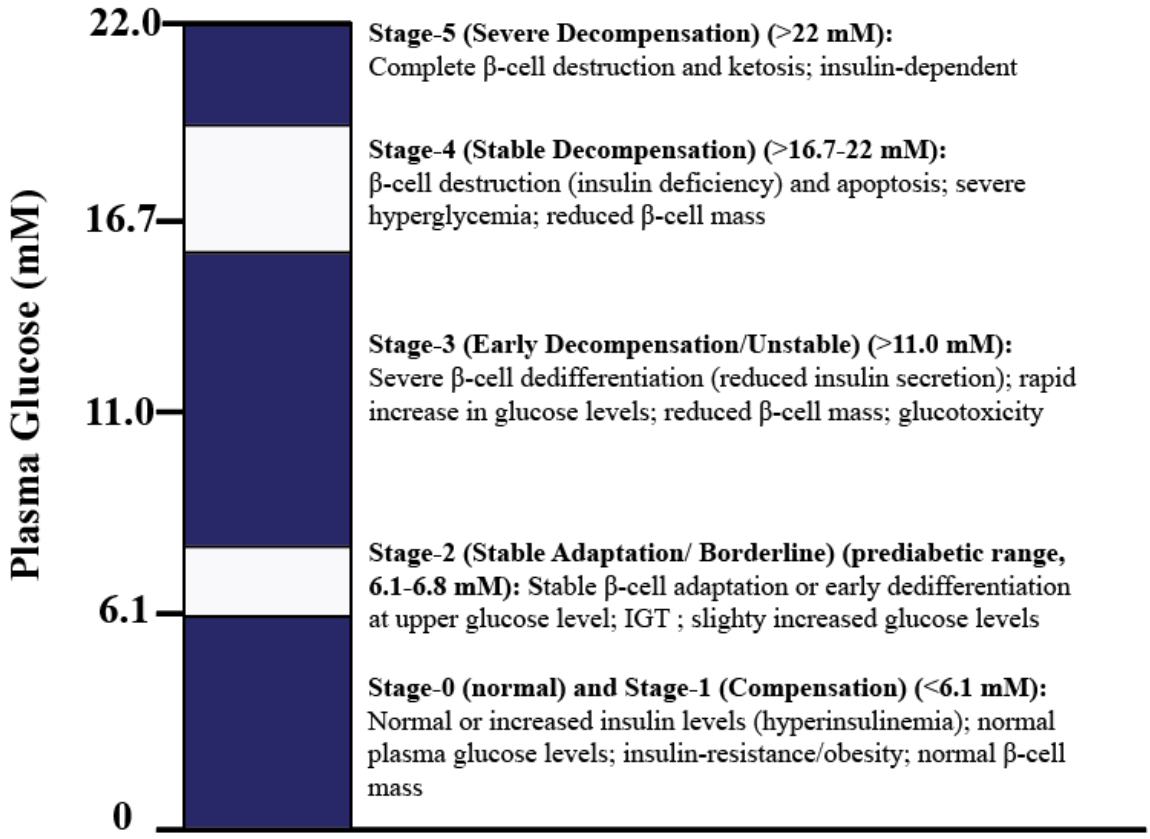

Fig. 1-10: Stages of T2D progression. (Reproduced with kind permission from Weir and Bonner-Weir, 2004.)

Stage-5 (Severe decompensation): typically resembles type-1 diabetes and is characterized by loss of β-cells and development of ketoacidosis, a condition where liver breaks down body fat at a higher rate into ketones in the absence of insulin and making blood more acidic. At this stage, patients are entirely dependent on insulin.

1.3 T2D-PSN

1.3.1 Clinical manifestations and assessment of T2D-PSN

Nearly half of the T2D patients worldwide are affected by PSN (Said, 2013; Feldman et al., 2017). PSN typically presents as symmetric damage to the distal peripheral nerve resulting in impaired somatosensation, affecting large sensory A-fibers and small C-fibers; motor and autonomic functions. PSN initially presents in the distal feet followed by gradual progression to hands, thus displaying a 'stocking-glove pattern' (Campbell and Meyer, 2006; Zochodne, 2007). The major risk factors of T2D-PSN are chronic hyperglycemia, age, duration of T2D, hypertension, increased body weight, and macrovascular complications. T2D PSN patients can be presented with positive (a painful or unpleasant sensation) or negative ('numbness') symptoms (Ziegler et al., 2014). Out of 50% of T2D PSN patients, 13-22% present positive sensory symptoms that are characterized by paresthesia (tingling, electric-shock-like, pinprick, and crawling), burning or stabbing-like pain, tactile allodynia or thermal hyperalgesia. These symptoms are more prominent at night and can be intermittent or persistent lasting over 3 months to several years (Spallone and Greco, 2013; Lee-Kubli and Calcutt, 2014; Ziegler et al., 2014). Negative symptoms are characterized by a progressive sensory loss resulting in numbness. Numbness accounts for almost 50% of the total T2D-PSN patients with a risk of developing foot ulcers. Of these, 25% of the patients can get

infections with a danger of amputation or mortality. T2D is linked to 85% of foot amputations worldwide (Cheer et al., 2009; Boulton, 2014). Paradoxically, numbness often coexists with ongoing pain (Bansal, 2006; Bril et al., 2018). Next, motor impairment is marked by weakness in the lower foot muscles, muscle cramps with pain (~5% in T2D patients), foot drop, decrease or lack of ankle and knee reflex as well as loss of proprioception leading to imbalance (Freeman, 2014). Because of this variability of T2D-PSN symptoms, no single diagnostic approach is reliable.

According to the Diabetic Neuropathy Study Group (NEURDODIAB), a requirement for careful and detailed neurologic assessment was proposed not only to identify the presence of T2D-PSN but to also diagnose the signs, symptoms as well as overall severity of T2D-PSN (Tesfaye et al., 2010; Dyck et al., 2011). Composite scales such as the Neuropathic Pain Questionnaire, Neuropathic Pain Symptom Inventory, Toronto Clinical Neuropathy Score or Brief Pain Inventory can be used to evaluate pain-severity (Veves et al., 2008; Didangelos et al., 2014). T2D-PSN patients can be assessed for negative symptoms using standard tests such as Neuropathy Disability Score to predict risk of foot ulceration, Semmes-Weinstein 10-gram monofilament to diagnose for tactile impairment as a result of cutaneous sensory loss, pinprick test to depict sensory loss, 128 Hz tuning fork to diagnose impairment to vibration sensation (Bansal, 2006; Zochodne, 2007; Boulton, 2014). The clinical neurologic examination can be further extended to investigate large-sensory and motor nerve impairment using electrophysiological nerve conduction and electromyography studies (Perkins and Bril, 2014). Small-sensory nerve impairment can be screened by performing Quantitative Thermal Threshold test to assess thermal sensitivity as well as Laser Doppler Image Flare (LDI Flare) test to assess axon-reflex for C-fiber dysfunction (Tesfaye et al., 2010; Javed et al., 2014). The most reliable test to assess small sensory fiber

denervation is the skin-punch biopsy that assesses the density of plantar paw intra-epidermal nerve fibers (IENFs) (Chao et al., 2010).

1.3.2 Abnormal axonal excitability in T2D-PSN

Prediabetes and prolonged hyperglycemia in T2D is deleterious to the peripheral sensory nerve and alters the anatomy as well as the function of both A- and C-fibers. Hyperglycemia induces oxidative stress in DRGNs making them more susceptible to irreversible damage (Feldman et al., 2017). Nerve injury sensitizes nociceptive and non-nociceptive DRGN axons which then show ectopic activity (Campbell and Meyer, 2006; Schreiber et al., 2015). This spontaneous discharge is due to a reduction in activation threshold with increased responsiveness to stimulus modalities resulting in tactile allodynia and hyperalgesia (Campbell and Meyer, 2006; Zochodne, 2007; Basbaum et al., 2009; Schreiber et al., 2015; Feldman et al., 2017). In addition to enhanced activity, altered expression of Nav, TRP channels, particularly TRPV1 (noxious heat) and TRPA1 (noxious cold), have been implicated in modulating axonal excitability and pain pathogenesis, as previously reported in T2D PSN animal models (Facer et al., 2007; Pabbidi et al., 2008; Feldman et al., 2017).

Another possible cause of modulated DRGN axonal sensitivity is due to sensitization by inflammatory mediators released from immune cells (macrophages, mast cells, monocytes, platelets, fibroblasts) following nerve injury. These mediators such as neuropeptides (substance P, CGRP, bradykinin, histamine), pE_2, cytokines (interleukin, IL-1β, IL-6, tumor necrosis factor α , TNFα), neurotrophin NGF, protons, or adenosine triphosphate (ATP) not only activate the sensory afferents by binding to their specific receptors, but also make them hypersensitive (Woolf and Ma, 2007; Zochodne, 2007; Basbaum et al., 2009). Binding of the inflammatory molecules to their

receptors activates several downstream cascades mediating hypersensitivity in T2D-PSN. Modulation of TRP channels in T2D-PSN, sustained inflammation, and sensory nerve damage also alters the expression of neurotrophins and neuropeptides in DRGNs (Tosaki et al., 2008; Kou et al., 2014). Some studies have shown NGF-mediated upregulation of CGRP and substance P in T2D-PSN (Cheng et al., 2009). However, others have shown downregulation, or no expression change of these neuropeptides in T2D DRG and their axonal free nerve endings (Zochodne et al., 2001; Verge et al., 2014; Li et al., 2017). In summary, ion-channel dysfunction and release of inflammatory mediators play a central role in enhancing axonal excitability and require thorough investigation at the molecular and electrophysiological level to understand their contribution to T2D-PSN.

1.3.3 Altered function of Nav in T2D-PSN

Nav are complex transmembrane channels composed of highly conserved large single 260 kDa α-subunits (principle subunit) comprising 4 homologous domains (DI-DIV) with α-helix transmembrane segments (S1-S6) while segments S5 and S6 form the pore region and S4 acts as a voltage sensor (Fig. 1-4A). The α-subunit also contains the selective filter for Na^+. Nav have 1 or more β-subunits which regulate the voltage-dependence and gating properties plus localization of the channel. The conformational change in the α-subunit either results in channel opening (open state or activation) to allow inward Na^+ current or an inactive and subsequently closed non-conducting state (Fig. 1-4B).

Nav are categorized into 9 isoforms (Nav1.1-Nav1.9). These isoforms differ slightly in the polypeptide sequences of their α-subunits and can be further distinguished based on their sensitivity

to tetrodotoxin (TTX), a neurotoxin extracted from puffer fish (Black and Waxman, 2013; Persson et al., 2016). 'TTX-sensitive' Nav isoforms (Nav1.1-1.4, Nav1.6, Nav1.7) are blocked by nanomolar TTX concentrations (Fang et al., 2002; Ho and O'Leary, 2011; Black and Waxman, 2013). The remaining Nav isoforms (Nav1.5, Nav1.8, Nav.1.9) require micromolar TTX for the blockade and are thus called 'TTX-resistant' (Fang et al., 2002; Ho and O'Leary, 2011; Nieto et al., 2012). The TTX-resistant Nav1.8 and Nav1.9 and the TTX-sensitive Nav1.7, are widely studied in T2D-PSN animal models and are linked to neuropathic pain (Khan et al., 2002; Cummins et al., 2007; Xia et al., 2016; Hoffmann et al., 2017). 'Gain- or 'loss-of-function mutation' affects Nav functionality by modulating neuronal excitability. Increased expression or gain-of-function mutation of Nav1.7 and Nav1.9, and the downregulation of Nav1.8 have been reported in T2D-PSN animal models.

Nav1.7 is expressed in all DRGN subtypes, but most robustly in small, nociceptive DRGNs (Rogers et al., 2006; Black et al., 2012). These channels rapidly activate and inactivate and then recover slowly from inactivation (Dib-Hajj et al., 2013; Waxman and Zamponi, 2014). Therefore, Nav1.7 remain available for activation and generate substantial gating current at small slow depolarizations close to the resting membrane potential (about -70 mV) (Dib-Hajj et al., 2012; Dib-Hajj et al., 2013; Bennett and Woods, 2013; Waxman and Zamponi, 2014). Therefore, Nav1.7 is also considered as a 'threshold channel'. The gain-of-function of Nav1.7 increases neuronal excitability and inflammatory thermal hyperalgesia suggesting its essential role in nociceptive signaling (Hong and Wiley, 2005; Chattopadhyay et al., 2008; Huang et al., 2014). Previous studies reported an increase in Nav1.7 currents and Nav1.7 protein and mRNA expression in DRGNs of T2D-PSN models (Dib-Hajj et al., 2012; Dib-Hajj et al., 2013). Conversely, loss-of-function

Nav1.7 mutation attenuated mechanical and thermal hyperalgesia in T2D-PSN animals (Dib-Hajj et al., 2010; Hoeijmakers et al., 2014; Emery et al., 2016; Blesneac et al., 2017).

Nav1.8 is responsible for ~60% of the slowly-inactivating inward Na^+ current underlying the AP upstroke (Han et al., 2016). These channels rapidly recover from inactivation in response to sustained depolarizations and thus supports repetitive AP firing (Waxman and Zamponi, 2014; Han et al., 2016). The distribution of Nav1.8 in DRGNs is similar to Nav1.7 with robust expression in small nociceptive cells. These channels have been widely studied in other pain models where Nav function is modulated by inflammatory mediators resulting in DRGN hyperexcitability (Belkouch et al., 2014). Previous studies have demonstrated downregulation of Nav1.8 expression in DRGNs in a T2D model (Hirade et al., 1999; Hong and Wiley, 2005). Thermal and mechanical hyperalgesia, as well as ectopic DRGN firing in association with Nav1.8, is regulated by post-translational modifications that are induced by methylglyoxal, a glycolytic metabolite (Bierhaus et al., 2012).

Nav1.9 is also primarily expressed in small-diameter nociceptive DRGNs. It activates already close to resting membrane potential (around -80mV) and is responsible for mediating 'persistent' Na^+ currents (Dib-Hajj et al., 2015; Hoffmann et al., 2016). Thus, Nav1.9 is also considered as a 'threshold channel' as it opens in response to weak stimuli and contributes to prolonged depolarization for ectopic firing (Dib-hajj et al., 2010) and therefore affects AP frequency in nociceptive DRGNs. Nav1.9 expression has been shown to be upregulated in the DRGNs in addition to Nav1.9 currents in painful T2D-PSN and inflammation illustrating its link to hyperexcitability (Hirade et al., 1999; Hong and Wiley, 2006; Chattopadhyay et al., 2008; Dib-

Hajj et al., 2015). Similarly, knocking out Nav1.9 reduces hypersensitivity and hyperalgesia (Chattopadhyay et al., 2008; Dib-Hajj et al., 2015). These Nav may, therefore, act as a potential target for therapeutic interventions to treat inflammatory-mediated pain as well as painful PSN as they solely mediate and regulate neuronal excitability.

1.4 NGR

A commonly used rodent model relies on streptozotocin-induced β-cell destruction to evoke Type-1 diabetes (Yorek, 2016; Barragán-Iglesias et al., 2018). After 2-4 weeks, these animals show acute hyperglycemia and other features of metabolic syndrome and are therefore also used as a T2D model. However, this model has the limitation of short T2D progression and the absence of increased body weight (2-4 weeks) over spontaneous long-progression of T2D in patients (Biessels et al., 2014). Additionally, it lacks structural changes in the nerve fibers that is likely observed in advanced T2D-PSN patients. Another T2D model is developed by injecting low dose (25 mg/kg) streptozotocin in combination with high-fat/high-fructose diet to mimic its long-progression (~56 weeks). These animals demonstrate some features of T2D-PSN complications such as tactile allodynia, hyperalgesia and slower motor NCV (Barrière et al., 2018). However, the approach still relies on pharmacological manipulations to cause β-cell dysfunction and induce T2D-PSN.

Among genetic T2D-PSN models, Zucker diabetic fatty rats are often used. They are deficient in a leptin receptor and develop obesity with insulin resistance at an early stage followed by progressive hyperglycemia after 8-10 weeks (Wattiez and Barrière, 2012; Biessels et al., 2014; Al-Awar et al., 2016). These rats demonstrate features of PSN such as IENFs loss, slowed motor NCV, structural changes in the nerve as well as mechanical allodynia. However, this model is limited by their high

costs to maintain sexual organ hygiene in males and increased mortality rates after 4-6 months (Biessels et al., 2014). Another lectin-deficient Bio-Breeding Zucker diabetic rat/Worchester rat has been studied for T2D-PSN, and this model showed IGT and insulin-resistance within 10 weeks similar to human patients (Tirabassi et al., 2004; Islam, 2013; Gao and Zheng, 2014). Within 4 months, these rats develop T2D-PSN-associated symptoms such as slowing of motor NCV, mechanical and thermal hyperalgesia. Although these rats serve as an important model to study T2D-PSN due to their development of spontaneous hyperglycemia, they are expensive to maintain, genetically-modified and require supplementation of insulin (Biessels et al., 2014).

Among mouse T2D models, leptin receptor-deficient db/db mice, ob/ob mice with mutated leptin gene as well as streptozotocin-high fat diet-fed mice are commonly used as they develop T2D and obesity within 4-6 weeks. These mice show hyperinsulinemia, dyslipidemia as well as progressive hyperglycemia (Islam, 2013; Gao and Zheng, 2014; O'Brien et al., 2014). They exhibit motor and sensory impairment, epidermal denervation and peripheral nerve structural abnormalities with impaired somatosensation. However, this model has a high mortality rate after 24-30 weeks.

Collectively these rodent models encompass salient features of T2D-PSN for unraveling its etiopathogenesis. However, it appears there is no single animal model available to date that accurately mirrors all characteristic features of the human disease for developing yet unavailable effective therapeutic intervention. This is when NGRs come into play. This species, *Arvicanthis niloticus*, is a herbivorous rodent that inhabits African grasslands, woodlands, and the savanna and resides in underground burrows, feeding on seeds, grains, nuts, grass, stem, flowering plants and insects (Refinetti, 2004; Subramaniam et al., 2018) (Fig. 1-11). NGRs exhibit diurnal habits unlike

nocturnal rodents (including laboratory rats and mice) and have been initially used for studying circadian rhythms (Blanchong et al., 1999). Besides, NGRs are rich in retinal cones (33%) and rods (67%), a percentage 10 times higher than other rodent species and have therefore been used in retina research (Bobu et al., 2010).

NGRs are established as a model of T2D, and they developed T2D when fed with a standard laboratory rat 'chow' high-fat/low-fiber diet, while they remained healthy on a 'chinchilla' high-fiber (Hfib) diet resembling more their natural nutrition (Chaabo et al., 2010; Noda et al., 2010; Yang et al., 2016). Specifically, the chow-fed males develop T2D complementing human T2D regarding insulin-resistance, obesity, hyperglycemia, dyslipidemia, increased cholesterol levels, hypertension as well as ketosis in advanced stages (Chaabo et al., 2010; Noda et al., 2010; Yang et al., 2016; Subramaniam et al., 2018) (Tab. 1-1). In addition, NGRs with severe T2D exhibit microvascular complications such as retinopathy, eye lesions, cataracts, cardiac impairment (atherosclerosis) as well as kidney complications potentially leading to renal failure (Noda et al., 2014; Han et al., 2017; Subramaniam et al., 2018). Like human patients (Fig. 1-10), NGRs undergo 5 stages of T2D progression. Specifically, they show hyperinsulinemia at 2 months (stage-1) followed by hyperglycemia at 6 months (stage-2) and progression to advanced stages 3-5 by 12 months and later (Yang et al., 2016). At the advanced stages 3-5, T2D NGRs demonstrate β-cell impairment, increased β-cell mass and ultimately their destruction resulting into decreased or no insulin-secretion. These stages are also marked by increased mitochondrial and endoplasmic reticulum stress. NGRs with advanced chronic hyperglycemia also showed cataracts and retinopathy, an enlarged discolored liver and swollen kidneys, hypertension (hyperlipidemia) and progressive nephropathy impairment as well as signs of ketosis. Notably, T2D NGRs have reduced

T2D symptoms upon feeding them with a green lentil diet similar to a high-fiber and protein-rich lentil diet that somehow helps managing T2D in humans (Bolsinger et al., 2017). All of these essential features should make NGRs a powerful model to understand the pathogenesis of PSN in T2D.

Fig. 1-11: Nile grass rat (NGR). *Arvicanthis niloticus* is a herbivorous rodent that inhabits African grasslands, woodlands, and the savanna resides in underground burrows and feeds on seeds, grains, nuts, grass, stem, flowering plants, and insects. NGR develops T2D when fed with a laboratory 'chow' diet and have been established as a model of T2D.

Pathophysiology of T2D NGRs						
Hyperinsulinemia		✓	✓	✓	✓	
Hyperglycemia		✓	✓		✓	✓
Pancreatic β-cell dysfunction	✓				✓	
Increased body weight		✓			✓	✓
Dyslipidemia		✓	✓	✓		
Hypertension		✓				
Glucosuria/Ketonuria		✓				
Retinopathy				✓	✓	
Nephropathy	✓					
T2D recovery on diet restriction		✓	✓			
Peripheral sensory neuropathy						✓
References	(Noda et al., 2010)	(Chaabo et al., 2010)	(Bolsinger et al., 2013, 2017)	(Noda et al., 2013)	(Yang et al., 2016, Han et al., 2017)	(Singh et al., 2018)

Tab. 1-1: Metabolic phenotype in ‘chow-fed’ T2D NGRs.

1.5 Rationale, hypothesis and aims

1.5.1 Rationale

As outlined above, millions of T2D patients develop multifactorial PSN which negatively affects their quality of life. The mechanisms underlying PSN need to be elucidated to develop effective therapies. According to NEURODIAB, existing animal models to study these mechanisms all have limitations, thus pointing out the need for a new model that shows all aspects of human T2D-PSN. NGRs are a promising model in that regard as they develop T2D when fed on chow diet and display the classic non-neurological symptoms (1.4). I aimed at studying whether NGRs display the hallmark features of T2D-PSN such as altered electrical and mechanical excitability of excised tactile peripheral sensory nerve fibers (for allodynia), distal sensory loss and numbness/hypoesthesia at the paw (altered tactile behavior), slowing of motor NCV, satellite glial cell activation, macrophage infiltration as well as altered Nav expression in DRGNs.

1.5.2 Hypothesis

I hypothesize that diet-induced T2D causes in NGRs human-like PSN due to pathological changes in DRGNs, particularly at their distal axons including the sensory nerve terminals.

1.5.3 Aims

1.5.3.1 To demonstrate clinical hallmark features of T2D-PSN in NGRs

I will investigate the classic symptoms of T2D-PSN in the NGR model including footpad IENF changes and altered behavioral sensitivities to touch and heat stimuli. Regarding IENFs, skin-biopsy is a valuable diagnostic test for unmyelinated C-fibers and myelinated Aδ-fibers under the

pathological condition like T2D-PSN (McCarthy et al., 1995). Both Aδ- and C-fibers extend their terminals into the epidermis as 'free nerve endings' (Kennedy and Wendelschafer-Crabb, 1993; McCarthy et al., 1995). T2D-PSN patients demonstrate decreased IENF density that often results in altered tactile and thermal sensitivity (Calcutt et al., 1996; Shun et al., 2004; Beiswenger et al., 2008). Thus, I will immunohistochemically determine the IENF density in the plantar footpad skin of T2D NGRs for denervation. In some animal models and clinical examples, PSN initially presents with hyperalgesia which turns later into hypoalgesia (Calcutt, 2004; Chen et al., 2005; Drel et al., 2006; Obrosova, 2009; Islam, 2013). Therefore, I will apply the behavioral Von-Frey (Chaplan et al., 1994, Field et al., 1999; Deuis et al., 2017) and Hargreaves (Hargreaves et al., 1988, Deuis et al., 2017) tests to determine if IENF impairment affects the tactile and thermal (heat) sensitivity in T2D NGRs.

1.5.3.2 To examine neuropeptide expression, satellite glial activation and inflammation in the DRGs of T2D NGRs

C-fibers of DRGNs comprise subtypes that are peptidergic (expressing neuropeptide, CGRP) or non-peptidergic (labeled by IB4). These subtypes are typically nociceptive and carry pain sensations as a result of injury, disease or tissue damage (Dubin and Patapoutian, 2010; Nickel et al., 2012). Some studies showed downregulation of CGRP mRNA in DRGN somata and CGRP loss in IENFs as a result of chronic hyperglycemia (Iyengar et al., 2017) while others demonstrated no change in CGRP expression (Zochodne et al., 2001; Terenghi et al., 1994). I will study if T2D-PSN alters CGRP expression in DRGNs. I will also determine if satellite glial cells that surround DRGNs, undergo functional and morphological alterations related to nerve injury or inflammation, thus potentially contributing to perturbed DRGN excitability. GFAP is a standard marker to

identify activated satellite glial cells including in diabetes (Hanani et al., 2014). Finally, I will determine if there are signs of macrophage infiltration at DRG as a result of putative T2D-PSN-associated inflammation.

1.5.3.3 To determine Nav expression in DRGNs of T2D NGRs

Nav contribute to AP generation and propagation and thus regulate neuronal excitability. Gain-of-function or loss-of-function mutation in Nav contribute to severe pain or alleviate pain transmission, respectively. Particularly Nav1.7, -1.8 and -1.9 are altered in T2D-PSN (Hong and Wiley, 2005; Lauria et al., 2014). These Na^+ channels are expressed predominantly in the DRGNs (Dib-Hajj et al., 2010; Ho and O'Leary, 2011). Studies have mostly focused on TTX-resistant Nav1.8 and Nav1.9 and TTX-sensitive Nav1.7 in association with hyperalgesia and tactile allodynia as result of neuronal hyperexcitability (Dib-Hajj et al., 2015; Hoffmann et al., 2017). It has been reported that Nav1.9 and Nav1.7 expression in DRGNs is upregulated whereas Nav1.8 expression is downregulated in T2D-PSN (Craner et al., 2002; Hong et al., 2004). Using immunohistochemical and molecular techniques such as quantitative RT-PCR (qRT-PCR), I will investigate the expression of Nav protein and mRNA in DRGNs that could alter in T2D NGRs to cause PSN.

1.5.3.4 To determine the excitability of single DRGN axons of NGRs

For this, the skin-nerve preparation for electrophysiological extracellular SFAP recordings (Reeh, 1986; Zimmermann et al., 2009) will be adapted for the first time to NGRs. Electrophysiological parameters such as RF mapping, adaptation properties, SFAP amplitude, activity-dependent latency changes, and NCV will be studied. Thinly myelinated Aδ-fibers and unmyelinated C-fibers

mediate the peripheral perception of pain, temperature, and itch (and to a small degree, touch and pressure). Previous studies have demonstrated hyperexcitability of these cutaneous sensory fibers in T2D-PSN model resulting in tactile allodynia and hyperalgesia (Khan et al., 2002; Suzuki et al., 2002; Bierhaus et al., 2012). I will study if electrophysiological parameters of Aδ- and C-fibers are changed in T2D.

CHAPTER-2

MATERIALS AND METHODS

2.1 Animals

In the current study, only male NGRs were used for data analysis due to their increased susceptibility to develop T2D compared to females as reported previously (Chaabo et al., 2010; Yang et al., 2016)[1]. In addition, some female NGRs were also used to practice the *ex-vivo* skin nerve preparation. NGRs were housed at the University of Alberta animal facility and maintained on a 12:12 h light-dark cycle at room temperature (21 ± 2 °C) and ~40 % humidity. The animals were obtained from Dr. Yves Sauvé's breeding colony with ad libitum access to food and water. Pups were weaned at 3 weeks and separated into 2 groups based on diet. Control NGRs were fed with Hfib ('Mazuri chinchilla' diet; 5M01, Purina Mills, St Louis, MN) containing 4.1 % fat, 15 % fiber, 21 % protein and 42.5 % carbohydrates. Prospective T2D NGRs were fed with chow diet (Prolab® RMH 2000, LabDiet, Nutrition International, Richmond IN) containing 9.6 % fat, 3.2 % fiber, 19.9 % protein and 50.8 % carbohydrates. At the experimental endpoint, NGRs were deprived of food for 16-18 h for baseline FBG measurements to assess altered glucose metabolism. Next, the animals were euthanized with a lethal dose (0.2-0.4 ml) of intraperitoneally injected Euthanyl (Bimeda-MTC Animal Health Inc., Cambridge, ON, Canada) (Yang et al., 2016). All protocols were approved by the University of Alberta Animal Ethics Committee, and all experiments were carried out per Canadian Council on Animal Care guidelines. Important to note, I only used live NGRs for the Von Frey and Hargreaves behavioral tests. All the tests were performed blinded to the experimental groups.

[1] Portions of this chapter have been published (Singh et al., 2018, Journal of Neuropathology & Experimental Neurology; 77(6):469-78

2.2 FBG, plasma insulin, and tissue collection

Before NGR euthanization, a blood sample from the tail vein was collected to measure FBG using an Accu-Chek Compact Plus glucose monitoring system (Roche, Mississauga, ON, Canada). NGRs with FBG >5.6 mM were considered hyperglycemic, and the cut-off was selected based on previous work of our collaborator Dr. Sauvé (Yang et al., 2016)[2]. Next, the body weight of NGRs was measured. Following Euthanyl injection, when the animal reached the surgical plane of anesthesia, confirmed by no response to the toe pinch, 1 ml blood was collected by puncturing the apex of the heart's left ventricle using 23-gauge needle. The blood sample was immediately transferred to the collection tubes containing dipotassium ethylenediamine tetra-acetic acid (EDTA) (BD Microcontainer tubes No. 365974) and centrifuged at 2000 rpm for 20 min at 4 °C. The collected plasma was either stored at -80 °C or used for measurement of insulin levels using an ELISA kit (Ultra-Sensitive Mouse Insulin ELISA kit#90080, Crystal Chem Inc., Downers Grove, IL, USA). Animals were considered 'compensating' if their average plasma insulin levels were above 2 ng/ml, which indicates more insulin secretion by β-cells to maintain a normal FBG (Weir and Weir, 2004; Yang et al., 2016).

To reduce NGR numbers, they were shared among users from different laboratories. Specifically, immediately following euthanization isolated tissues including the eyes, heart, pancreas, kidneys, mesenteric arteries and liver were collected within 10-15 min to study non-neurological T2D pathology. Immediately afterwards, I used the carcass to isolate the skin-nerve preparation, DRGs, and footpads.

[2] The euthanization, blood collection and measurement of FBG, insulin levels and body weight of NGR was performed with the help from Sharee Kuny, Ted Han and Hui Huang in Dr, Yves Sauvé laboratory.

2.3 Electrophysiology

The skin-nerve preparation is an established *ex-vivo* model to study in rats and mice sensory SFAPs (Zimmermann et al., 2009). In the second half of my thesis, I visited in April 2016 for one month to the laboratory of Dr. Peter Reeh who developed this model at the Institute of Physiology and Pathophysiology of the Friedrich-Alexander University Erlangen-Nürnberg in Germany. The goal was to learn advanced features of this technique and apply them to NGRs in Dr. Ballanyi's laboratory. During this training, I learned how to discriminate different subgroups of Aδ- and C-fibers based on their responses to heat and cold stimulation plus effects of (inflammatory) compounds. Besides, I learned how to apply suction-electrodes in this model to record Aδ- and C-fiber SFAP responses. Due to the limited number of available NGRs, these detailed studies could though not be carried out after my return to Edmonton.

2.3.1 Dissection of skin-nerve preparation

For dissection, both hind feet were shaved using an electric razor, and the foot was mounted on a small inclined platform using double-sided tape. A small circular incision of approximately 10-15 mm around mid-thigh was made, 1-2 mm proximal to the knee joint. Under a Zeiss stereomicroscope 305 (Carl Zeiss, Oberkochen, Germany), the region where the saphenous nerve emerges from the femoral nerve and intersects into the inguinal ligament was exposed by making two parallel incisions, laterally and medially to the saphenous nerve (Fig. 2-1). The exposed nerve was kept moist by dripping with superfusate of close-to physiological salt and glucose content containing (in mM) 107.8 NaCl, 26.2 $NaHCO_3$, 3.5 KCl, 1.53 $CaCl_2$, 0.69 $MgSO_4$, 1.67 NaH_2PO_4,

9.64 Na-gluconate, 5.55 D-glucose, 7.6 sucrose (Sigma Aldrich, ON, Canada); pH was adjusted to 7.4 by gassing with 95% O_2 + 5% CO_2 ('carbogen').

The saphenous nerve was then isolated from surrounding connective tissue and blood vessels using a pair of superfine Dumont #5 forceps (Fine Science Tools, BC, Canada) proximally to the point where it emerges from the femoral nerve (Fig. 2-2). The femoral nerve containing a branch of saphenous nerve was then gently and carefully lifted by placing the forceps underneath and tying a knot around it using 5-0 USP, 1.0 metric surgical silk thread (Ethicon, ON, Canada). After tying the knot, the femoral nerve was transected at the level of the inguinal ligament using a pair of angled spring scissors (No. 15008-08, Fine Science Tools). The saphenous nerve was then detached from the side branches, adhered muscles and connective tissues of the thigh up to the site where it branches into the skin. It was then covered with a superfusate-moist piece of Kimwipe®. Subsequently, the dorsal foot skin was carefully dissected to include the intact saphenous nerve branches. For this, a straight incision was made using a #11 Sterisharps scalpel blade® on the back of the calf, starting from the region of Achilles tendon and proximally up to the mid-thigh. The cut ensured that the nerve was positioned centrally within the dissected skin and equidistant to each side of the incision. Next, the dorsal skin attached to the paw phalanges was separated from the subcutaneous tissue using the above-mentioned scissors and forceps. By removing the adhered connective tissues, muscles and tendons, the dorsal toe skin was gently dissected proximally to the ankle and then up to the thigh where the saphenous nerve branches into the skin. The separated dorsal skin along with the innervating saphenous nerve was then transferred into a 100 ml glass beaker filled with carbogenated superfusate kept at ~26-28 °C.

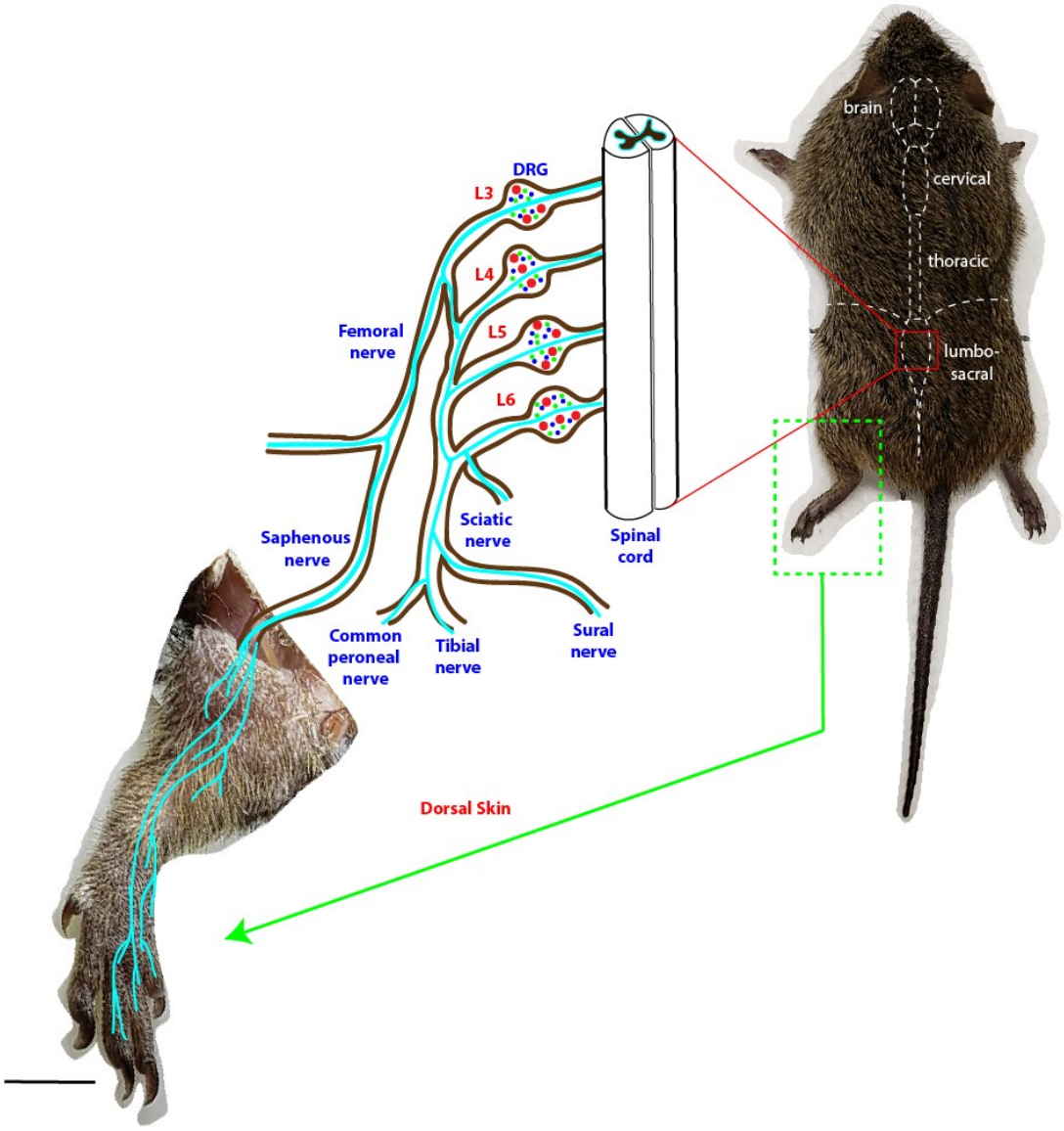

Fig. 2-1: Lumbar L3-L6 segment with DRGs and nerve locations in the spinal column of NGRs. Regions of the spinal column are indicated in the photograph of a NGR. The saphenous nerve is one branch of the femoral nerve and originates from the L3 and L4 lumbar vertebrae of the spinal cord. It descends in the foot and innervates the medial region of the foot skin (not shown). (Scale bar is 5 mm)

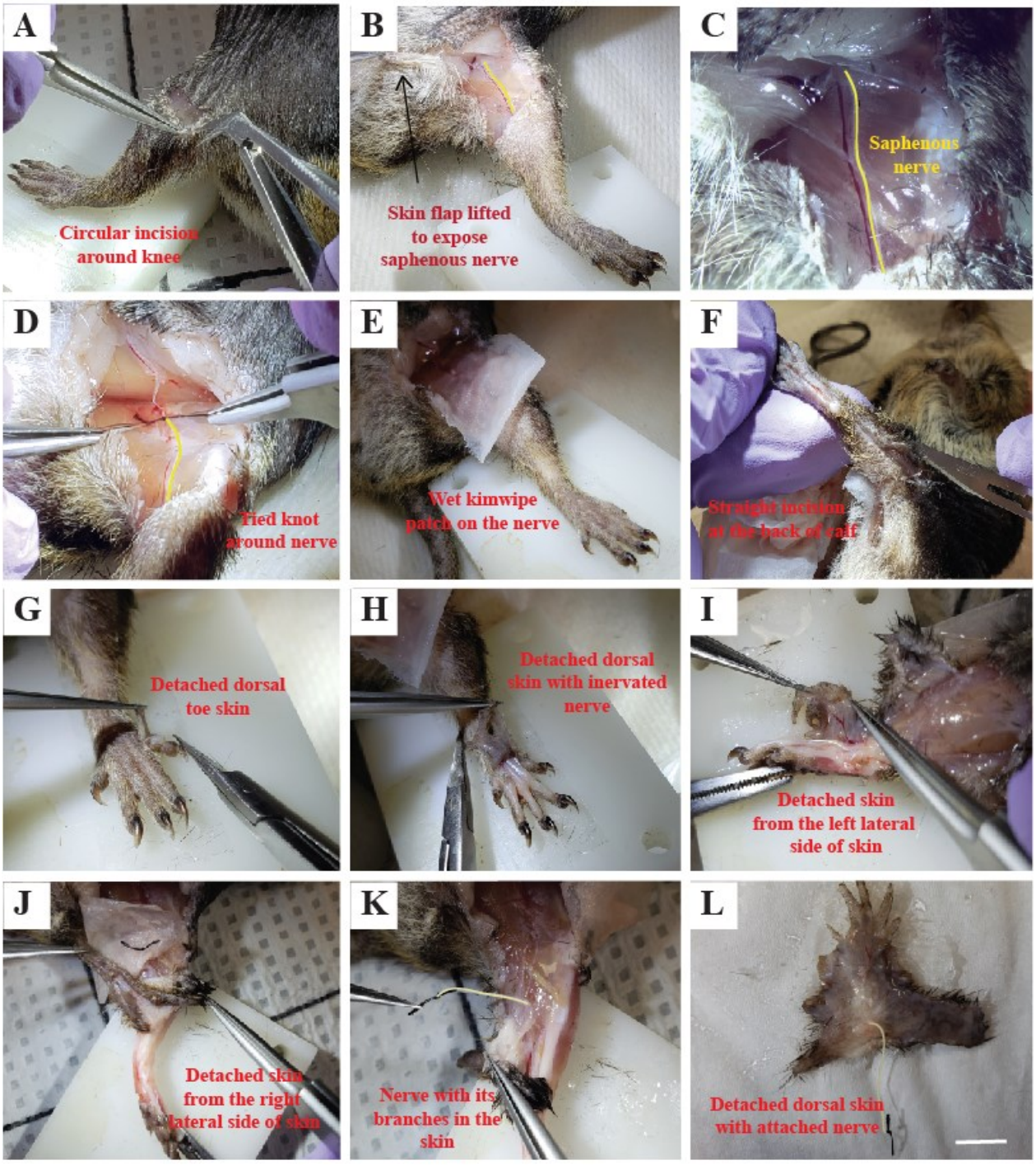
A
Circular incision around knee
B
Skin flap lifted to expose saphenous nerve
C
Saphenous nerve
D
Tied knot around nerve
E
Wet kimwipe patch on the nerve
F
Straight incision at the back of calf
G
Detached dorsal toe skin
H
Detached dorsal skin with inervated nerve
I
Detached skin from the left lateral side of skin
J
Detached skin from the right lateral side of skin
K
Nerve with its branches in the skin
L
Detached dorsal skin with attached nerve

Fig. 2-2: Dissection of NGR saphenous nerve along with dorsal foot skin. A-C, An incision (A) was made around the forefoot above the thigh to expose the saphenous nerve (C) joining the femoral nerve by lifting the skin flap (B). D, E, The knot was tied around the nerve (D) and nerve detached from the surrounding muscles and connective tissue to the point it branched into the skin and covered with Kimwipe® briefly soaked in superfusate of close-to-physiological ion and glucose content (E). F-I, A straight incision (F) was made at the back of the calf and the dorsal skin, attached to the paw phalanges, was separated (G-I). J-L, The intact nerve along with dorsal skin was carefully separated from the foot. (Scale bar is 10 mm)

Subsequently, another skin-nerve preparation was obtained from the contralateral foot applying the same procedure. Preparations from both foot were then kept in superfusate in the fridge at 4 °C for recordings later on the same day or up to 24 h to record the next day. The dissection required 35-50 min depending on the age and diet-related size of the animal.

2.3.2 Experimental Setup, stimulation and recording

The skin-nerve preparation was transferred to an acrylic 'organ bath' in which carbogenated superfusate was continuously supplied at 30 ± 2 °C at a flow rate of 3 ml/min using a peristaltic pump (New Era Pump Systems Inc., NY, USA) while fluid was removed with a syringe connected to a vacuum flask (Figs. 2-3, 2-4). It was mounted at the bottom of the bath with the dermal side up on Vaseline®, gently flattened using a 'L-shaped' glass rod, and fixed at the edge of the skin with insect pins (Fig. 2-4). The saphenous nerve was threaded (by pinching the knot with the fine forceps) through an acrylic interface and placed on a mirrored platform (1 x 2 cm) in a separate compartment comprising the recording chamber. This chamber was then filled with carbogenated superfusate up to the level of the platform. Low-viscosity mineral oil (Sigma Aldrich) was placed on top of the superfusate layer in the recording chamber to keep the platform superfusate-free and prevent the nerve from floating. Both, the organ bath and the recording chamber contained grounding electrodes to minimize electrical noise during recording.

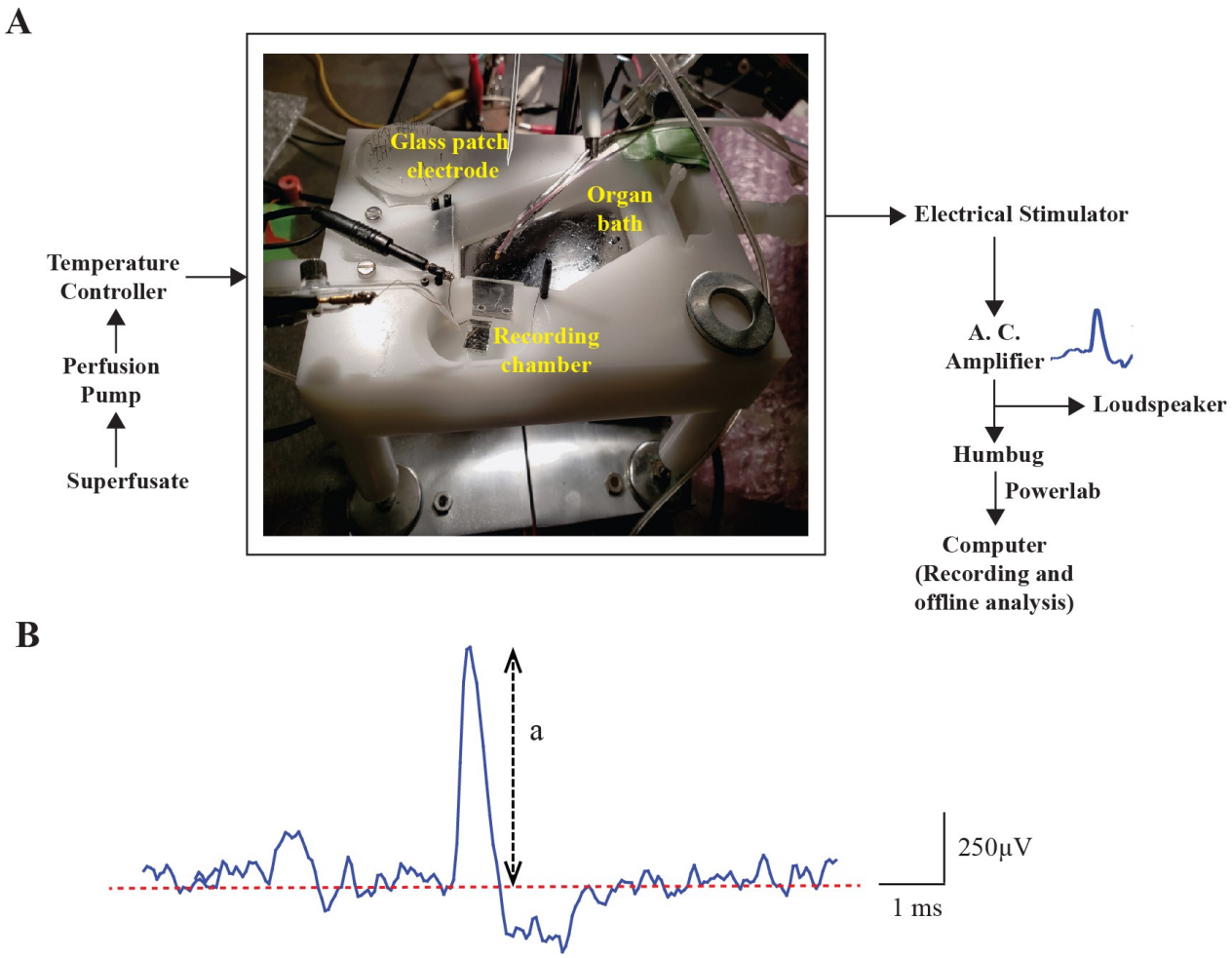

Fig. 2-3: Experimental setup for single-fiber AP (SFAP) recording in skin-nerve preparation. A, The organ bath and recording chamber are perfused with superfusate via a peristaltic pump at 30 ± 2 °C maintained by the temperature controller. The electrical stimulation was applied using patch electrode at the mounted dorsal skin. The output voltage of the recording amplifier was amplified 10k-fold. 60 Hz noise was filtered using a 'humbug' device plus an analog notch filter in Labchart software. The signal was also fed into a loudspeaker for auditive signal control. B, SFAP amplitude was measured (a). The red dotted line indicates the center of the baseline from which 'a' was measured.

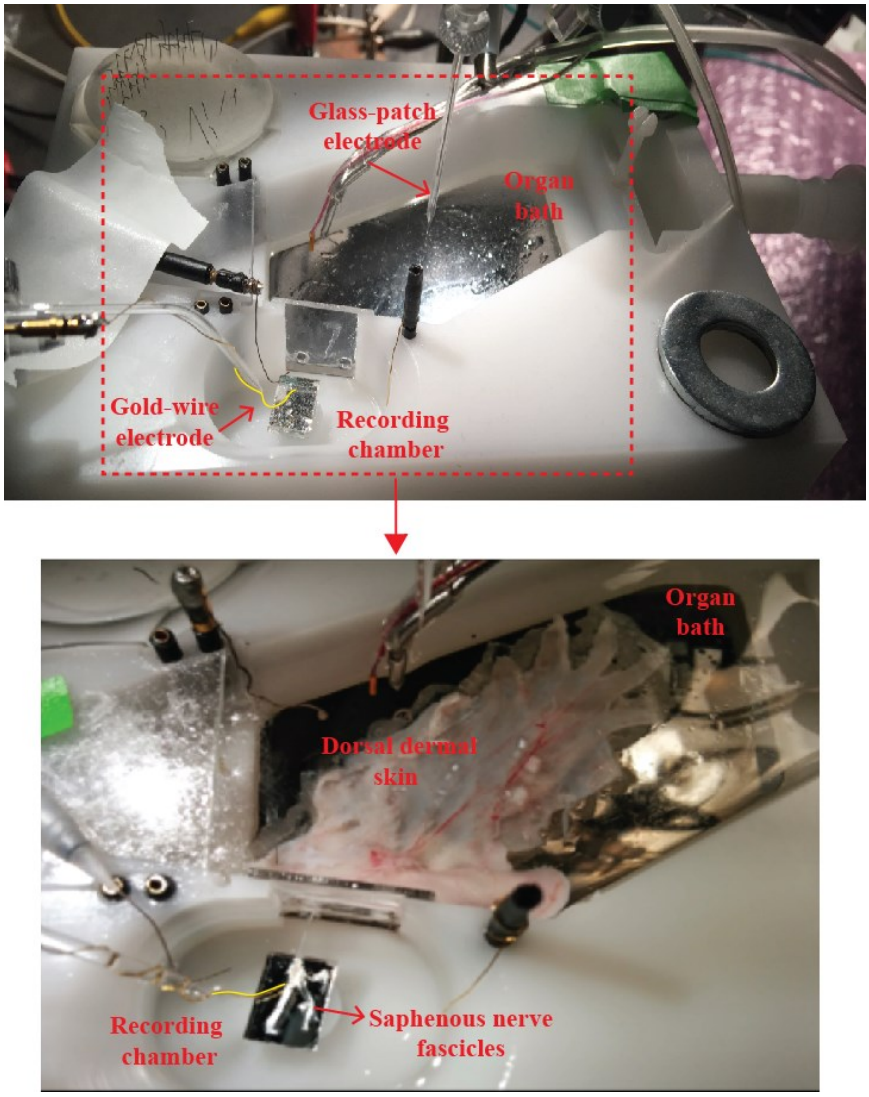

Fig. 2-4: Skin-nerve preparation recording chamber. Top panel consists of recording chamber and organ bath. In the organ bath, the dorsal skin was mounted with the dermal side up and stimulated electrically using a superfusate-filled patch electrode. The recording chamber was for SFAP recording from sensory fibers using gold electrode. The bottom panel shows a magnified view of the system. The nerve was placed and teased into fascicles on a mirror platform submerged into low-viscosity mineral oil and was superfusate-free to prevent nerve floating.

After cutting a threaded knot under a stereomicroscope (Model No. CO-EM-600, Scienscope™), the nerve was exposed by removing the epineurium with superfine Dumont #5SF forceps (Fine Science Tools). The nerve was then teased apart into fascicles to increase the probability for successful SFAP recording. Next, one of the smallest isolated fascicles was placed gently onto a 0.20 mm diameter gold wire electrode (Goodfellow Cambridge Ltd., Huntingdon, England) (Fig. 2-4). Electrical signals were amplified (x10k) and 60 Hz noise was eliminated by notch-filtering using a 'Humbug' device (Quest Scientific, BC, Canada) for digital recording at a sampling rate of 20 kHz and further 60 Hz filtering using a Powerlab 8/35 device and LabChart software (AD Instruments, CO, USA). A loudspeaker was connected in parallel to the recording amplifier output to enable auditive control of evoked SFAP or mixed AP responses. After a RF point with a robust response was determined via rod stimulation, electrical stimulation was performed followed by mechanical stimulation using Von Frey filaments as follows:

Electrical Stimulation: Patch electrodes were pulled from borosilicate glass capillaries (#30-0057, Harvard Apparatus, Quebec, Canada) on a single-stage glass microelectrode puller (Model No. PP-830, Narishige, Tokyo, Japan) to an outer tip size of ~2 µm. After filling with carbogenated superfusate, the electrodes were positioned at the optimal RF point under the binocular microscope using a manual micromanipulator (Model No. M3301L, World Precision Instruments, Sarasota, USA). Via a chlorided silver wire, d.c. current pulses of 0.2 ms duration and 1.5-5 mA amplitude were delivered at a frequency of 0.5 Hz to the patch electrode using the stimulation module of the Labchart software and the Powerlab output to trigger an Isoflex isolation unit (A.M.P.I., Jerusalem, Israel). For determining the NCV of a fiber, the latency between the time point of the beginning of the electrical stimulation artifact and the SFAP peak was determined as well as the distance

between the stimulation and recording electrodes. Fibers with an NCV >1-13 m/s were classified as Aδ-fibers and C-fibers were assigned to have an NCV <1.0 m/s. To further confirm the fiber type, a 'latency test' (George et al., 2007; Hoffmann et al., 2015) was performed by first stimulating the fiber at a frequency of 0.25 Hz for 3 min, then increasing the frequency to 2 Hz for 3 min and finally returning to 0.25 Hz for 3 min. C-fiber identification was confirmed if the latency increased (Fig. 2-5).

Mechanical Von Frey Stimulation: After completion of electrical stimulation, the same RF point of the identified fiber was mechanically stimulated using 0.02-1 g Von Frey filaments to determine the mechanical threshold ('the minimum force required to evoke an SFAP response') for mechanosensitive Aδ- and C-fibers. Such filaments are used in behavioral tests to assess tactile allodynia (Chaplan et al., 1994, Field et al., 1999; Deuis et al., 2017). Under the stereomicroscope, the Von Frey filament was placed manually perpendicularly to the dermal skin at the responsive RF spot for 5-7 s until it bent stably. The mechanical threshold of a SFAP response was determined by starting with the 0.02 g filament (also used in the behavioral studies in 2.7.1), and then proceeding to the next higher stimulus strength until a response was evoked. The stimulation of the RF field point was repeated three times to confirm the mechanical threshold for evoked SFAP responses. The stimuli were separated by 5-10 s lasting pauses to avoid SFAP adaptation or fiber desensitization.

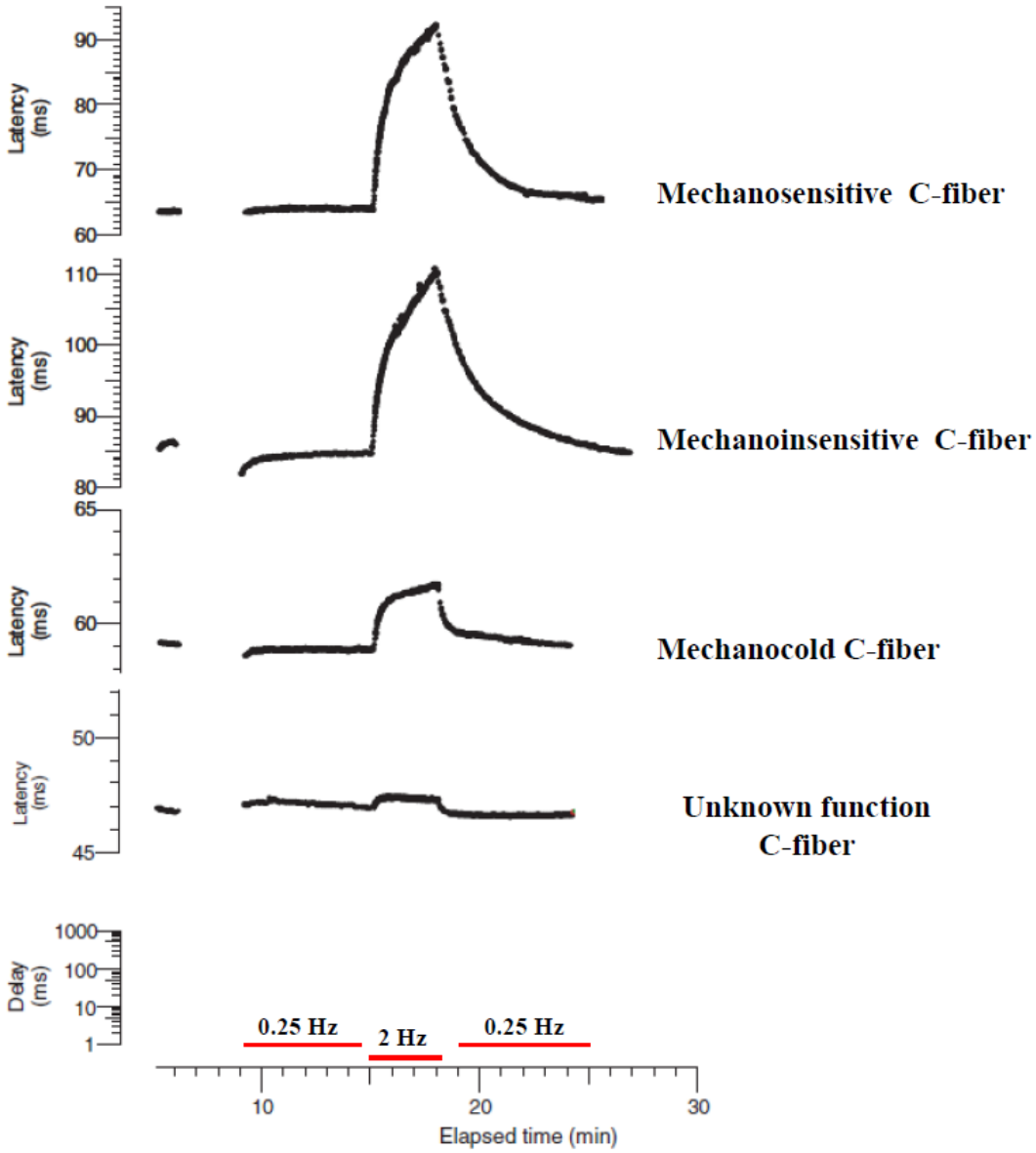

Fig. 2-5: Activity-dependent latency increase in C-fiber subtypes. Different types of C-fibers (i.e., mechanosensitive, mechano-insensitive, cold and unknown function) are displaying activity-dependent changes in their latency at 2 Hz instead of 0.25 for 3 min. (Reproduced with permission from George et al., 2007.)

2.3.3 Data Analysis

The amplitude of individual SFAP's were analyzed using LabChart and Clampfit software (Molecular Devices, CA, USA) (Fig. 2-3B). Overlaying and averaging of sweeps was also performed in Clampfit software. The activity-dependent latency changes in Aδ- and C-fibers at 2 Hz repetitive electrical stimulation were analyzed in LabChart software.

2.4 Immunohistochemistry

Footpad skin punch biopsy was performed using a 3 mm diameter tool (Acu Punch, Acuderm Inc., FL, USA) to generate 2-3 mm thick tissue plugs which were then chemically fixed in 2% paraformaldehyde, lysine, periodate fixative overnight at 4 °C[3]. Next day, the tissues were washed 5 times in 0.1 M Sorenson's phosphate buffer and cryoprotected in 20 % glycerol/0.1 M Sorenson's phosphate buffer overnight at 4 °C (Brussee et al., 2008; Cheng et al., 2013). Next day, tissues were washed 4 times in 1X phosphate-buffered saline (PBS) solution (Thermo Fisher Scientific, MA, USA) and embedded in 'Optimal Cutting Temperature freezing fluid' (Tissue Tek, Tokyo, Japan) under dry ice before cutting them perpendicular to the skin surface into 20 µm thin sections and placing them onto 'Superfrost Plus' microscope slides (Thermo Fisher Scientific). They were then processed for antigen retrieval in sodium citrate buffer (10 mM sodium citrate, 0.05 % Tween 20, pH 6.0) for 20 min at 85 °C. The slides were then washed in 1X PBS and permeabilized in 1 % Triton-X for 10 min. The tissues were 'blocked' for 1 h at room temperature in 10 % normal goat serum, 1 % bovine serum albumin (Sigma Aldrich), 0.3 % Triton-X, and 0.05 % Tween 20 in 1X PBS and incubated overnight at 4 °C in primary rabbit polyclonal antibody (PGP9.5) solution

[3] The footpad immunohistochemistry studies were performed with the help from Paige Shelemey and the DRG and footpad sections were obtained with the help from Twinkle Joy and Haecy Macandili in Dr. Christine A. Webber Laboratory.

(1:200, EnCor Biotechnology, FL, USA). After rinsing in 1X PBS, the tissues were incubated for 2 h with Cy3 anti-rabbit IgG (1:500, Jackson ImmunoResearch Laboratories, West Grove, PA, USA), washed, and mounted with polyaquamount (Polysciences Inc., PA, USA). Images were captured at 40X magnification with a Zeiss Observer Z1 inverted fluorescence microscope. IENFs labeled with PGP9.5 were counted in 4-6 adjacent fields of at least 3 sections per animal for a total of 12-18 fields per NGR using ImageJ (Russell et al., 1999; Beiswenger et al., 2008) and IENF density (i.e. the number of PGP9.5-positive axons/mm) was calculated. DRGs of lumbar spinal segments L4 and L5 were isolated by firstly removing the skin and exposing the sciatic nerve at mid-thigh level. The muscle and the tissue on the side of the exposed spinal column were removed using Dumont #5 forceps and fine scissors No. 14090-09. The sciatic nerve was traced back to the pelvic bone, and shallow bend fine rongeurs (No. 16015-17, Fine Science Tools) were used to crush the pelvic bone to allow the course of the sciatic nerve to be traced proximally to expose the L4 and L5 nerve roots. Dumont #5 forceps were used to firmly pull the nerve roots until the DRG emerged from the intervertebral foramen. The L4 and L5 DRGs were separated from their axon roots using angled spring scissors No. 15008-08 and fixed in 4 % paraformaldehyde overnight at 4 °C. After 16-18 h, the L4 and L5 DRGs were washed 4X in PBS and cryoprotected in 30 % sucrose overnight at 4 °C. DRGs were rewashed after 16-18 h 3X in PBS and then embedded immediately in Optimal Cutting Temperature freezing fluid. DRGs were cut into 12 µm thick sections as noted above and slides with sections were processed for antigen retrieval, washed and permeabilized as above. The slides were incubated for 1 h in blocking solution containing 10 % normal goat serum and 3 % bovine serum albumin and incubated overnight at 4 °C in the following primary antibodies: mouse anti-peripherin (1:500, Sigma Aldrich), rabbit anti-NF200 (1:500, Sigma Aldrich), rabbit anti-CGRP (1:500, Sigma Aldrich), rabbit anti-GFAP (1:500, Dako, ON, Canada), rabbit anti-

ionized calcium-binding adapter molecule (Iba1) (1:500, Wako, VA, USA), rabbit anti-Nav1.7, rabbit anti-Nav1.9 and rabbit anti-Nav1.8 (1:500, Alomone Labs, Jerusalem, Israel). The sections were washed in PBS and incubated with Cy3 anti-rabbit IgG or AlexaFluor 488 secondary antibodies (1:500). Nuclei were labeled with NucBlueTM Live Cell Stain (Life Technologies, NY, USA). The DRG sections were then imaged at 20X magnification on a Zeiss AxioCam MRm camera using Zeiss Observer Z1 inverted fluorescence microscope. Using the freehand selection tool (ImageJ software), each DRGN soma with a visible nucleus was circled and the fluorescent intensity (average grey intensity/μm^2) in this region of interest was represented as arbitrary units (au) (Collins, 2007; Jensen, 2013). Using ImageJ software, an intensity threshold was set (Jensen, 2013) and all DRGNs with pixel intensity in their region of interest above this threshold were considered labeled. These data were represented by scatterplots prepared using Prism 5.0 software (Graphpad software, CA, USA). The average of at least three DRG sections from two separate slides was determined for each animal.

2.5 Motor NCV

NGRs were anesthetized with 5 % isoflurane (Fresenius Kabi Inc., ON, Canada) applied orally at a flow rate of 500-1000 ml/min until recumbent with stable respiration[4]. Once the animal reached a surgical plane, confirmed by testing for the withdrawal reflex with toe pinching, the flow rate was changed to 100-200 ml/min with 2-3 % isoflurane. The areas of the skin, hip, knee, and foot were cleaned with 70 % ethanol, and sites of sciatic nerve stimulation (sciatic notch and popliteal fossa) were located. Pediatric subdermal needle electrodes (7 mm x 30 ga, Consolidated Neuro Supply, Inc., OH, USA) were connected to a biopotential amplifier (D440 amplifier, Digitimer

[4] The motor NCV studies were performed by Dr. Kelvin Jones and Dr. Christine A. Webber.

Ltd., Hertfordshire, UK). They were aseptically inserted into the interossei foot muscles for stimulation to record a compound muscle AP as well as under the skin near hip for ground (Brusse et al., 2008). The electromyographic signals were band-pass filtered at 10-1000 Hz and recorded at a sampling rate of 10 kHz. Electrical stimulation (DS5 stimulator, Digitimer Ltd., Hertfordshire, UK) was performed at the sciatic notch or popliteal fossa. The tibial nerve was stimulated at 1.0 Hz, and the amplitude was increased until a response was evoked. The distance from the stimulation points to the site of recording at the foot muscles was measured to determine the motor NCV.

2.6 qRT-PCR

Isolated DRGs were processed for qRT-PCR as described (Yousuf et al., 2017)[5]. Total ribonucleic acid (RNA) (200 ng) was converted to cDNA using Superscript III Reverse Transcriptase (Invitrogen, CA, USA) and oligo $(dT)_{12-18}$ primers (Invitrogen). Resulting complementary deoxyribonucleic acid (cDNA) was transcribed in a FAST Sybr Green (Applied Biosystems CA, USA) qRT-PCR reaction using StepOne Plus System (Life Technologies, CA, USA). The following primers were used to for qRT-PCR reaction: Nav1.7, Nav1.9 and Nav1.8 (Qiagen, Hilden, Germany); LCGRP (peptide): Fw-CCAGATAAGCCAGAACCATGC, Rev-CCCTTCTCCCTATGACAGGAAA; ACGRP (receptor): Fw-AGCTAAGATGAGC GCAA GT, Rev-CCCTTCTCCCTATGACAGGAAA; HPRT:Fw-AGCCTAAGATGAGCGCAAGT, Rev-TTACTAGGCAGATGGCCACA. Data were analyzed on a base-2 logarithmic scale.

[5] The RT-PCR experiments were performed with the help from Muhammad Saad Yousuf in Dr, Bradley J. Kerr Laboratory.

2.7 Behavioral tests

2.7.1 Von Frey test

The mechanical sensitivity in regard to tactile allodynia and hyperalgesia is most commonly determined by a Von Frey test (Fig. 2-6) for which rodents are placed unrestrained in a small closed chamber with a mesh platform (Chaplan et al., 1994; Field et al., 1999; Deuis et al., 2017). The Von Frey filament with lowest 'gram' force is then applied through the penetrable meshed bottom, perpendicular to the plantar surface of the hind paw constantly for 5 s and the force is increased till the paw-withdrawal response is elicited. NGRs were transferred into the chamber and allowed to habituate for 1 h, and then their foot withdrawal response was measured as described above with 0.02-6 g filaments (Fig. 2-6). Tests were repeated 5 times per filament on both the left and the right paw, and the threshold was noted if a positive response (paw withdrawal, flinching or licking) was observed in at least 3 of the 5 tests (Deuis et al., 2017; Alles et al., 2017). The thresholds from both paws were averaged for each NGR.

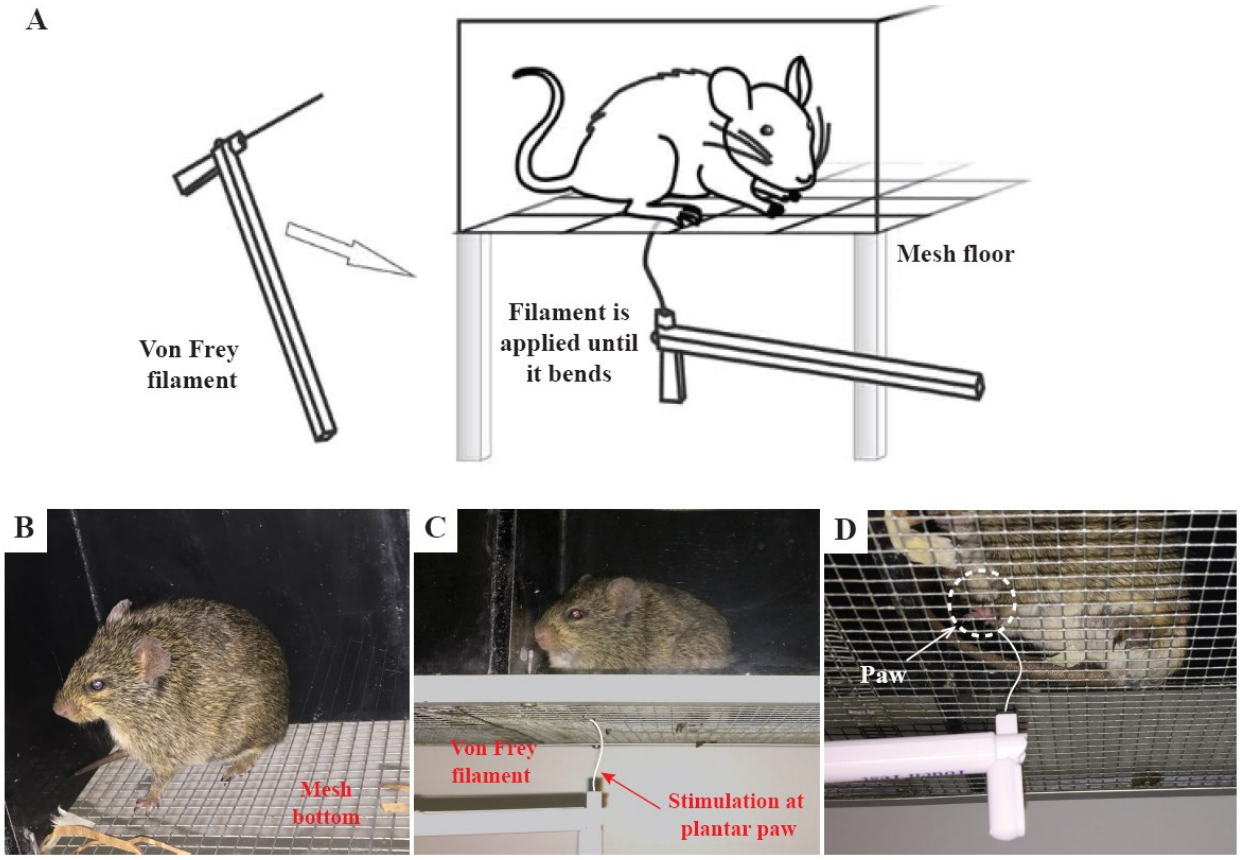

Fig. 2-6: Von Frey mechanical stimulation of NGR paw. A, Cartoon showing a Von Frey chamber for mechanical stimulation of rodent paws. B, NGRs were habituated for 1 h before testing. C, The plantar surface of the NGR paw was stimulated with Von Frey filaments starting with a lower gram (g) force until a paw withdrawal (and licking) response occurred. D, Magnified view of the plantar paw where the Von Frey stimulation is applied. (A reproduced with permission from Deuis et al., 2017.)

2.7.2 Hargreaves test

The Hargreaves test is the most common method for quantifying heat sensitivity and is carried out by applying infrared radiant heat stimulus on the plantar surface of the paw (Hargreaves et al., 1988; Deuis et al., 2017) (Fig. 2-7). NGRs were transferred from cages to Hargreaves chamber very gently in a closed chamber with glass bottom surface and habituated for 1 h before heat application. A beam of infrared radiant heat at 52 °C was then applied manually to the plantar paw surface (Fig. 2-7). The paw withdrawal latency was then recorded in a notebook that is displayed automatically on the apparatus. The cut-off time of 30 s was preset in the apparatus for heat stimuli to avoid potential damage to the NGR paw tissue. Each test was repeated 3 times on both the left and right paws, and the latency for paw withdrawal was averaged from both paws for final analysis.

2.8 Statistical analysis

Statistical analysis of all data and preparation of all scatter plots was performed in Prism 5.0 software. All results are presented as means ± standard error of the means (sem). Unpaired Student's t-test was used to obtain statistical significance between control and T2D groups, with a significance criterion of at least $p<0.05$. P values less than 0.05 are denoted by one asterisk while p values less than 0.01 and 0.001 are illustrated by two and three asterisks in the figures in chapter-3.

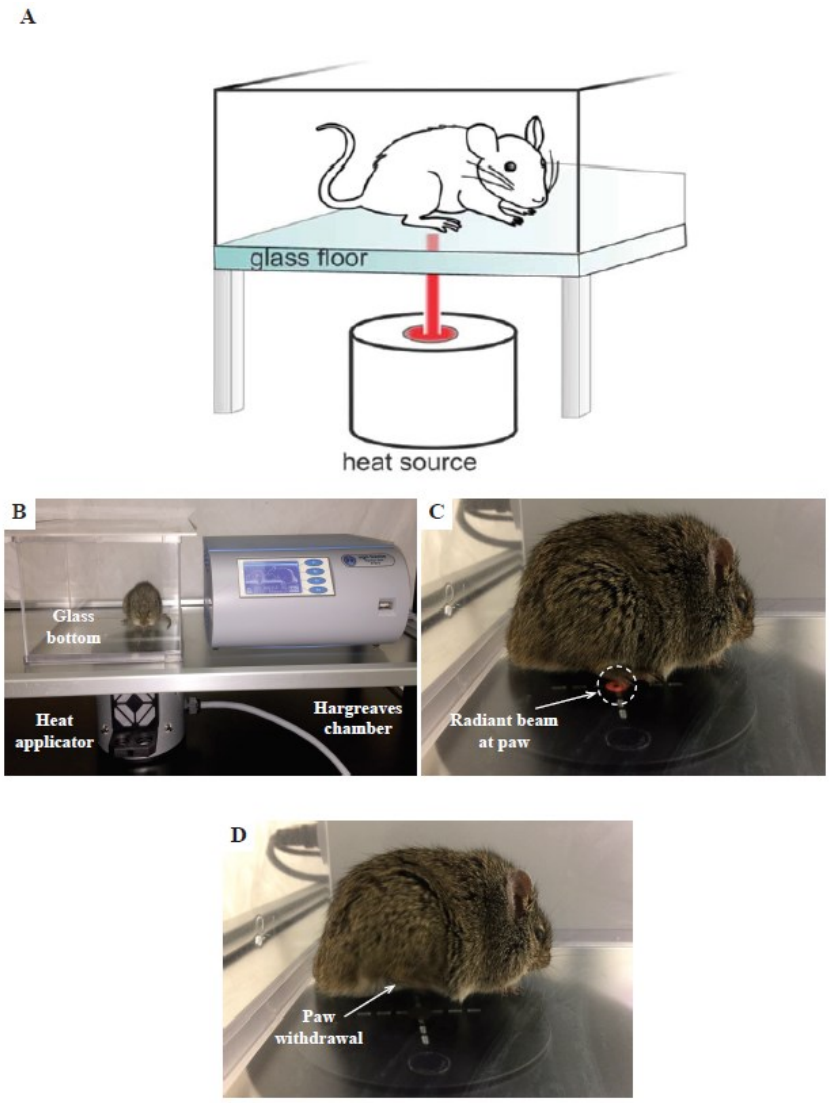

Fig. 2-7: Heat stimulation of NGR plantar paw for Hargreaves test. A, Cartoon showing heat stimulation on rodent paw in Hargreaves chamber. B, NGRs were habituated for 1 h before heat testing in the Hargreaves chamber. C, Heat stimulation was applied to the plantar foot surface by manually positioning the infrared radiant heat source (red spot within a dotted circle). D, Paw withdrawal response automatically turned off the heat and the latency between the start of heat pulse and response (in s) were recorded. (A reproduced with permission from Deuis et al., 2017.)

CHAPTER-3

RESULTS

This chapter begins with a summary of the metabolic phenotype of T2D NGRs, followed by my first author publication (Singh et al., 2018) which shows that this model demonstrates hallmark features of PSN (3.1-3.4)[6]. The final part describes the feasibility of the skin-nerve preparation in NGRs to analyze T2D-related changes in nerve fiber properties.

3.1 Metabolic Phenotypes

The primary diagnostic criterion to determine T2D in NGRs is hyperglycemia with a FBG>5.6 mM (Yang et al., 2016; Han et al., 2017). The mean FBG in 14 control NGRs was 2.83 ± 0.15 mM (Fig. 3-1A), whereas 20 out of 25 chow-fed NGRs were hyperglycemic as their mean FBG was 10.78 ± 1.33 mM (n=25; $p<0.001$) (Fig. 3-1A). Another criteria to determine T2D was increased body weight and BMI. The average body weight of T2D NGRs was higher (120 ± 2.86 g; n=19) compared to controls (90.5 ± 4.05 g; n=14; $p<0.001$) (Fig. 3-1B). The average BMI of T2D NGRs was 5.96 ± 0.14 kg/m^2 (n= 18) compared to 5.12 ± 0.11 kg/m^2 in controls (n=14; $p<0.001$) (Fig. 3-1C). In T2D patients and animal models, pathology is also reflected by decreased fasting plasma insulin levels suggesting β-cell impairment (Weir and Bonner-Weir, 2004; Biessels et al., 2013). There was no difference in the mean fasting plasma insulin levels of T2D animals (2.17 ± 0.44 ng/ml; n=16; p=0.82) compared to control NGRs (2.04 ± 0.35 ng/ml; n=12) (Fig. 3-1D). This heterogeneity was similar to previously published results (Yang et al., 2016).

[6] Portions of this chapter have been published (Singh et al., 2018, Journal of Neuropathology & Experimental Neurology; 77(6):469-78

The T2D status of the 5 non-hyperglycemic animals was verified based on comorbidities such as body weight (T2D NGRs: 119.3 ± 5.68 g; n=5; control NGRs: 90.5 ± 4.05 g; n=14; $p<0.001$) and BMI exceeding control thresholds (T2D NGRs: 5.66 ± 0.12 kg/m^2; n=5; control NGRs: 5.12 ± 0.11 kg/m^2; n=14; $p<0.05$). Three of these animals demonstrated fasting plasma insulin levels below 2 ng/ml suggesting β-cell impairment (Table. 3-1) (Yang et al., 2016).

3.2 Hallmark features of T2D-PSN

Hallmark features of T2D-PSN include IENF denervation, thermal and mechanical hyposensitivity, and decreased motor NCV (McCarthy et al., 1995). Skin-biopsy is a valuable test to assess IENFs ('unmyelinated C-fibers and myelinated Aδ-fibers') under pathological conditions such as T2D-PSN (McCarthy et al., 1995). IENFs extend into the epidermis as 'free nerve endings' (Kennedy and Wendelschafer-Crabb, 1993; McCarthy et al., 1995). Footpad skin biopsies from NGRs were processed for immunocytochemistry against the small nerve fiber marker PGP9.5 to count IENFs. There was a marked IENF denervation in the footpads of T2D NGRs (16.6 ± 1.9 nerve terminals/mm, n=9) compared to control animals (25.8 ± 1.5 nerve terminals/mm, n=5, $p<0.01$) (Fig. 3-2A-C).

The response to mechanical stimuli was tested using calibrated Von Frey filaments (0.4-6.0 g) (Chaplan et al., 1994; Field et al., 1999; Deuis et al., 2017). T2D NGRs required greater mechanical force (2.1 ± 0.6 g, n=10) to withdraw their paws compared to control animals (0.7 ± 0.1 g, n=7, $p<0.05$) (Fig. 3-2D). Hargreaves analysis revealed a thermal hyposensitivity in T2D NGRs (Hargreaves et al., 1988; Deuis et al., 2017) as it took them significantly longer (16.0 ± 1.1 s, n=10) to remove their paws from a 52 °C heat stimulus compared to control animals (11.5 ± 1.1 s, n=7,

$p<0.05$) (Fig. 3-2E). Motor NCV slowing is an important clinical criterion to indicate sensorimotor nerve dysfunction in both experimental and human T2D-PSN (Biessels et al., 2013; Dunninan et al., 2013; Wilson and Wright, 2014). For example, streptozotocin-induced T2D mice displayed motor NCV slowing from 53.6 m/s to 47.9 m/s in controls (Wilson et al., 2014). Similarly, T2D patients demonstrated 38.5 m/s of common peroneal motor NCV compared to 51.6 m/s in healthy volunteers (Perkins and Bril, 2014). Sciatic motor nerve analysis revealed that NCV slowed to 26.9 ± 2.3 m/s ($n=7$, $p<0.001$) in T2D NGRs compared to 68.0 ± 0.8 m/s ($n=5$) in control NGRs when the sciatic notch or popliteal fossa was electrically stimulated and CMAPs were recorded at interossei foot muscles (Fig. 3-2F, G)[7]. Collectively, these data indicate that T2D NGRs display hallmark features of human T2D-PSN.

[7] The motor NCV studies were conducted by Drs. Kelvin Jones and Christine A. Webber.

Age (months)	FBG (mM)	Fasting plasma insulin (ng/ml)	Body weight (g)	BMI (kg/m^2)
18	2.8	4.6	114.3	5.5
12	2	3	110.7	5.5
12	5.2	0.28	109.9	5.2
19	3.6	0.5	121.1	5.7
18	4.3	1.89	140.6	6.1

Table. 3-1: Chow-fed NGRs with T2D comorbidities. Systemic status of 5 chow-fed NGRs with non-hyperglycemic FBG. These animals were included in this study as they had at least 2 comorbidities such as low fasting plasma insulin level below control (2 ng/ml) indicating β-cell impairment in T2D, increased body weight compared to mean body weight of 90.5 g in control NGRs; increased body mass index in Chow-fed NGRs compared to a mean control threshold of 5.12 kg/m^2.

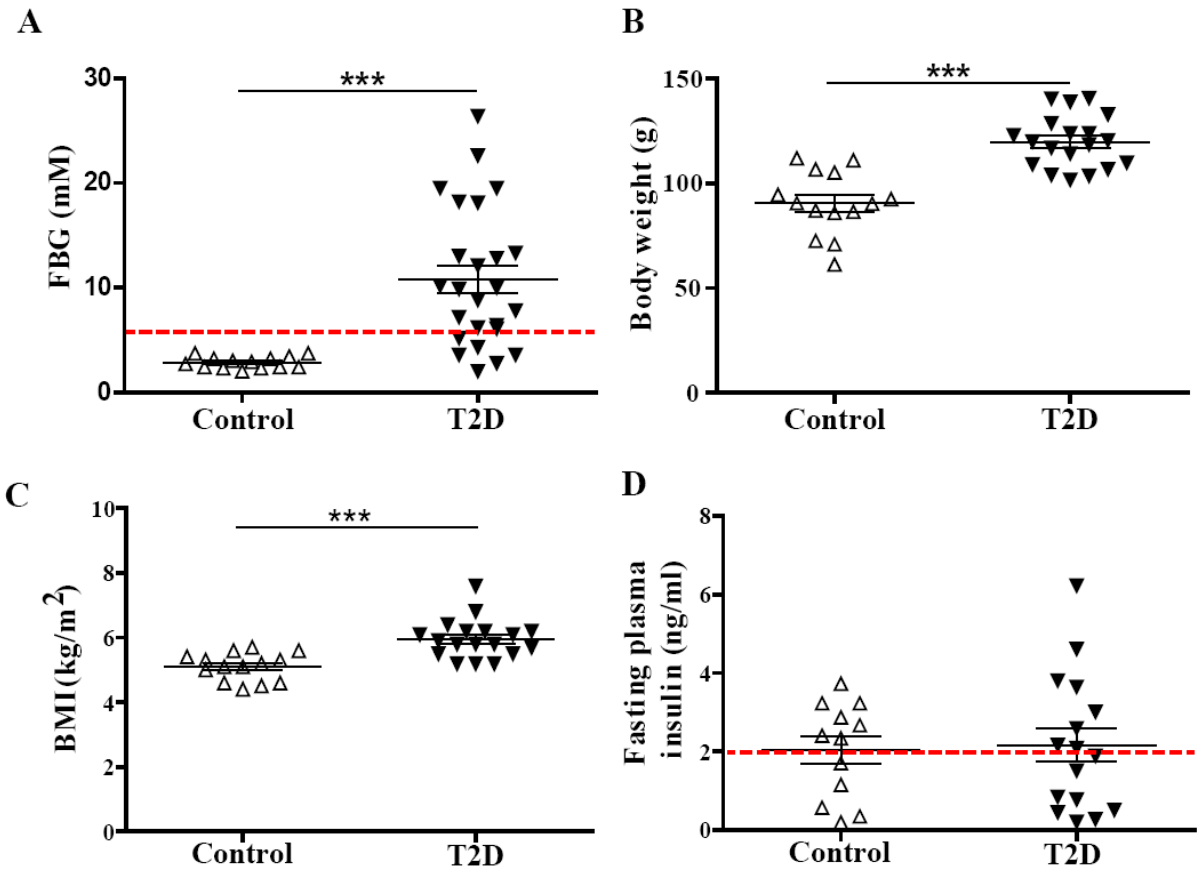

Fig. 3-1: Metabolic phenotype in NGRs. A, 20 of 25 chow-fed NGRs had increased FBG compared to controls (n=14; ***p<0.001). The red dotted line represents the hyperglycemia cut-off at 5.6 mM. B, C, T2D NGRs had increased body weight (C, n=19; ***p<0.001) and body mass index, BMI (D, n=18; ***p<0.001)) compared to controls (C, n=14; D, n=14). D, Fasting plasma insulin levels did not change in T2D NGRs (n=16) compared to control animals (n=12; p=0.82). (Reproduced with kind permission from Singh et al., 2018.)

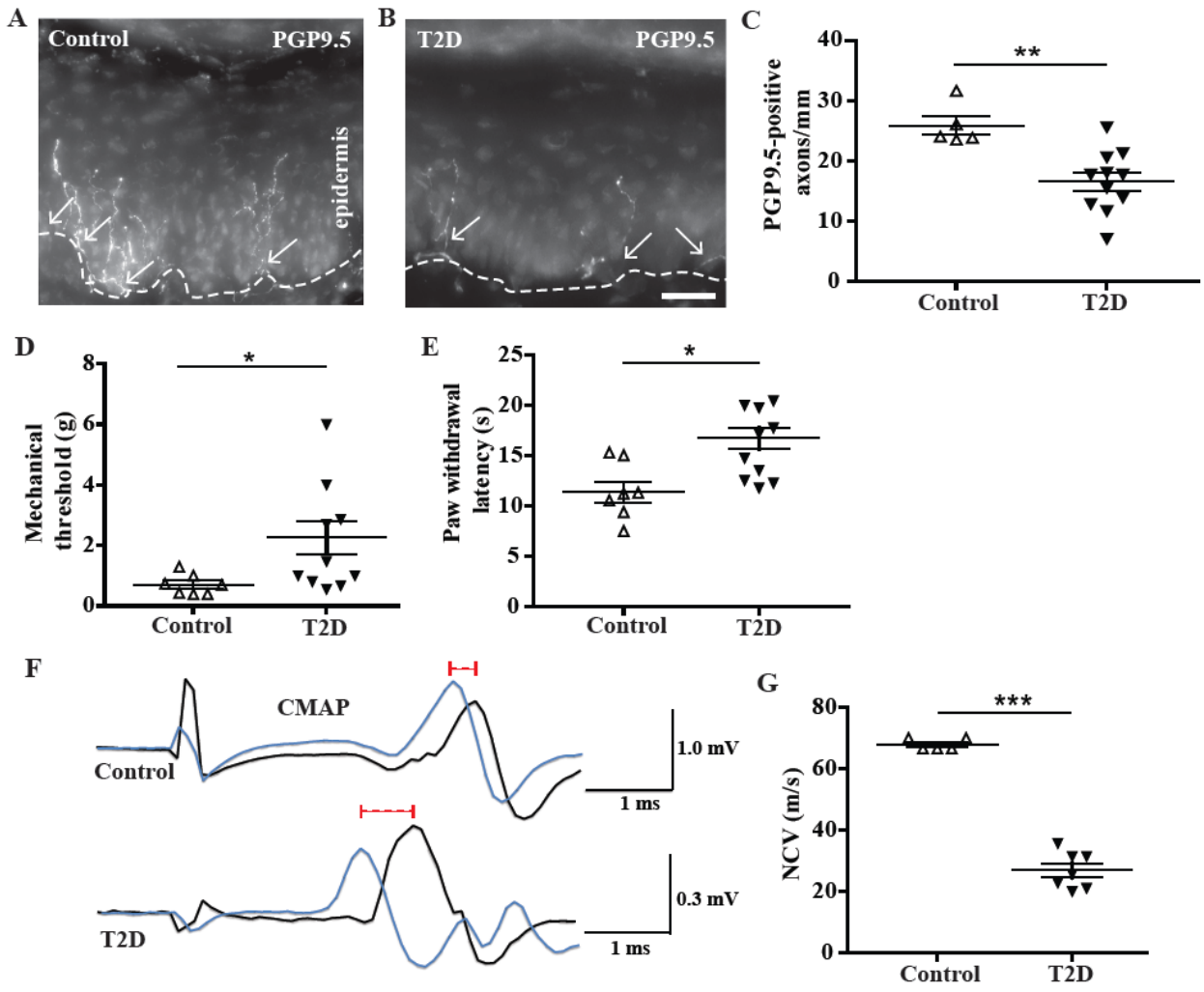
A
Control
PGP9.5
epidermis
B
T2D
PGP9.5
C
PGP9.5-positive axons/mm
40
30
20
10
0
**
Control
T2D
D
Mechanical threshold (g)
8
6
4
2
0
*
Control
T2D
E
Paw withdrawal latency (s)
25
20
15
10
5
0
*
Control
T2D
F
CMAP
Control
1.0 mV
1 ms
T2D
0.3 mV
1 ms
G
NCV (m/s)
80
60
40
20
0
***
Control
T2D

Fig. 3-2: T2D NGRs demonstrate hallmark pathological features of PSN. A, B, Epidermal innervation of plantar footpads of (A) control and (B) in T2D NGRs. IENFs were immunolabeled against PGP9.5 (arrows), and each IENF that crossed the dermal-epidermal junction (dashed lines) was counted. C, T2D NGRs (n=9; black triangles) had less epidermal innervation compared to control (white triangles) (n=5; **$p<0.01$). D, *In-vivo* behavioral assessment by force application using Von Frey filaments on the plantar paw demonstrated an increased mechanical threshold in T2D NGRs (n=10) compared to controls (n=7; *$p<0.05$). E, Hargreaves heat test (52 °C) demonstrated an increased plantar paw withdrawal latency in T2D NGRs (n=10) compared to control animals (n=7; *$p<0.05$). F, Compound muscle AP (CMAP) traces in control and T2D NGRs; black trace displayed stimulation at sciatic-notch, while blue trace illustrated stimulation at popliteal-fossa. G, T2D NGRs (n=7) had decreased motor nerve NCV compared to controls (n=5; ***$p<0.001$). Scale bar is 25 μm. (Reproduced with kind permission from Singh et al., 2018.)

3.3 Effect of T2D on DRGNs and surrounding satellite glial cells

Next, the effect of T2D on DRGNs was analyzed. Firstly, large and small diameter DRGNs were co-immunolabeled with established markers to ensure T2D did not affect the overall number or relative distribution of DRGN subpopulations. Specifically, large diameter (>30 μm) mostly mechanosensory and proprioceptive DRGNs were immunolabeled against NF200, whereas small diameter, primarily nociceptive, neurons (Woolf and Ma, 2007; Dubin and Patapoutian, 2010; Nickel et al., 2012), were immunolabeled against peripherin (Fig. 3-3A-F). The DRGN soma diameter versus fluorescence intensity of immunolabeled tissue sections was plotted for NF200 (Fig. 3-3G, H) and peripherin (Fig. 3-3I, J). A semi-quantitative analysis determined there was no change in the NF200 labeling intensity of T2D DRGNs (48.8 ± 1.1 au, n=3, 10 DRGs) compared to control animals (51.0 ± 1.7 au, n=3, 11 DRGs, p=0.30) (Fig. 3-3K). Similarly, there was no difference in the percentage of large diameter DRGNs expressing NF200 in T2D NGRs (38.7 ± 4.6%, n=3, 10 DRGs) compared to control animals (52.4 ± 5.2%, n=3, 11 DRGs, p=0.06) (Fig. 3-3L). There were no changes in peripherin labeling intensity of T2D DRGNs (31.6 ± 2.5 au, n=3, 10 DRGs) compared to control animals (28.0 ± 2.2 au, n=3, 9 DRGs, p=0.29) (Fig. 3-3M). Finally, there was no difference in the percentage of small diameter DRGNs expressing peripherin in T2D NGRs (68.6 ± 8.4%, n=3, 10 DRGs) compared to control NGRs (55.9 ± 6.2%, n=3, 9 DRGs, p=0.25) (Fig. 3-3N).

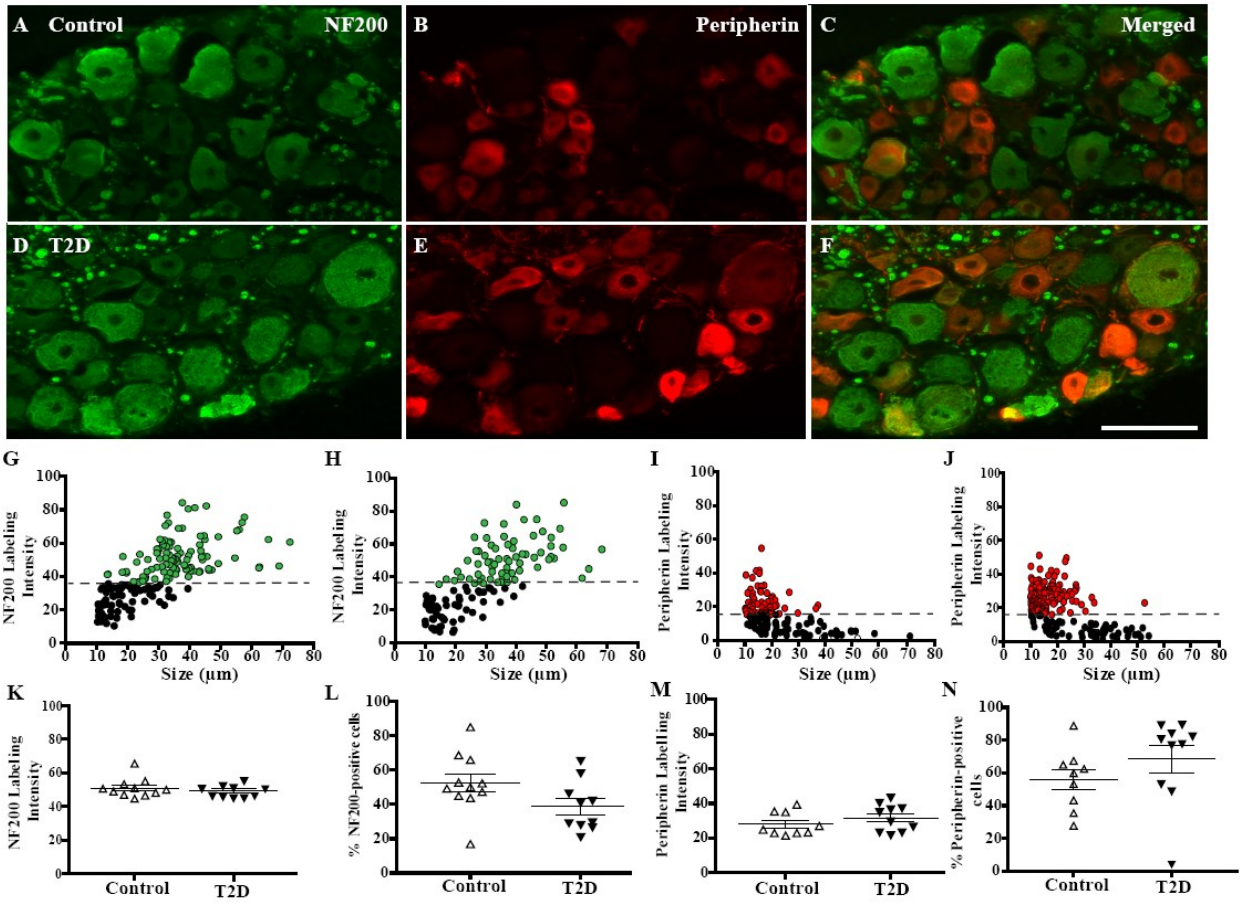
A Control
NF200
B
Peripherin
C
Merged
D T2D
E
F
G
H
I
J
NF200 Labeling Intensity
Peripherin Labeling Intensity
Size (µm)
K
L
M
N
% NF200-positive cells
% Peripherin-positive cells
Peripherin Labelling Intensity
Control
T2D

Fig. 3-3: T2D does not cause DRGN death. A-F, Immunofluorescent labeling of DRGNs from control (A-C) and T2D (D-F) NGRs (scale bar is 100 μm). Large soma diameter (>30 μm) mechanosensitive and proprioceptive control (A) and T2D (D) DRGNs were immunolabeled against neurofilament 200 (NF200, green). Small diameter control (B) and T2D (E) DRGNs were immunolabeled against peripherin (red). Merged images of DRGNs labeled with NF200 and peripherin in control (C) and T2D (F) NGRs. G, H, Scatterplots of sections in one control (G) and one T2D (H) DRG labeled with NF200; dashed line represents the threshold of NF200-positive DRGNs (green dots). DRGNs below the threshold were considered NF200-negative (black dots). I, J, Scatterplots of control (I) and T2D (J) NGRs; the dotted line represents the threshold of peripherin-positive DRGNs (red dots) whereas DRGNs below this range were considered peripherin-negative (black dots). K, Semi-quantitative analysis of DRGNs labeled with NF200 did not show a change in NF200-labeling intensity in T2D NGRs (n=3, 10 DRGs) compared to controls (n=3, 11 DRGs; p=0.29). L, There was no change in the percentage of NF200-positive DRGNs in T2D NGRs (n=3, 10 DRGs) compared to controls (n=3, 11 DRGs; p=0.06). M, Semi-quantitative analysis of peripherin-labeled DRGNs showed no change in labeling intensity in T2D NGRs (n=3, 10 DRGs) compared to controls (n=3, 9 DRGs; p=0.29). N, There was no change in the percentage of peripherin-positive DRGNs in T2D NGRs (n=3, 10 DRGs) compared to controls (n=3, 9 DRGs; p=0.2539). Scale bar is 50 μm. (Reproduced with kind permission from Singh et al., 2018).

Next, I determined if T2D affected peptidergic or non-peptidergic DRGNs. Peptidergic (i.e., CGRP-expressing) DRGNs have a nociceptive role, and in T2D-PSN, they demonstrate altered CGRP expression (Malon et al., 2011; Malon and Cao., 2016; Iyengar et al., 2017). T2D and control DRGs were immunolabeled against CGRP (Fig. 3-4A, B) and scatterplots of these tissue sections depicted the neuronal soma diameter and CGRP labeling intensity (Fig. 3-4C, D). Semi-quantitative analysis of CGRP immunolabeling did not reveal changes in protein labeling intensity between T2D DRGNs (60.6 ± 4.5 au, n=3, 15 DRGs) and control DRGNs (58.4 ± 1.9 au, n=4, 11 DRGs, p=0.69) (Fig. 3-4E). Similarly, there was no change in the percentage of CGRP-positive small diameter T2D DRGNs (47.1 ± 7.2%, n=3, 15 DRGs) compared to control DRGNs (44.8 ± 5.8%, n=4, 11 DRGs; p=0.81) (Fig. 3-4F). Furthermore, there was no change in the percentage of IB4-positive (non- peptidergic) small diameter T2D DRGNs (40.7 ± 7.1%, n=3, 9 DRGs) compared to control DRGNs (42.1 ± 5.2%, n=3, 9 DRGs; p=0.88) (Fig. 3-4G-I).

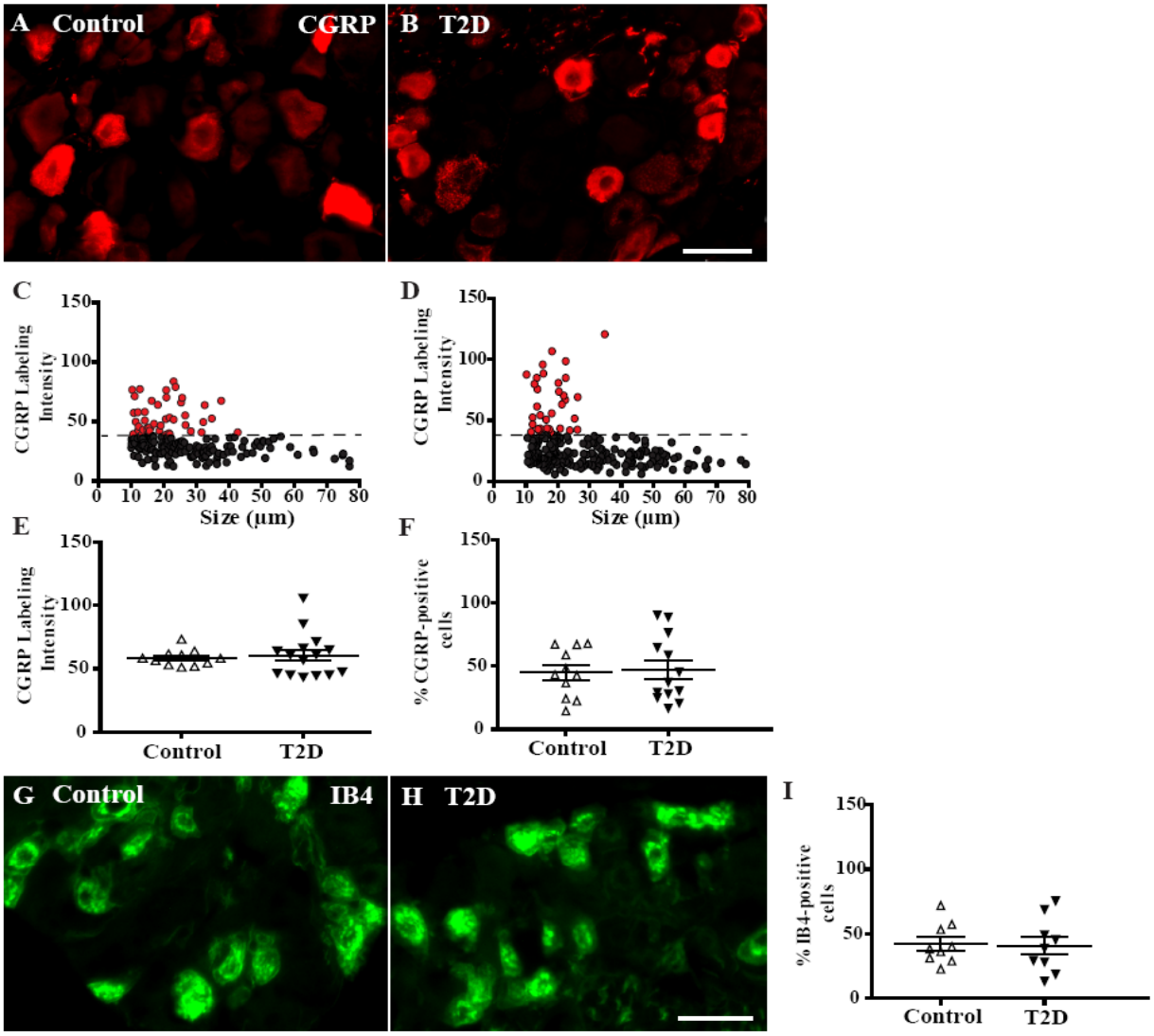
A Control
CGRP
B T2D
C
CGRP Labeling Intensity
150
100
50
0
0 10 20 30 40 50 60 70 80
Size (µm)
D
CGRP Labeling Intensity
150
100
50
0
0 10 20 30 40 50 60 70 80
Size (µm)
E
CGRP Labeling Intensity
150
100
50
0
Control
T2D
F
% CGRP-positive cells
150
100
50
0
Control
T2D
G Control
IB4
H T2D
I
% IB4-positive cells
150
100
50
0
Control
T2D

Fig. 3-4: T2D DRGNs show no change in CGRP and IB4 immunoreactivities. A, B, CGRP immunofluorescent labeling of control (A) and T2D (B) NGRs DRG sections. C, D, Scatterplots of sections from one control (C) and one T2D (D) DRG labeled against CGRP. The dashed line indicates the threshold of individual CGRP-positive DRGNs (red dots) and DRGNs below this threshold were considered CGRP-negative (black dots). These plots illustrate that CGRP-expressing DRGNs were primarily the smaller diameter DRGNs (<30 μm). E, Semi-quantitative analysis of CGRP-labeled DRGNs revealed no change in the expression of CGRP in T2D (n=3, 15 DRGs) compared to control DRGNs (n=4, 11 DRGs; p=0.85). F, There was also no change in the percentage of CGRP-expressing DRGNs in T2D NGRs (n=3, 15 DRGs) compared to controls (n=4, 11 DRGs; p=0.81). G, H, IB4-immunofluorescent labeling in one control (G) and one T2D (H) DRG. I, There was no change in the percentage of IB4-labeled DRGNs in T2D NGRs (n=3, 9 DRGs) compared to controls (n=3, 9 DRGs; p=0.88). Scale bar is 50 μm. (Reproduced with kind permission from Singh et al., 2018.)

GFAP, a marker of satellite glial cell activation, is elevated in T2D-PSN (Warwick and Hanani, 2013; Hanani et al., 2014; Nascimento et al., 2014; Costa and Neto, 2015). In T2D NGRs, 36.5 ± 2.7 % of DRGNs were surrounded by activated satellite glial cells (n=5, 8 DRGs) compared to 13.6 ± 1.9% in control animals (n=4, 8 DRGs, $p<0.001$) (Fig. 5A-C). Iba1, a macrophage marker that is upregulated in streptozotocin-T2D models (Ton et al., 2013; Ellis and Bennett, 2013), was used to determine macrophage infiltration (indicative of an increased inflammatory response) in DRGs of T2D NGRs. It was revealed that T2D NGRs had an elevated percentage area of Iba1 labeling (0.11± 0.02%; n=3) compared to control animals (0.04 ± 0.01%; n=4; $p<0.01$) (Fig. 3-5D-F).

Collectively, these results show that T2D NGRs have activated satellite glial cells and macrophage infiltration surrounding the unchanged prototypical DRGN subpopulations.

3.4 Effect of T2D on Nav expression

Nav are important to regulate neuronal excitability and mediate AP propagation (Black and Waxman, 2013; Lauria et al., 2014). Nav 1.7, Nav 1.8 and Nav1.9 are expressed in DRGNs and are involved in the mediation of thermal hyperalgesia, inflammation and chronic pain syndromes in T2D-PSN (Khan et al., 2002; Hong and Wiley, 2005; Chattopadhyay et al., 2008; Dib-Hajj et al., 2015). Moreover, Nav1.9 and Nav1.7 expression in DRGNs is upregulated whereas Nav1.8 is downregulated in T2D-PSN streptozotocin rat models (Craner et al., 2002; Hong et al., 2004).

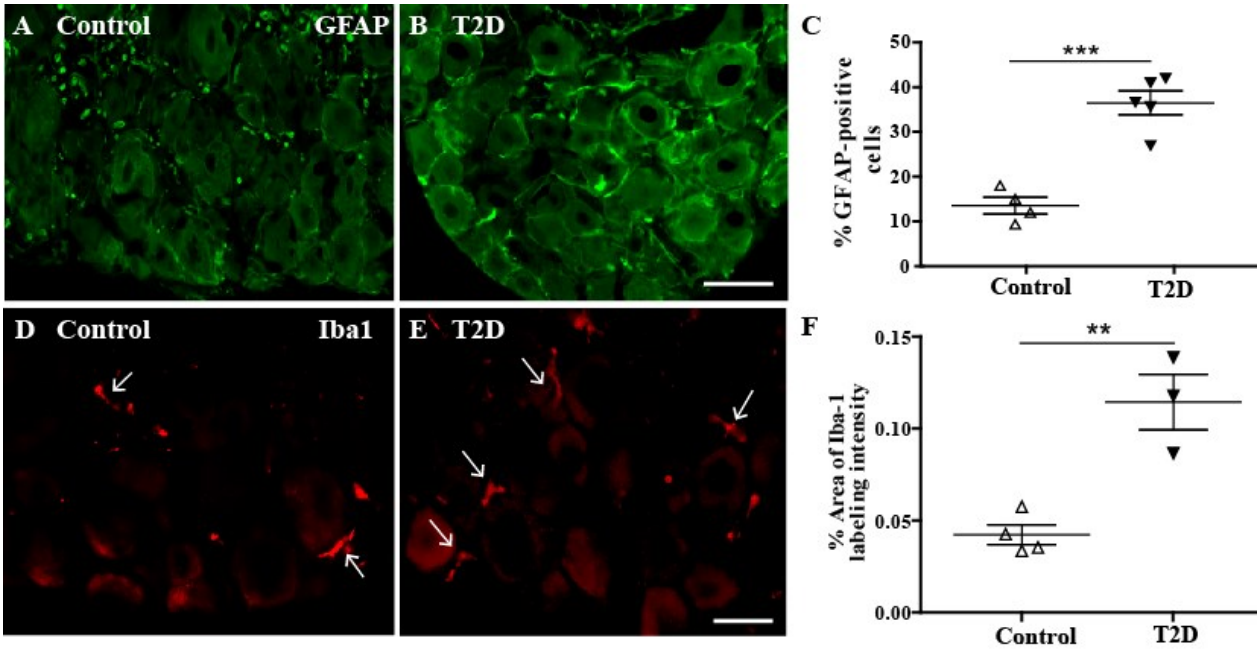

Fig. 3-5: Activation of satellite glial cells and macrophage infiltration in T2D DRGNs. A, B, Glial fibrillary acidic protein (GFAP) immunofluorescent labeling of satellite glial cells surrounding DRGNs in one control (A) and one T2D (B) DRG. C, There is an increase in the percentage of DRGNs surrounded by GFAP-positive satellite glial cells in T2D (n=5, 8 DRGs) compared to controls (n=4, 8 DRGs, ***$p<0.001$). D, E, DRGNs from one control (D) and one T2D (E) NGR showing macrophage labeling with ionized calcium binding adaptor molecule 1 (Iba1) marker. F, There was an increase in Iba1-labeled percent area in T2D DRGNs (n=3) compared to controls (n=4, **$p<0.01$). Scale bar is 50 µm. (Reproduced with kind permission from Singh et al., 2018.)

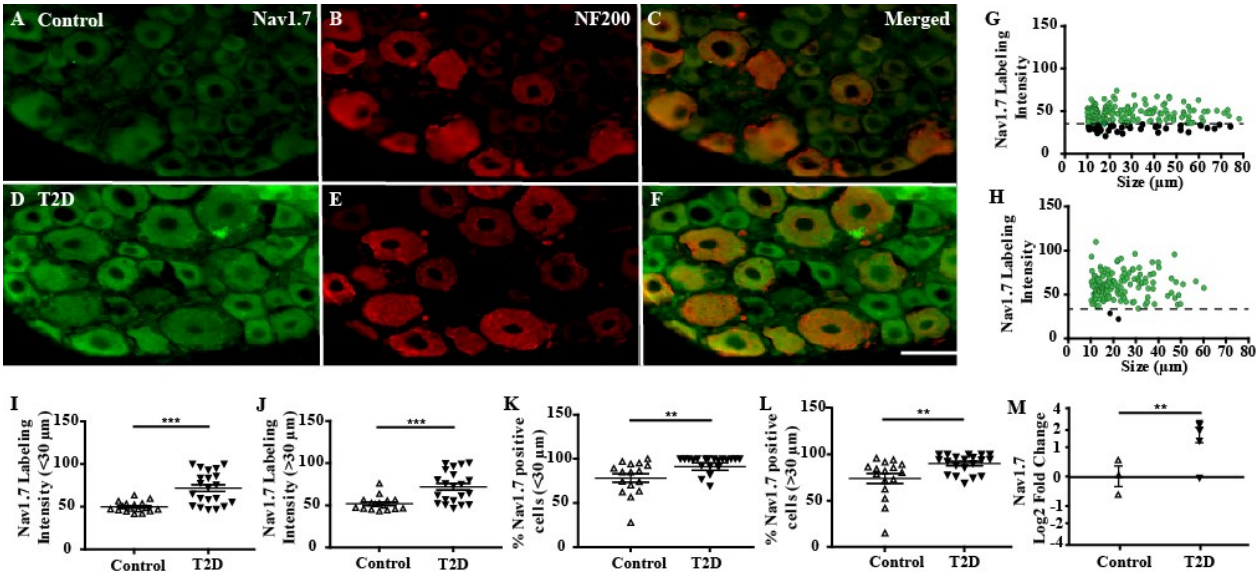

Fig. 3-6: Nav1.7 expression in T2D DRGNs. A-F, Immunofluorescence images of control (A-C) and T2D (D-F) DRGNs co-labeled against Nav1.7 and NF200. G, H, Scatterplots of control (G) and a T2D (H) DRGNs labeled for Nav1.7. The dashed line indicates the threshold of individual DRGNs Nav1.7-positive (red dots) and DRGNs below this threshold were considered Nav1.7-negative (black dots). I, J, The average labeling intensity of each DRG section revealed a significant increase in Nav1.7-protein expression in both small (I) and large (J) diameter T2D DRGNs (n=6, 21 DRGs) compared to controls (n=4, 21 DRGs, ***p<0.001). K, L, There was an increase in the percentage of small (K) and large (L) diameter (n=4, 20 DRGs) Nav1.7-positive DRGNs in T2D NGRs compared to controls (n=4, 16 DRGs, **p<0.01). M, qRT-PCR revealed an overall increase in Nav1.7 mRNA expression in T2D DRGs (n=4) compared to controls (n=3, **p<0.01). Scale bar is 50 µm. (Reproduced with kind permission from Singh et al., 2018.)

Nav1.7-labeled DRGNs from T2D and control NGRs were co-immunolabeled against NF200 to identify the large (NF200-expressing) and small (NF200-negative) DRGNs (Fig. 3-5A-F). Scatterplots illustrated the DRGN soma size and Nav1.7 labeling intensity. These studies revealed an increase in Nav1.7 labeling intensity in both the small and large diameter T2D DRGNs, respectively (72.0 ± 4.1 au; 72.1 ± 4.0 au, n=6, 21 DRGs) compared to controls (49.9 ± 1.5 au; 52.0 ± 2.1 au, n=4, 17 DRGs), $p<0.001$) (Fig. 3-6I, J). Further, there was an increase in the percentage of both small and large diameter T2D DRGNs expressing Nav1.7 (95.0 ± 2.0%; 90.1 ± 2.3%, n=4, 20 DRGs compared to control DRGNs (78.4 ± 4.8%; 74.0 ± 5.4%, n=4, 16 DRGs, $p<0.01$) (Fig. 3-6K, L). Quantitative RT-PCR confirmed there was an increase in Nav1.7 mRNA expression in T2D DRGs (2.11 ± 0.27 $M_{(log2)}$, n=4) compared to control DRGs (0.0001 ± 0.27 $M_{(log2)}$, n=3; $p<0.01$) (Fig. 3-6M)[8].

There was also an increase in Nav1.9 labeling intensity of small diameter T2D DRGNs (56.6 ± 3.2 au, n=4, 12 DRGs) compared to control DRGNs (47.4 ± 1.1 au, n=3, 13 DRGs, $p<0.05$) (Fig. 3-7A-I). Conversely, there was no change in the percentage of small diameter T2D DRGNs expressing Nav1.9 (88.0 ± 4.5%, n=4, 12 DRGs) compared to controls (85.2 ± 3.5%, n=3, 13 DRGs, p=0.63) (Fig. 3-7K). There was also no change in labeling intensity of Nav1.9 protein in T2D large diameter DRGNs (54.9 ± 2.9 au, n=4, 12 DRGs) compared to controls (50.0 ± 1.2 au, n=3, 13 DRGs, p=0.23) (Fig. 3-7J) and in the percentage of large diameter T2D DRGNs expressing Nav1.9 (85.8 ± 6.5%, n=4, 12 DRGs) compared to controls (86.5 ± 5.7%, n=3, 13 DRGs, p=0.93) (Fig. 3-7L).

[8] The RT-PCR studies were conducted with help from Muhammad Saad Yousuf in Dr. Bradley J. Kerr laboratory

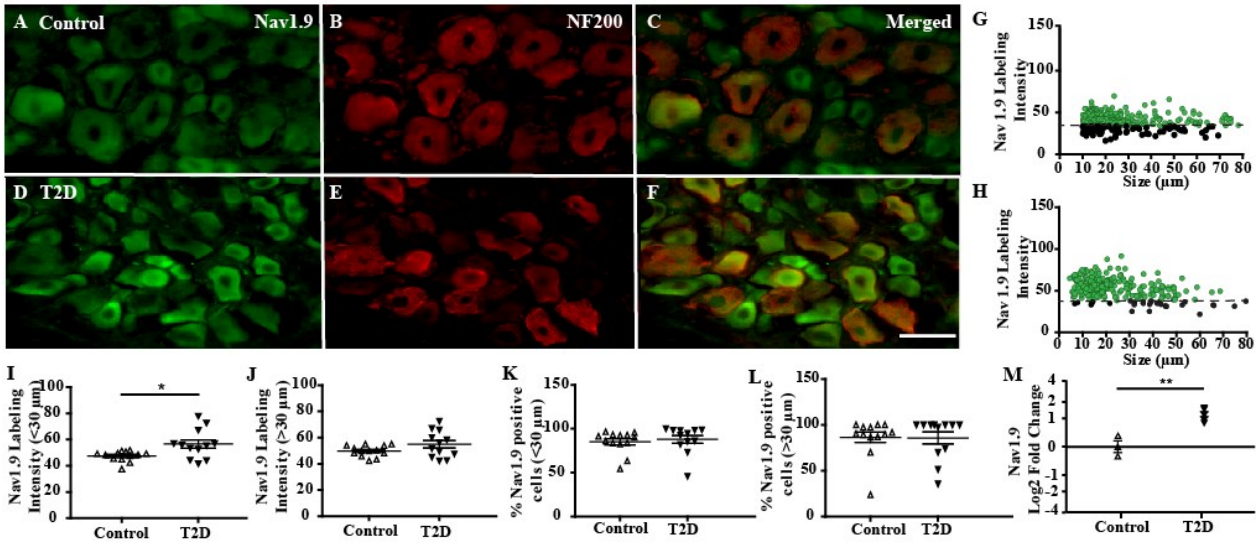

Fig. 3-7: Nav1.9 expression in T2D DRGNs. A-F, Immunofluorescent images of control (A-C) and T2D (D-F) DRGNs co-labeled against Nav1.9 and NF200. G, H, Scatterplots of control (G) and T2D (H) DRGNs labeled for Nav1.9. The dashed line indicates the threshold of individual Nav1.9-positive DRGNs (green dots), and DRGNs below this threshold were considered Nav1.9-negative (black dots). I, J, Semi-quantitative analysis of the average Nav1.9-labeled DRGNs revealed a significant increase in labeling intensity in small (I), but not large (J) diameter T2D DRGNs (n=4, 12 DRGs) compared to controls (n=3, 13 DRGs; I, *$p<0.05$; J, $p=0.23$). K, L, There was no change in the percentage of small-diameter (K) or large-diameter (L) Nav1.9-positive T2D DRGNs compared to controls (n=3, 13 DRGs; K, $p=0.63$; L, $p=0.93$). M, qRT-PCR revealed a significant increase in Nav1.9 mRNA expression in T2D (n=5) compared to control DRGs (n=3, **$p<0.01$). Scale bar is 50 µm. (Reproduced with permission from Singh et al., 2018.)

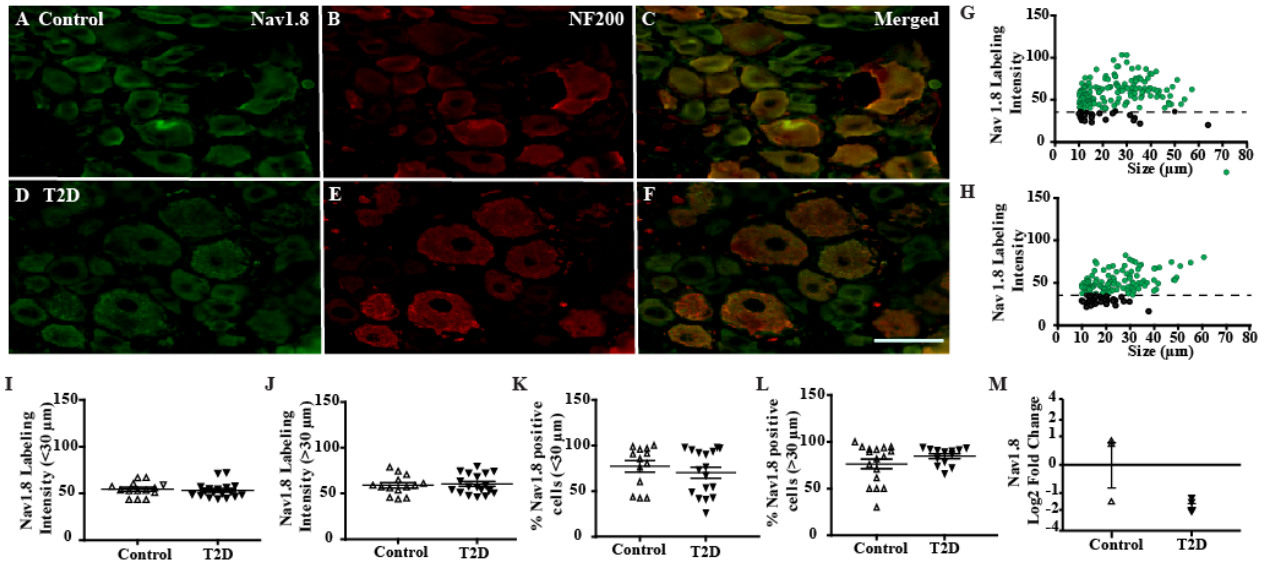

Fig. 3-8: Nav1.8 expression in T2D DRGNs. A-F, Immunofluorescent images of control (A-C) and T2D (D-F) DRGNs co-labeled against Nav1.8 and NF200. G, Scatterplots of individual control (G) and T2D (H) DRGNs expressing Nav1.8; dashed line represents the threshold of Nav1.8-positive DRGNs (green dots), and neurons below this threshold were considered Nav1.8-negative (black dots). I, J, Semi-quantitative analysis of Nav1.8-labeled DRGNs revealed no change in Nav1.8-protein expression in both small (I) and large-diameter (J)) DRGNs in T2D NGRs (n=6, 18 DRGs) compared to controls (n=4, 14 DRGs; I, p=0.69; J, p=0.96). K, L, There was no change in the percentage of (K) small-diameter or (L) large diameter Nav1.8-positive T2D DRGNs (n=5, 17 DRGs) compared to controls (n=4, 13 DRGs; K, p=0.43; L, p=0.19). M, quantitative RT-PCR revealed no change in Nav1.8 mRNA expression in T2D DRGs (n=5) compared to control (n=3, p=0.19). Scale bar is 50 µm. (Reproduced with kind permission from Singh et al., 2018.)

Quantitative RT-PCR identified an increase in Nav1.9 mRNA expression in T2D DRGNs (1.312 ± 0.18 $M_{(log2)}$, n=5) compared to controls (0.0004 ± 0.16 $M_{(log2)}$, n=3; $p<0.01$) (Fig. 3-7M).

There was no change in Nav1.8 labeling intensity in either small or large T2D DRGNs (53.3 ± 1.9 au; 60.3 ± 2.5 au, respectively, n=6, 18 DRGs) compared to controls (small, 54.4 ± 2.1 au, p=0.69; large, 60.5 ± 2.8 au, p=0.96; n=4, 14 DRGs) (Fig. 3-8A-J). Similarly, there was no change in percentage of small or large diameter T2D DRGNs expressing Nav1.8 (small, 70.2 ± 6.0%; large, 76.5 ± 5.1%, n=5, 17 DRGs) compared to controls (small, 77.2 ± 6.2%, p=0.43; large, 84.9 ± 2.6%, p=0.19; n=4, 13 DRGs) (Fig. 3-8K, L). Quantitative RT-PCR confirmed there was no change in Nav1.8 mRNA expression in T2D DRGN (-1.773 ± 0.15 au, n=5) compared to controls (-0.020 ± 0.75 au, n=3, p=0.14) (Fig. 3-8M).

Collectively, these results support findings from other T2D-PSN models that show elevated expression of Nav1.7 and Nav1.9 in DRGNs. My results demonstrate an upregulation of Nav1.7 in all T2D DRGNs, whereas Nav1.9 is elevated primarily in small diameter cells. However, they do not support that Nav1.8 is downregulated in T2D DRGNs.

3.5 SFAP recording

The above data show there is a retraction of IENFs in T2D NGRs without the death of DRGNs. To determine whether Aδ- and C-fibers functions were changed in T2D, I used the *ex-vivo* skin-nerve preparation to identify their mechanosensitive subtypes and their electrical and mechanical properties. For this, the saphenous nerve fiber terminals were mechanically and electrically

stimulated at the dermis side of the dorsal foot skin, and their AP responses were recorded proximally at the branch site of saphenous nerve.

As such recordings have not been performed in NGRs, my first goal was to demonstrate the feasibility of the approach which was done in 33 male and 11 female NGRs, aged 2, 6 or 12-24 months. Of these NGRs, 16 males that were 12-24 months-old were then used to identify and analyze the nerve fiber properties as this age group corresponds to that studied in the previous sections of this thesis. In all preparations, rod stimulation at the RF points evoked either one type of AP response or multiple AP responses. Thus, I will either use the term 'SFAP' or 'mixed AP' to describe the AP response.

The first step was to determine the viability of nerve fibers in the skin-nerve preparation. Using a blunt glass rod, I manually applied a sustained mechanical stimulus to the dermal side of the mounted dorsal foot skin to evoke a response (3.5.1). If the nerve fascicle was viable and a response was recorded, I went on to characterize it with electrical stimulation (3.5.2). Next, I identified the fiber type based on stimulation-evoked latency changes and NCV determination (3.5.3). Finally, I analyzed the mechanical excitability of the fiber with Von Frey filaments (3.5.4).

3.5.1 Establishing the skin-nerve preparation

In the initial phase, the dissection was challenging to perform in NGRs due to large amount of adipose and connective tissue compared to mice in previous studies (Zimmermann et al., 2009), particularly in T2D animals with increased body weight and BMI (Fig. 3-1C, D). Moreover, technical difficulties were experienced that contributed to the diminished viability of the nerve such as cutting, pinching, stretching and drying out during dissection. These difficulties, in addition to the subsequent initially ~50 min lasting dissection procedure, substantially decreased the viability of the nerve with progressive attenuation of SFAP or multiple AP responses within less than 20 min.

Changing the position of the rod principally enables the determination of the extension of a RF which is a region of the foot skin innervated by collateral terminal branches of single nerve fiber (Hudspeth et al., 2013).

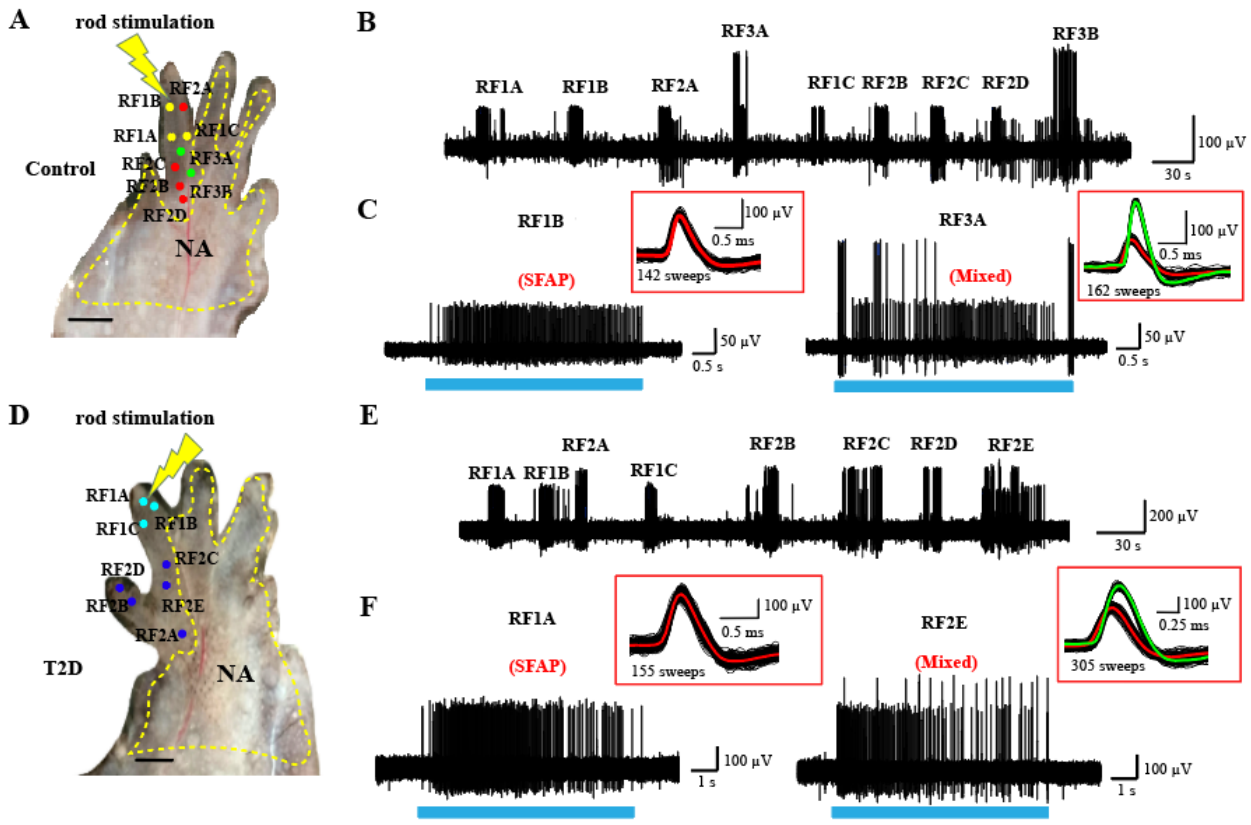

Fig. 3-9: SFAPs at distal digits in NGRs dissected under optimized conditions. A, D, Images of dermis side of the dorsal skin from one control (A) and one T2D NGR (D); scale bars are 3 mm. Yellow dotted lines indicate NA regions. B, C, E, F, Continuous recordings of rod-evoked responses (blue bars) from RF points shown in A and D. C, F, Traces at higher time resolution from B (RF1B and RF3A points) and E (RF1A and RF2E points) show SFAPs (RF1B and RF1A points in C and F) as well as mixed AP responses (RF3A and RF2E in C and F).

After few months, the experimental conditions were optimized by changing the order of tissue removal and allowing foot dissection to begin 5-10 min following euthanasia. In addition, this approach decreased the dissection time from ~50 min to ~30 min and increased the probability of obtaining a viable preparation to >85% with stable recording conditions for at least 20 min. Furthermore, I was able to record up to 9 stimulation points, likely from 3 different RFs per fascicle in 5 control and 9 T2D NGRs (Fig. 3-9). Note that several stimulation points in the figures that are assumed to be from the same RF are designated by different letters, for example, RF1A, RF1B, and RF1C represent three points within RF1, whereas the numbers indicate different RFs (Fig. 3-9). Because responses at various RF points could comprise either SFAPs or mixed APs from different fibers, their amplitudes and shapes were discriminated by overlaying them and calculating the average trace (see boxes in Fig. 3-9C, F). As discussed later (4.5.2), mixed AP responses were due to overlapping RFs. For trying to obtain SFAPs, the nerve was further split into smaller fascicles in every preparation.

Now, the viability of the skin nerve preparation was improved, more than one foot was routinely dissected. This was helpful as, depending on the outcome of breeding, the preparations needed to be isolated from 2 NGRs (in this case, one preparation per NGR) on a single day. Mostly, the first dissected preparation was immediately used and the other was stored at 4 °C for use either later on the same day or the following day, depending on whether responses were obtained from the first one. 13 preparations (4 control and 9 T2D NGRs) from either the first dissected foot or the NGR preparation from the contralateral foot were tested ~24 h after the dissection. The success rate for stable recording was >75% with mapping of ~9 RF points in the central area and also at the digits.

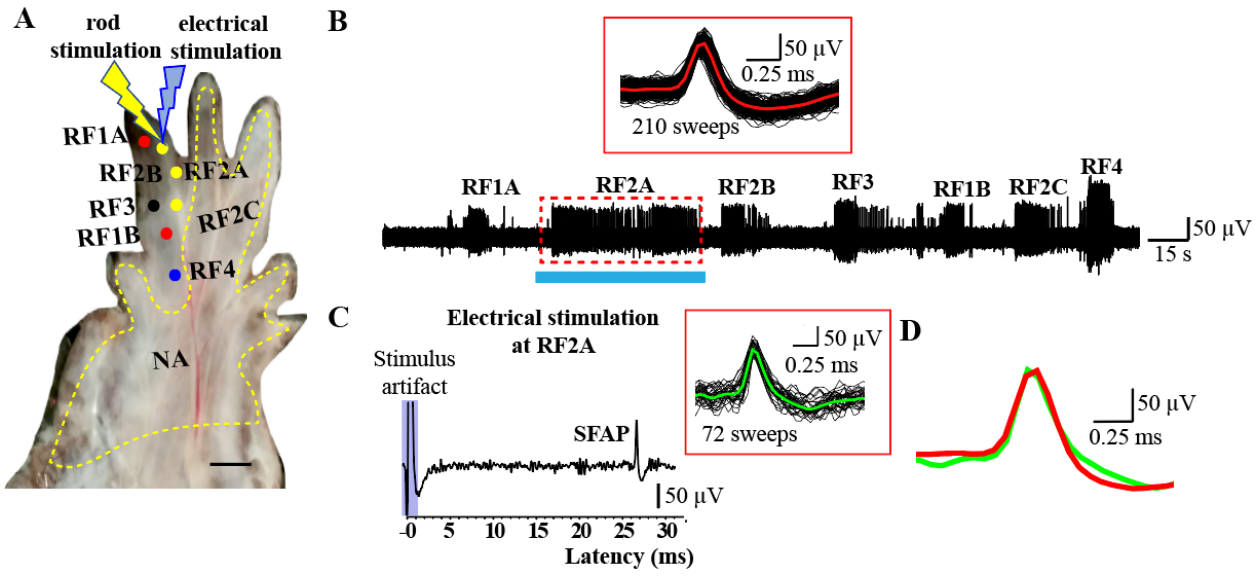

Fig. 3-10: Rod and electrical stimulation of RF point on the dissection. A, Image of dermis side of the same dorsal skin from control NGR. Yellow dotted lines indicate NA regions and scale bar is 3 mm. RF point (RF2A) from B was selected to subsequently evoke SFAP by electrical stimulation applied via a superfusate-filled patch-electrode. The traces from rod and electrical stimulation were overlaid and averaged as shown in insets. D, Average spike overlay of traces in B and C identified SFAP from the same fiber.

3.5.2 Characterization of nerve fibers by electrical stimulation

In RF points with reproducible responses to rod stimulation, fibers were characterized further with electrical stimulation. Firstly, the activation threshold was determined by increasing the amplitude of a repetitive 0.2 ms-lasting d.c. electrical pulse applied at a rate of 0.5 Hz. In the example of Fig. 3-10, the SFAPs recorded upon mechanical (Fig. 3-10A, B) and the electrical stimulation (Fig. 3-10C, D) were overlaid and averaged. The similarity of both signals indicated that both types of stimulation activated the same fiber type which was characterized by latency test and NCV.

In total, 24 Aδ- and 22 C-fibers were electrically identified from control and T2D NGRs. All Aδ-fibers displayed a post-stimulus latency <30 ms whereas in the C-fibers latency ranged from 30-100 ms (Fig. 3-11A), consistent with previous studies in mice (Zimmermann et al., 2009). Corresponding to these latencies and the distance between the stimulation and recording site, NCV in Aδ-fibers ranged from 1-13 m/s and in C-fibers from 0.3-1 m/s (Fig. 3-11B). Specifically, repetitive mechanical and electrical stimulation at a single RF point did not alter the shape and size of SFAP from Aδ-fiber (Figs. 3-12, 13). The spike overlay and average SFAP from mechanical and electrical stimulation demonstrated, as above, an identical SFAP shape and size and confirming recordings from the same type of mechanosensitive Aδ- (Fig. 3-12) or C-fiber (Fig. 3-13). In some preparations, a rod stimulation evoked AP responses whereas electrical stimulation failed.

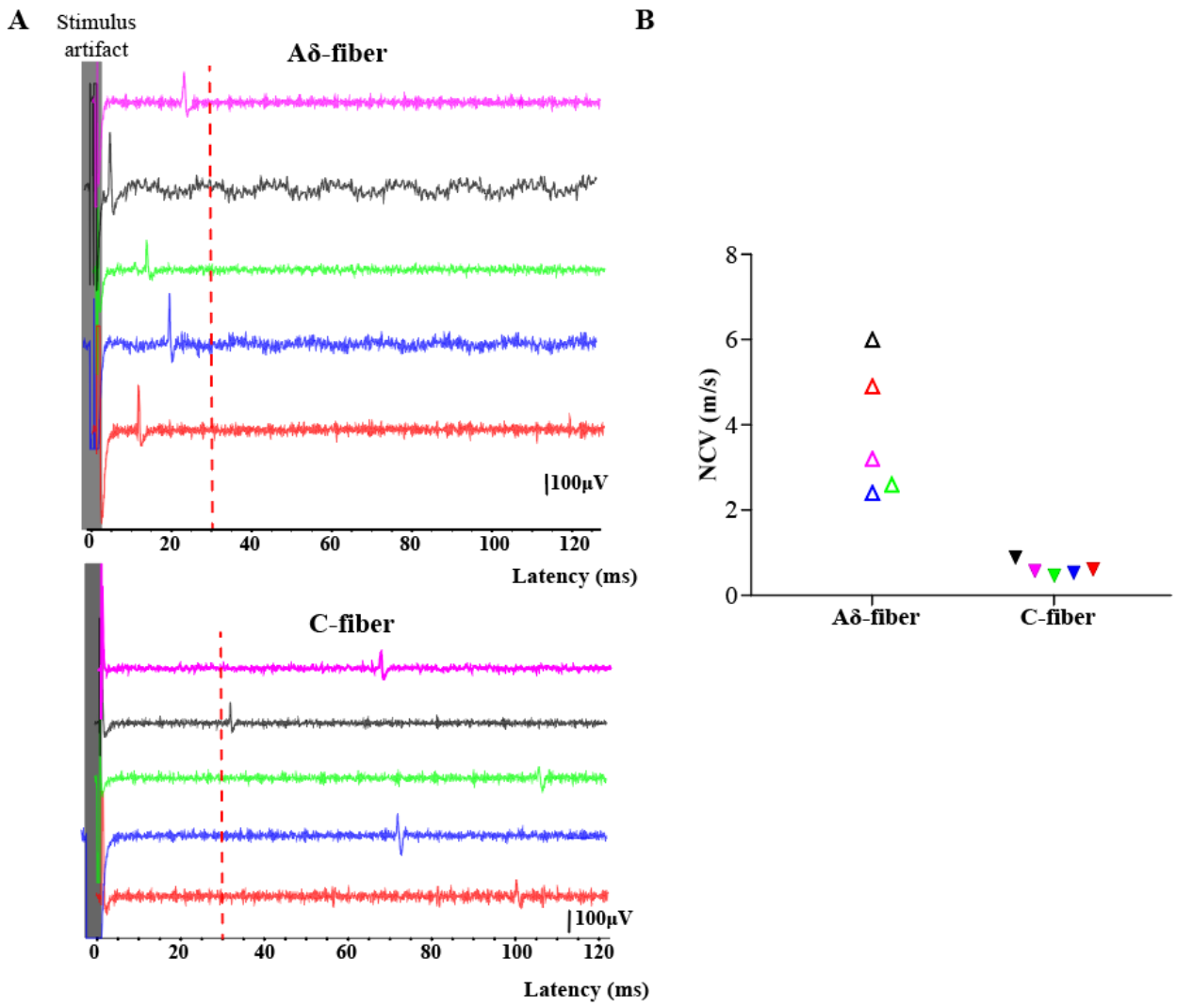

Fig. 3-11: Range of SFAP latency and NCV in sensory nerve fibers from control NGRs. A, Top 5 traces exemplify electrically-evoked SFAPs from Aδ-fibers in control NGRs with latency cut-off set to 30 ms as indicated by the red line; bottom 5 traces exemplify corresponding SFAPs from C-fibers in control NGRs with a latency larger than the cut-off. B, the plot of NCVs of the 5 Aδ- and C-fibers in A.

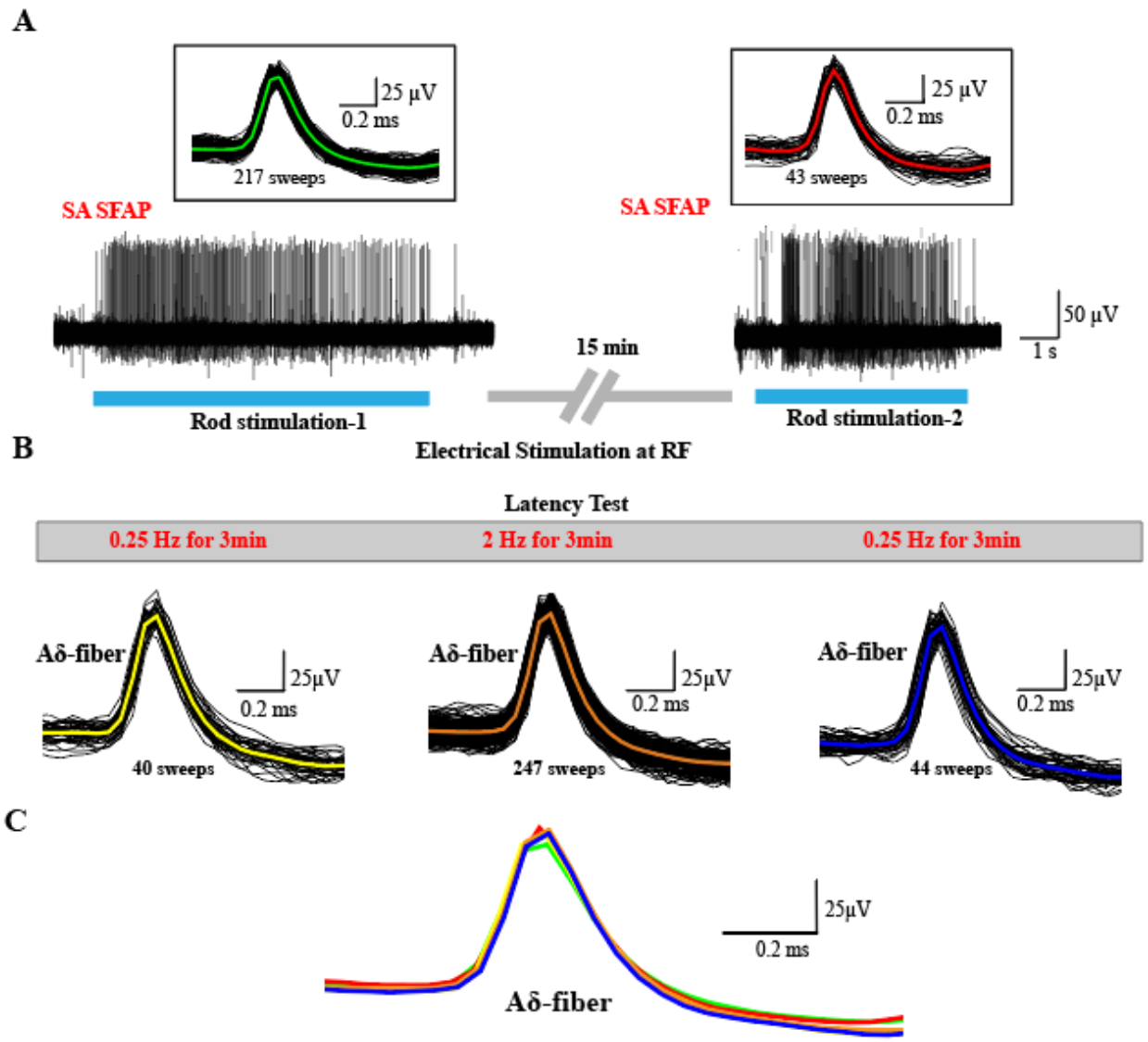
A
25 μV
0.2 ms
217 sweeps
SA SFAP
25 μV
0.2 ms
43 sweeps
SA SFAP
50 μV
1 s
15 min
Rod stimulation-1
Rod stimulation-2
B
Electrical Stimulation at RF
Latency Test
0.25 Hz for 3min
2 Hz for 3min
0.25 Hz for 3min
Aδ-fiber
25μV
0.2 ms
40 sweeps
Aδ-fiber
25μV
0.2 ms
247 sweeps
Aδ-fiber
25μV
0.2 ms
44 sweeps
C
25μV
0.2 ms
Aδ-fiber

Fig. 3-12: Aδ-fiber SFAP responses evoked by mechanical and electrical stimulation at the same RF point. A, Traces displaying SFAP responses evoked by rod stimulation applied for nearly 10 s at the selected RF point (left bottom panel in A). Shorter-lasting rod stimulation after 15 min at the same RF point (right bottom panel in A) prior to electrical stimulation demonstrated a consistent and same type of SFAP response. B, Electrical stimulation at the same RF point as in A evoked a very similar-looking SFAP response identified as originating from an Aδ-fiber via 'latency test' and NCV of 2.8 m/s. Latency test means here that the stimulation rate was increased for 3 min from 0.25 to 2 Hz (0.25 Hz, yellow trace; 2 Hz, cyan trace; 0.25 Hz, pink trace). This test revealed a SFAP shape identical to that for the SFAP in A. Overlaid and then averaged SFAP traces are shown in the insets above the original traces. D, Spike overlay and average of signals from A and B demonstrate identical SFAP amplitude and shape, identified as an Aδ-fiber that did not change in shape and size during repetitive stimulation.

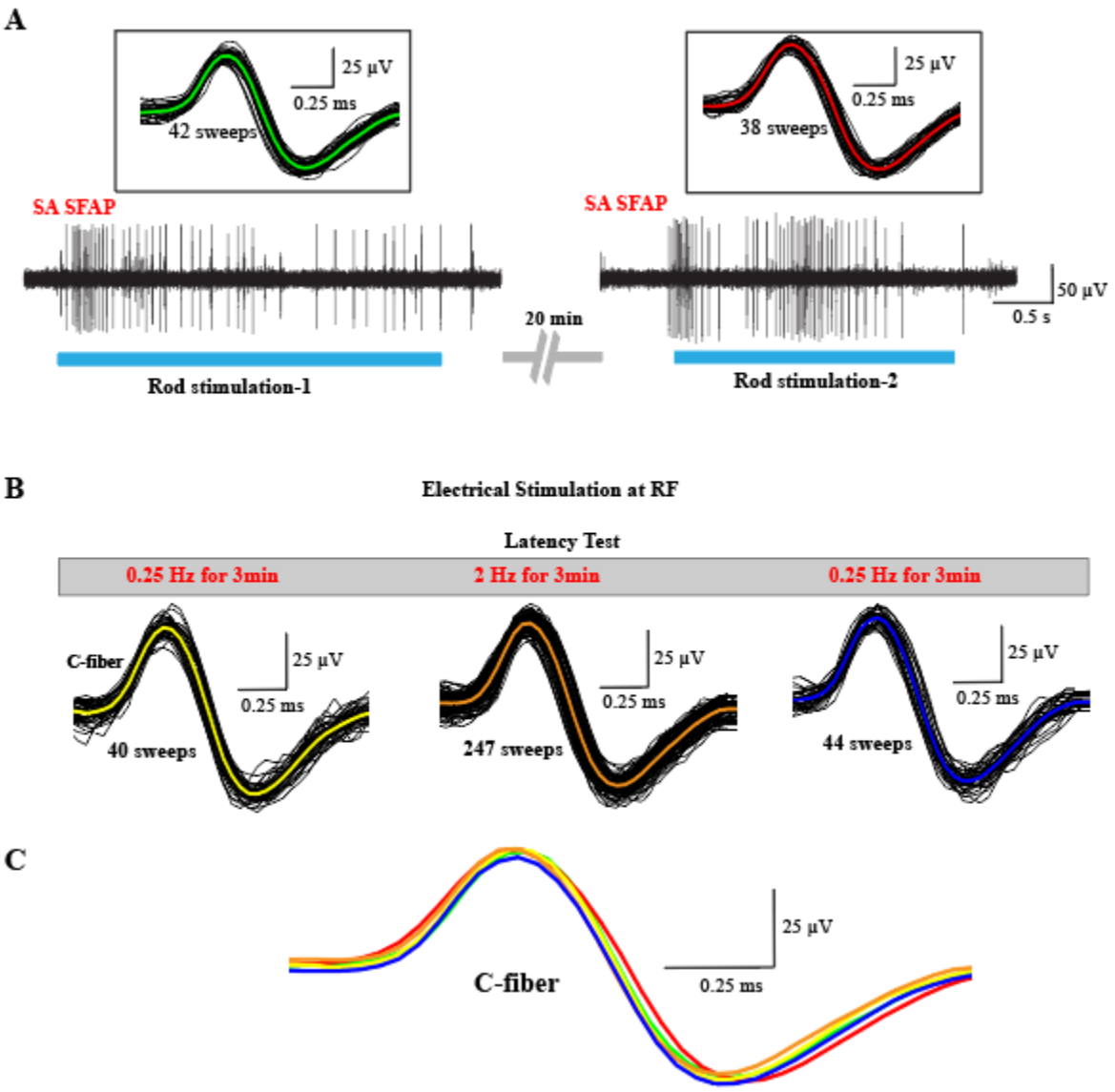
A
25 μV
0.25 ms
42 sweeps
38 sweeps
SA SFAP
SA SFAP
50 μV
0.5 s
20 min
Rod stimulation-1
Rod stimulation-2
B
Electrical Stimulation at RF
Latency Test
0.25 Hz for 3min
2 Hz for 3min
0.25 Hz for 3min
C-fiber
40 sweeps
247 sweeps
44 sweeps
C
C-fiber

Fig. 3-13: C-fiber SFAP responses evoked by mechanical and electrical stimulation at the same RF point. A, Traces displaying SFAP response evoked from constant mechanical rod stimulation applied for ~6 s at the selected RF point (left bottom panel in A). Shorter-lasting rod stimulation after 20 min at the same RF point (right bottom panel in A) prior to electrical stimulation demonstrated a consistent and same type of SFAP response. B, Electrical stimulation at the same RF point as in A evoked a very similar-looking SFAP response identified as originating from a C-fiber via 'latency test' and NCV of 0.58 m/s. Latency test means here that the stimulation rate was increased for 3 min from 0.25 to 2 Hz (0.25 Hz, yellow trace; 2 Hz, cyan trace; 0.25 Hz, pink trace). This test revealed a SFAP shape identical to that for the SFAP in A. Overlaid and then averaged SFAP traces are shown in the insets above the original traces. D, Spike overlay and average of signals from A and B demonstrate identical SFAP amplitude and shape, identified as a C-fiber that did not change in shape and size during repetitive stimulation.

C-fibers that were further characterized by activity-dependent latency changes upon increasing the rate of repetitive stimulation from 0.25 to 2 Hz. This demonstrate a latency increase in C-fibers from both control and T2D NGRs (Fig. 3-18). The range of latency increases in control NGRs was 5.7-50% and 2-57% in T2D NGRs. C-fibers showing a >10% increase in latency are typically nociceptive, whereas C-fibers with <10% increase in latency are non-nociceptive (Schmelz et al., 1995; Gee et al., 1996; George et al., 2007; Zimmermann et al., 2009). Out of 22 C-fibers identified electrically in both control (n=4, 5 cases) and T2D NGRs (n=10, 17 cases), 20 fibers in control and 9 fibers in T2D NGRs showed >10% latency increase (Fig. 3-14A) and were thus likely nociceptive, whereas the remaining C-fibers were likely non-nociceptive (Fig. 3-14B). The fibers identified as Aδ-fibers did mostly not show a notable change in latency (Fig. 3-14).

3.5.3 Analysis of electrical properties of nerve fibers

After I obtained stable recordings from Aδ- and C-fibers in the skin-nerve preparation from NGRs, their characterization in controls versus T2D animals included 3 criteria as follows:

A. SFAP amplitude: The amplitude (measured as the upstroke of SFAP) of recorded Aδ- and C-fiber APs was analyzed in control and T2D NGRs. Specifically, Aδ-fiber APs had a mean amplitude of 136.9 ± 22.97 μV (n=5, 13 fibers) in control NGRs that decreased in T2D NGRs to 75.63 ± 8.26 μV (n=8, 11 fibers; *$p<0.05$) (Fig. 3-15A). Similarly, the amplitude of C-fiber APs in control NGRs was 81.04 ± 11.35 μV (n=4, 5 fibers) that decreased in T2D NGRs to 39.85 ± 6.58 μV (n=10, 17 fibers; **$p<0.01$) (Fig. 3-15B).

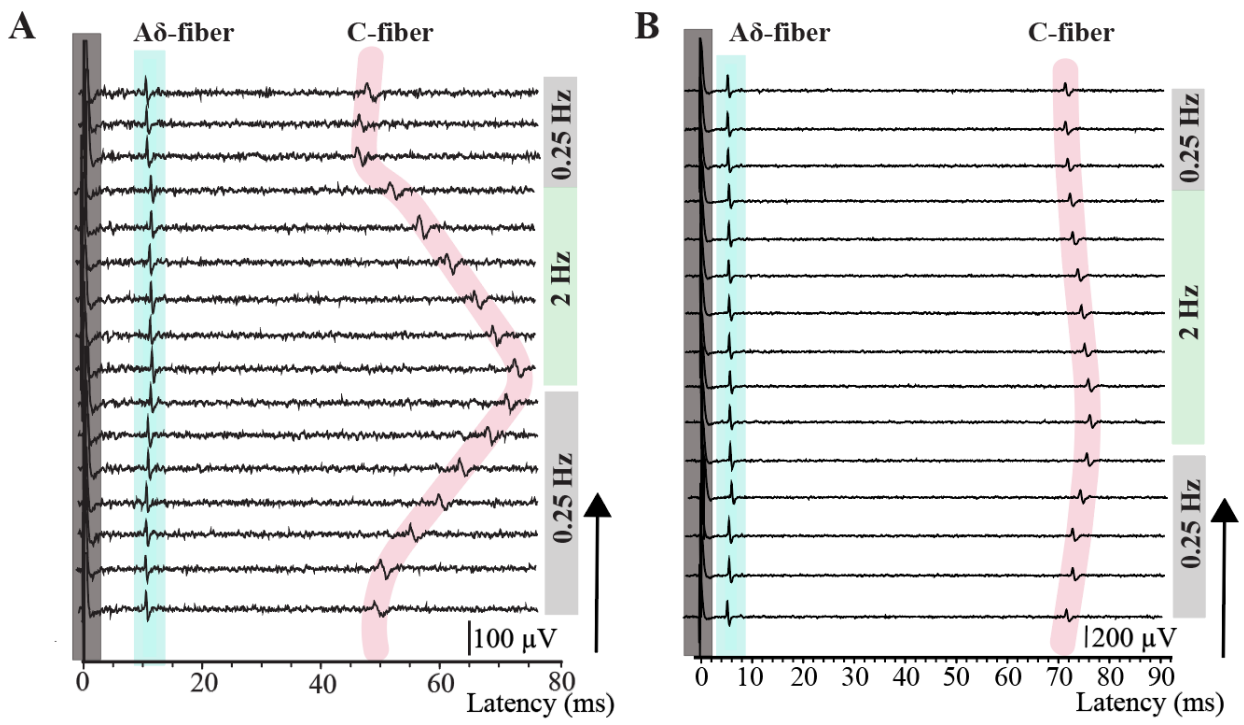

Fig. 3-14: Activity-dependent latency changes in sensory nerve fibers. A, B, Activity-dependent changes in Aδ- and C-fibers SFAP latency at 2 Hz stimulus frequency for 3 min instead of 0.25 Hz in control. A, An Aδ-fiber (NCV: 3.8 m/s) does not show an increase in latency from 10 ms; however, a C-fiber (NCV: 0.56 m/s) displays a 24 ms increase from 48 ms (>10%). B, An Aδ-fiber (NCV: 7.6 m/s) does not show an increase in latency from 5 ms; however, a C-fiber (NCV: 0.57 m/s) displays a 4 ms increase from 72 ms (<10%).

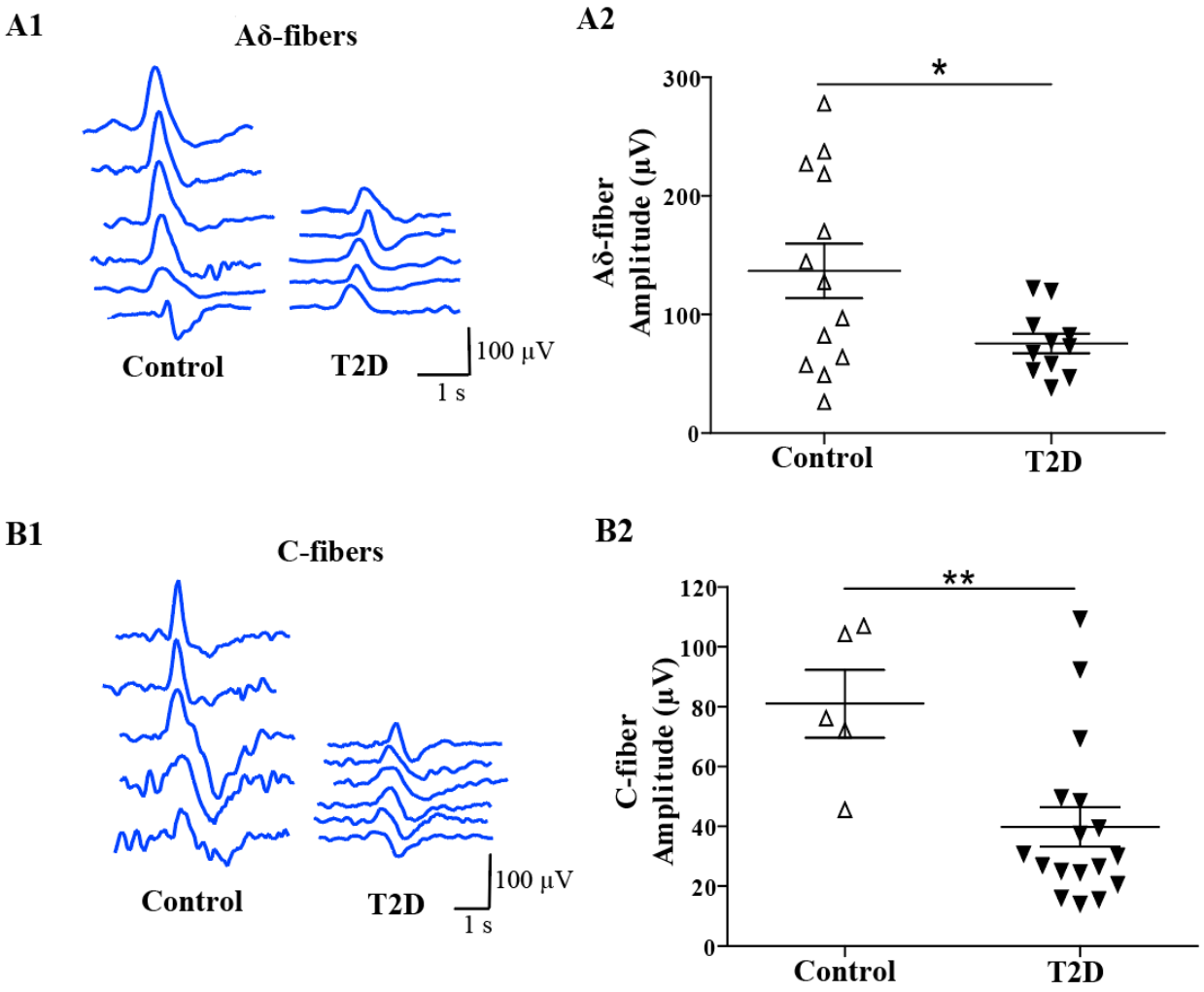

Fig. 3-15: Analysis of amplitudes of electrically characterized Aδ- and C-fibers. A1, Examples of SFAPs of Aδ-fibers in control and T2D NGRs. A2, Aδ-fiber SFAP amplitude was reduced in T2D NGRs (n=8, 11 fibers) compared to controls (n=5, 13 fibers, *p<0.05). B1, examples of SFAPs of C-fibers in control and T2D NGRs. B2, C-fiber SFAP amplitude was smaller in T2D NGRs (n=10, 17 fibers) compared to controls (n=4, 5 fibers, **p<0.01).

B. NCV: Although nerve fibers were classified as Aδ- or C-fibers via electrical stimulation and based on activity-dependent latency changes, their identity was further substantiated by their NCV. As stated above, fibers with a NCV of 1-16 m/s were classified as Aδ-fibers while C-fibers were classified based on a NCV <1 m/s. The range of NCV in Aδ-fibers in control was 1.88-13 m/s (n=5, 13 fibers) and 1.6-10 m/s in T2D NGRs (n=8, 11 fibers). Furthermore, the range of NCV in C-fibers in control NGRs was 0.46-0.89 m/s (n=4, 5 fibers) and in T2D NGRs 0.31-0.8 m/s (n=10, 17 fibers). Aδ-fiber NCV did not differ between controls (mean 4.89 ± 0.82 m/s) and T2D NGRs (mean 3.79 ± 0.72 m/s, p=0.34) (Fig. 3-16A). Similarly, there was no difference in C-fiber NCV between controls (mean 0.61± 0.07 m/s) and T2D NGRs (mean 0.54 ± 0.03 m/s, p=0.25) (Fig. 3-16B).

.

C. Electrical excitability: To determine if Aδ- and C-fibers in T2D NGRs differed in their excitability compared to controls, their electrical thresholds were compared. Specifically, Aδ-fibers in T2D NGRs had a mean electrical threshold of 0.16 ± 0.03 mA (n=8, 11 fibers) compared to 0.39 ± 0.03 mA in controls (n=5, 13 fibers; p<0.001) (Fig. 3-16C). C-fibers in T2D NGRs had an electrical threshold of 0.19 ± 0.03 mA (n=10, 17 fibers) compared to controls (n=4, 5 fibers, 0.35 ± 0.05 mA; n=4; p<0.05) (Fig. 3-16D). Accordingly, both Aδ- and C-fibers had decreased thresholds in T2D NGRs indicating increased excitability.

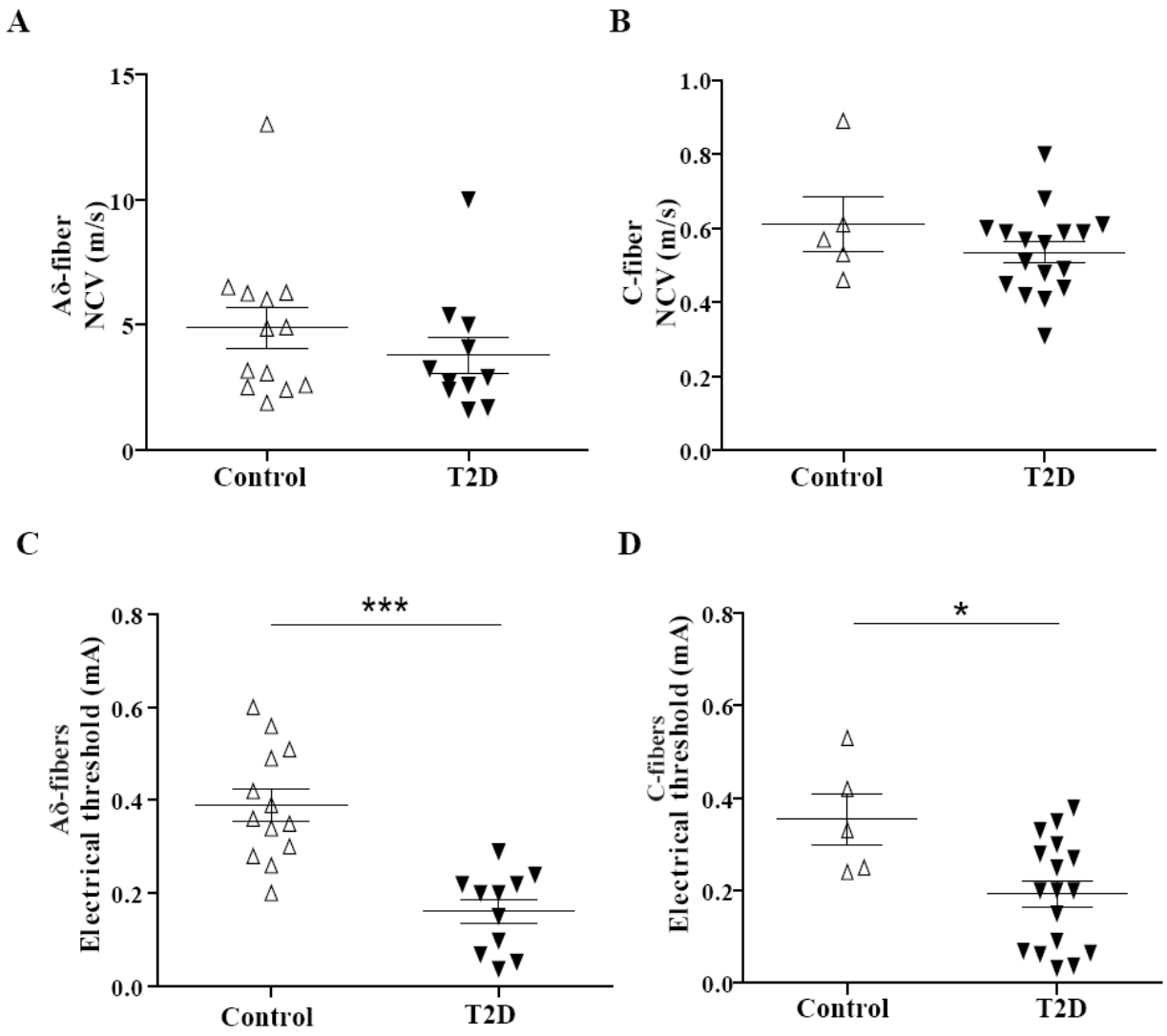

Fig. 3-16: Analysis of NCV and the electrical threshold of mechanosensitive Aδ- and C-fibers in T2D NGRs. A, B, Aδ- and C-fiber NCV did not differ in controls (n=5, 13 fibers) versus T2D NGRs (A, n=8, 11 fibers, p=0.34; B, p=0.34). C, D, Aδ- (C) and C-fibers (D) in T2D NGRs (C, n=8, 11 fibers; D, n=5, 13 fibers) had lower electrical (C, ***p<0.001; D, *p<0.05) thresholds than controls (C, n=5, 13 fibers; D, n=4, 5 fibers).

3.5.4 Assessment with Von Frey filaments of mechanical excitability

Finally, I measured the mechanical thresholds of sensory nerve fibers by manually stimulating the RF point with Von Frey filaments. The filaments were difficult to position at the selected RF point onto the skin due to the interference of surface tension of the superfusate (4.5.3). As stated above, both rod and electrical stimulation activated identical fibers (3.5.2). However, as indicated in the example of Fig. 3-17, SFAP spike overlay analysis from control (n=4, 6 fibers and T2D NGRs (n=4, 6 fiberss) revealed non-identical Von Frey-evoked responses. As the SFAP responses appeared to be from different fibers, they could not be identified as Aδ- or C-type by latency (test) recordings and are therefore labeled here as 'mechanosensitive fibers'. It is to note that the SFAP spike overlay analysis was not performed for all the mechanosensitive fibers recorded. Correlation of Von Frey thresholds revealed decreased values in T2D NGRs (0.16 ± 0.03 g; n=9, 24 fibers) compared to controls (0.39 ± 0.05 g; n=4, 15 fibers, $p<0.001$) (Fig. 3-18).

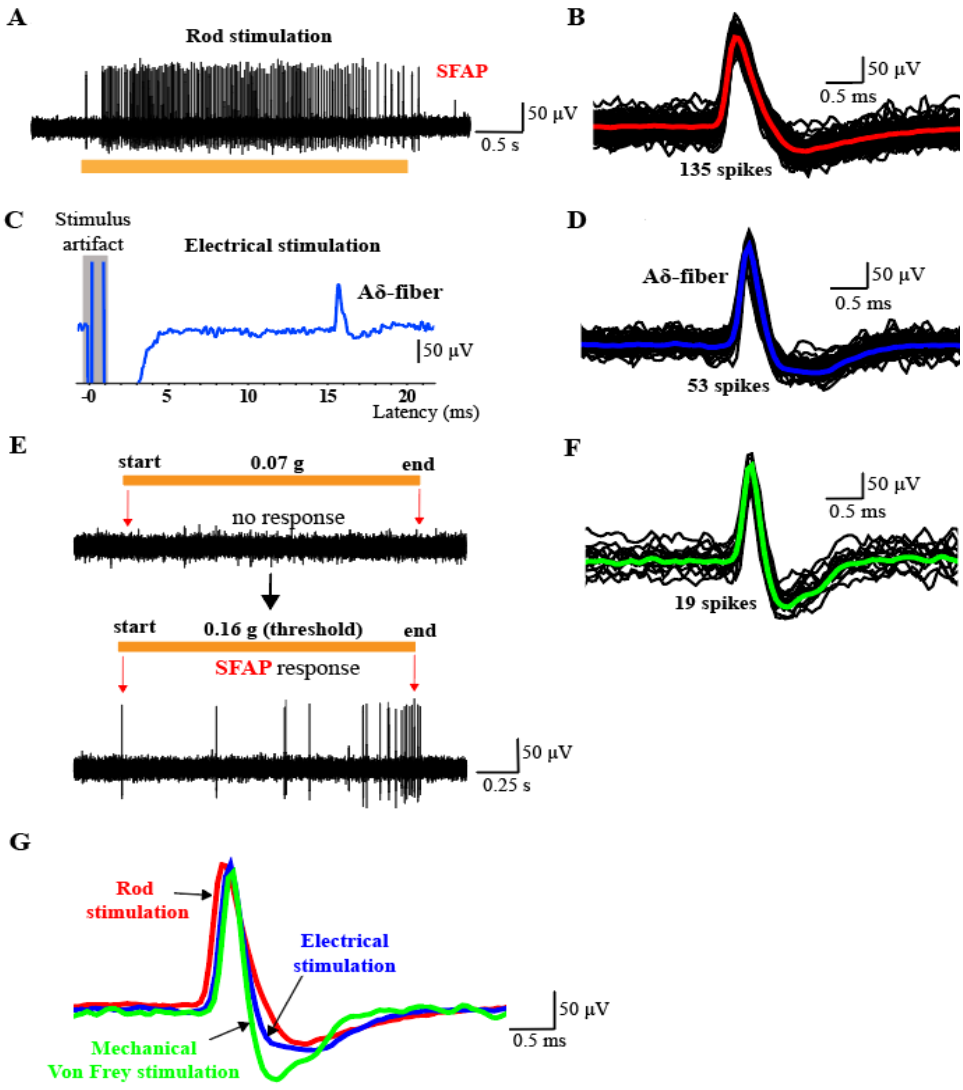

Fig. 3-17: SFAP responses evoked by the rod, electrical, and Von Frey filament stimulation. A, B, AP traces displaying SFAP response evoked by constant rod stimulation applied for ~5 s at the RF point (A). C, D, AP traces displaying SFAP responses evoked from Aδ-fiber (NCV: 2.6 m/s) by electrical stimulation (C). E, F, AP traces displaying SFAP response evoked at the mechanical threshold of 0.16 g by constant mechanical Von Frey stimulation (E). Overlaid and then averaged SFAP traces are shown in the insets above the original traces. G, Average spike overlay from B, D and F demonstrate identical SFAP spike from B and D, but non-identical to F.

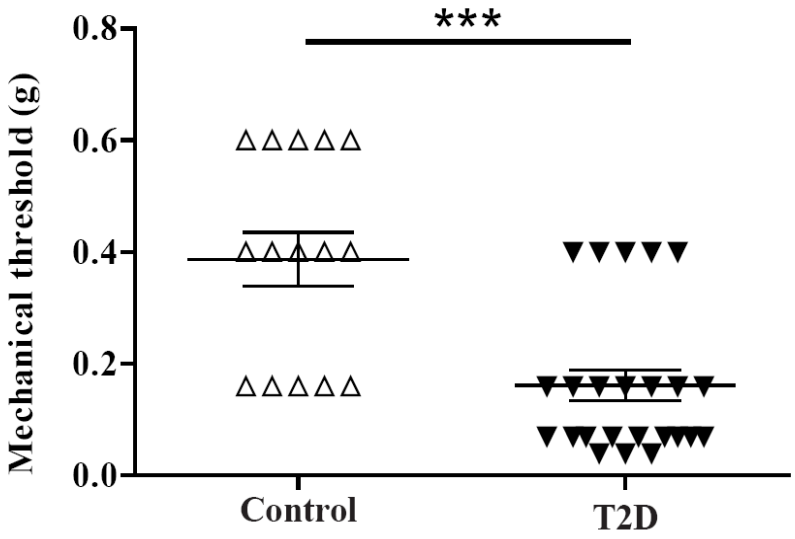

Fig. 3-18: Correlation of Von Frey thresholds in mechanosensitive nerve fibers. Mechanosensitive sensory nerve fibers stimulated at the dermal side of the dorsal skin using Von Frey force filaments had reduced thresholds (n=9, 24 fibers, ***$p<0.001$) in T2D NGRs compared to controls (n=4, 15 fibers).

CHAPTER-4

DISCUSSION

The primary goal of my thesis work was to establish T2D NGRs as a promising preclinical model to study PSN. NGRs are feral animals that were brought into captivity to study circadian rhythms and the retina as they are diurnal and they have a large number of cones comparable to humans. A secondary effect of their captivity was the development of increased body weight, hyperglycemia and hypertension by 12 months upon feeding them with chow diet typically used for rodsents. Specifically, this happened in 90% of males whereas only 50% of the chow-fed females developed these symptoms that are associated with T2D (Noda et al., 2010; Chaabo et al., 2010). One explanation for this sex difference could be a partially protective role of female sex hormones against β-cell injury as previously suggested for a streptozotocin T2D mouse model (Le May et al., 2006; Subramaniam et al., 2018). T2D NGRs also display 5 stages of T2D progression paralleling those in human patients with the presence of microvascular and macrovascular complications such as retinopathy, cataracts, atherosclerosis, renal failure and cardiovascular diseases (Chaabo et al., 2010; Noda et al., 2010; Yang et al., 2016; Han et al., 2017; Subramaniam et al., 2018). Also in my thesis, the 12-24 months male NGRs fed on standard chow diet developed T2D and signs of metabolic dysfunction such as insulin-resistance, increased body weight, hyperglycemia, dyslipidemia, increased cholesterol levels, hypertension as well as ketosis at advanced stages. Contrary, male NGRs fed on Hfib-diet remained normoglycemic and lacked T2D pathology. I first demonstrated through behavioral, immunohistochemical and molecular techniques T2D animals display PSN features. These data were published in my first author paper (Singh et al., 2018) comprising the first part of the Results section. In parallel, I demonstrated for the first time the feasibility of using in NGRs the skin-nerve preparation which is an established *ex-vivo* rodent model for studying peripheral nerve fiber properties (Zimmermann et al., 2009). In this preparation,

electrical and mechanical properties of sensory nerve fibers in NGRs were identified with AP recordings. All these findings are discussed as follows:

4.1 Metabolic Phenotypes

The first objective was to investigate the hallmark features of T2D. According to the IDF task force of T2D epidemiology and prevention, an important clinical criterion to diagnose this metabolic syndrome in humans is elevated FBG (>5.6 mM) (Alberti et al., 2009). Based on the above criterion and previous studies on NGRs (Yang et al., 2016; Bolsinger et al., 2017), the hyperglycemic threshold to diagnose T2D was correspondingly set at 5.6 mM. Also consistent with the latter studies, hyperglycemia was observed in 80 % of chow-fed NGRs with FBG >6.1 mM whereas, controls remained healthy with FBG ranging from 2.2-3.6 mM. Although not much is known about the prediabetic stage in NGRs, it is possible that an FBG range of >3.6-5.5 mM is indicative of prediabetes (Bolsinger et al., 2017). This stage can be validated in the future by IGT and IFG diagnostic methods (1.2.1). The degree of hyperglycemia and normal FBG varies for rodent species, and the criteria to define hyperglycemia are not explicitly stated in publications (Fajardo et al., 2014; Togashi et al., 2016). Some T2D models such as streptozotocin mice demonstrate a considerable variation and acute rise in FBG ranging from 5-25 mM depending on the toxin dose (Akbarzadeh et al., 2007; Graham et al., 2011; Premilovac et al., 2017).

Although the remaining 20% of chow-fed NGRs used in my study were non-hyperglycemic at the time of euthanization, they were considered T2D-positive based on their increased body weight and BMI, indicative of abundant fat accumulation and increased adiposity associated with T2D (Tab. 3-1, Fig. 3-4B, C). Possibly, they displayed hyperglycemia at other time points before their

euthanization and therefore it would have been beneficial to test in these animals FBG at multiple time points. Dysregulated insulin-glucagon balance may explain why these T2D animals have a seemingly normal FBG (Immerman et al., 1982; Workgroup on Hypoglycemia, American Diabetes Association, 2005; Mohseni et al., 2014). Insulin plus glucagon work in tandem to regulate blood glucose levels and glucagon functions as a counter-regulatory hormone to insulin and is secreted under low blood glucose levels or hypoglycemia (Girard, 2017; Hædersdal et al., 2018). The presence of pancreatic tumors or insulinomas might cause elevated insulin secretion from β-cells that in turn restricts glucagon secretion by α-cells (Immerman et al., 1982; Amiel et al., 2008; Mohseni et al., 2014; Iglesias et al., 2014). Elevated insulin levels (as with pancreatic tumors or insulinoma) may also result in decreased glucagon secretion resulting in plasma FBG <3.6 mM (Cryer, 2012). Although previous studies from our collaborator, Dr. Yves Sauvé, demonstrated no change in glucagon levels in hyperglycemic T2D NGRs (Yang et al., 2016), it is possible that glucagon might be present at low levels in the animals used in the current study suggesting impaired glucagon metabolism. Another possible explanation could be the potential development of hepatic or pancreatic tumors that may likely result in low FBG due to increased demand for glucose (Immerman et al., 1982; Forde et al., 2017). Previous studies have demonstrated the presence of hepatic tumors in ~40 % of T2D NGRs older than 12 months (Subramaniam et al., 2018); however, in the current study, the presence of pancreatic tumors in the non-hyperglycemic animals were not explored.

Here, blood tests at the time of euthanization revealed no difference in fasting plasma insulin levels between control and T2D NGRs (Fig. 3-4D). The fact that 51 % of T2D NGRs had fasting plasma insulin levels above 2 ng/ml indicates these animals may have compensated for increased demand

for insulin during hyperglycemia. Contrary, 32 % of these animals had <2 ng/ml fasting plasma insulin levels suggesting β-cell depletion. There were no data available for the remaining NGRs. In conclusion, it turned out all chow-fed NGRs used here showed T2D.

4.2 Hallmark features of T2D-PSN in NGRs

My published study (Singh et al., 2018) showed NGRs with T2D exhibit hallmark features of PSN such as IENF denervation with concomitant hyposensitivity to both touch and temperature, and slowing of motor NCV, consistent with previous findings in T2D patients and streptozotocin rodent models (Russel et al., 1996; Lennertz et al., 2011; Katon, 2013; Cortez et al., 2014; Fernyhough and McGavock., 2014) (Fig. 3-2A-E).

4.2.1 Loss in IENFs in T2D NGRs

It has been demonstrated that metabolic insult due to elevated FBG in T2D results in peripheral nerve damage and loss in both human T2D patients and streptozotocin rodent models (Beiswenger et al., 2008; Said, 2013; Feldman et al., 2017). A series of metabolic cascades are likely induced in response to elevated FBG that lead to a peripheral nerve injury in T2D-PSN. One such cascade is the activation of the polyol pathway that induces oxidative stress-induced nerve damage due to metabolic imbalance caused by overproduction of reactive oxygen species (ROS) (Oates, 2008; Fernyhough and McGavock, 2014; Feldman et al., 2017). The activity of aldose reductase in this pathway results in the formation and accumulation of sorbitol in the neurons disrupting the osmotic balance and causing cell lysis. This is followed by depletion of cellular nicotinamide dinucleotide phosphate (NADPH) that is required to generate the potent antioxidant glutathione (a scavenger of ROS), ultimately putting the peripheral nerve under oxidative stress. Therefore, the presence of

aldose reductase activity can be tested in T2D-PSN NGRs by investigating the accumulation of sorbitol in the distal peripheral nerve terminals. A further mechanism that promotes metabolic imbalance is hyperglycemia-induced protein kinase-C (PKC) activation which in turn inhibits Na^+/K^+-ATPase pump activity (Brownlee, 2001; Feldman et al., 2017). Previous studies have shown that overexpression of this enzyme accelerates peripheral nerve damage, whereas its inhibition improves IENF loss in T2D-PSN streptozotocin rodent models (Calcutt et al., 2004; Oates, 2008; Schemmel et al., 2010; Zochodne, 2014).

Another outcome of excessive glycolysis via elevated FBG is the formation of advanced glycation end-products (AGEs) that cause oxidative stress to the sensory neurons and their axons (Brownlee, 2001; Feldman et al., 2017). In addition, formation of AGEs activates downstream signaling cascades such as the nuclear factor-kappa B pathway to form proinflammatory cytokines that exaggerate sensory dysfunction (Sugimoto et al., 2008; Toth et al., 2008). Studies have demonstrated accumulation of AGEs in the footpad skin of T2D-PSN patients and it has been used as a marker to assess pathology associated to T2D-PSN (Meerwaldt et al., 2005; Vouillarmet et al., 2013).

4.2.2 Tactile and thermal hyposensitivity in T2D NGRs

The reduced sensitivity to touch and heat demonstrated here likely correlates with IENF loss and is consistent with previous findings in patients and rodent T2D-PSN models (Lennertz et al., 2011; Singh et al., 2014; Boulton, 2014). Lack of tactile sensitivity in T2D NGRs may suggest the involvement of large-diameter nerve fibers that are primarily analyzed using NCV studies. These fibers can be assessed in T2D NGRs by investigating the expression of various myelin proteins

such as myelin basic protein, or myelin-associated glycoprotein (Myers et al., 2013). Additionally, the distribution of mechanoreceptors in the dermal skin can be quantified by measuring, for example, the density of intrapapillary myelinated nerve endings that innervate Meissner corpuscles, as previously demonstrated in T2D-PSN patients (Myers et al., 2013). Although the skin-biopsy method only investigates the distribution of small diameter unmyelinated IENFs, this method limits the study of large diameter myelinated nerve fibers. Some reports have shown loss of myelinated afferent fibers and their respective mechanoreceptors in T2D-PSN patients in correlation with segmental demyelination (Steck et al., 2006; Myers et al., 2013). The thermal hyposensitivity in the epidermal skin of T2D NGRs might also suggest a selective loss of heat-sensing small-diameter sensory fibers. This sensory loss-associated reduced sensitivity can be further confirmed by investigating the reduced expression of heat-activated TRPV1 channels in these nerve terminals as previously demonstrated in T2D-PSN patients and T2D-PSN streptozotocin mouse models (Facer et al., 2007; Pabbidi et al., 2008; Beiswenger et al., 2008.

4.2.3 Motor NCV analysis in T2D NGRs

As one functional deficit of peripheral nerve damage in my published study (Singh et al., 2018), T2D NGRs showed slowing of motor NCV which correlates with the clinical presentation of T2D-PSN including weakened foot muscles, fatigue, muscle atrophy, unsteady gait and frequent falls (Dunnigan et al., 2013; Andersen, 2014; Biessels et al., 2014; Kakrani et al., 2014) (Fig. 3-2F-G). It remains unclear why distal sensory nerves are typically vulnerable early in T2D, whereas motor dysfunction occurs in a later phase of the disease. It is possible that T2D NGRs, the ~50% reduction in motor NCV indicates severe motor impairment which could not be evaluated and was beyond the scope of the current study. T2D-PSN-induced NCV slowing is often accompanied by

demyelination, Nav alteration at Nodes of Ranvier, functional and morphological changes at the neuromuscular junction (Dunnigan et al., 2013; Malik, 2014). Besides, segmental demyelination of internodes as a result of T2D-PSN has been well documented which would explain NCV slowing (Binnie et al., 1995; Mizisin, 2014). *In-vivo* electrophysiological threshold tracking is a non-invasive technique to study perturbed axonal excitability under pathological conditions such as T2D-PSN (Bostock et al., 1998; Krishnan and Kiernan, 2005). This technique demonstrated in T2D patients and rats reduced inward rectification with decreased Na^+/K^+-ATPase pump activity. This reduced pump activity resulted in intra-axonal Na^+ accumulation, a decreased transmembrane Na^+ gradient and Na^+ current attenuation, ultimately causing slowing of NCV (Yang et al., 2001; Misawa et al., 2004 George et al., 2007). Apart from studying Nav conductances, this technique has been further explored in T2D patients to measure K^+ channels. The latter study revealed that there was a reduced nodal-paranodal K^+ current under hyperglycemic conditions that partly contributed to the slowing of NCV (Misawa et al., 2004).

Previous nerve biopsy studies demonstrated a reduced density of myelinated and unmyelinated sensory fibers along with myelin thinning in humans and experimental T2D-PSN models indicating axonal degeneration (Herrmann et al., 1999; Mizisin., 2014; Biessels et al., 2014). Although I did not measure the extent of myelination in the T2D NGRs, morphometric analysis may reveal myelin impairment in the sensory nerve that can be correlated with motor NCV slowing (Zochodne et al., 2001; Lennertz et al., 2011; Webber et al., 2013).

4.3 Effect of T2D-PSN on DRGNs of NGRs

4.3.1 Neuropeptide expression and satellite glial cell activation

The numbers of NF200- and peripherin-positive DRGNs did not alter in T2D NGRs (Fig. 3-3) indicating DRGN survival was unaffected. However, these findings do not exclude that they might be functionally impaired. As the current studies only focused on measuring the neurofilament content in the cytoplasm of DRGNs, T2D-induced oxidative injury to the sensory nerve somata can be further explored by analyzing the DRGN at nuclear level in T2D NGRs. The population of immunoreactive-CGRP/IB4 DRGNs and the extent of CGRP immunoexpression in the same neurons did not change in T2D NGRs (Fig. 3-4). However, expression of CGRP could be further confirmed by analyzing its mRNA levels that have been suggested to decrease in DRGN of human and experimental T2D-PSN (Russell et al., 2014; Tellechea et al., 2018). IB4 serves as an immunomarker to identify non-peptidergic DRGNs; however, its function in T2D-PSN remains ambiguous and needs to be explored in depth.

Consistent with previous findings, activation of satellite glial cells and infiltration of macrophages in the DRGs of T2D NGRs indicate nerve injury-induced neuronal stress and inflammation (Fig. 3-5) (Warwick et al., 2013; Hanani et al., 2014; Rahman et al., 2016; Bolsinger et al., 2017). The underlying mechanisms of these responses to injury remain poorly understood; however, it has been suggested that hyperglycemia-induced oxidative stress might trigger them (Rahman et al., 2016; Gonçalves et al., 2018). It will also be important to study the expression of aldose reductase that has been shown to colocalize in satellite glial cells and Schwann cells as a result of hyperglycemia in T2D (Jiang et al., 2006; Gonçalves et al., 2018). The presence of aldose reductase

would indicate the direct role of hyperglycemia-induced stress in satellite glial cells that might be present in addition to neuronal stress. As GFAP is expressed in both satellite glial cells surrounding DRGNs and Schwann cells, its co-expression in both cells types can be further explored by labeling against glutamine synthetase that is not expressed by Schwann cells. It would also be interesting to determine if blocking the activation of satellite glial cells in the DRGNs can help to diminish the oxidative stress and inflammation exhibited in the nerve and its DRGN somata in T2D NGRs.

4.3.2 Nav expression at the DRG level in T2D NGRs

Altered Nav function and distribution have been demonstrated in association to various pathophysiological processes such as NCV slowing, axonal degeneration, hyperexcitability, hyperalgesia, and allodynia (Toth et al., 2004; Sima and Zhang, 2014; Schreiber et al., 2015; Feldman et al., 2017). In my studies, increased expression of Nav1.7 and Nav1.9 in the DRGNs indicates gain-of-function mutations of these channels and these findings are in line with previous studies in T2D-PSN patients and experimental models (Craner et al., 2002; Hong and Wiley, 2005; Dib-Hajj et al., 2012; Lauria et al., 2014; Waxman and Zamponi., 2014; Schreiber et al., 2015). The upregulation of these channels suggests injury to the peripheral nerve fibers which may also cause hyperexcitability at the level of somata. It has been demonstrated using whole-cell patch-clamp recordings in DRGNs that gain-of-function mutation in Nav1.7 produces TTX-enhanced ramp currents and impaired Nav activation (Dib-Hajj et al., 2009). Also, upregulation of Nav1.7 mediated by activation of PKC and p38 mitogen-activated protein kinase phosphorylation in response to hyperglycemia has been shown for T2D DRGNs (Igarashi et al., 1999; Chattopadhyay et al., 2008). It has been suggested that more than one isoform of Nav are involved in mediating hyperexcitability (Krishnan et al., 2009). Next, inflammation may occur in T2D-PSN, and it was

demonstrated that the inflammatory mediator pE_2 alters Nav1.9 activity via G-protein activation resulting in an increased persistent Nav1.9 current in the DRGNs when investigated using whole-cell patch technique (Rush and Waxman, 2004).

My study revealed no change in Nav1.8 expression, consistent with previous reports in streptozotocin T2D mice (Craner et al., 2002; Rogers et al., 2006; Bierhaus et al., 2012). Contrary, other studies have demonstrated an increase in slowly-inactivating TTXr Nav currents in cultured DRGNs of T2Dstreptozotocin rodent models (Dib-Hajj et al., 2009). Moreover, in cultured DRGNs of T2D rats, the amplitude of TTXr Na^+ currents increased in hyperglycemia (Singh et al., 2013; Schreiber et al., 2015). Previous study revealed that post-translational modifications of Nav1.8 by the glycolytic end-product methylglyoxal in streptozotocin T2D mice resulted in the increased firing of DRGNs and induced thermal and mechanical hyperalgesia (Bierhus et al., 2012). It was demonstrated that PKC-mediated phosphorylation of Nav1.8 increased inward currents in cultured DRGNs causing lowering of their activation threshold (Wu et al., 2012). Additionally, an increase in the level of serine/threonine phosphorylation of Nav1.8 and Nav1.7 was also studied in T2D rat DRGNs in association to painful T2D-PSN (Hong et al., 2004). The role of Nav isoforms in nerve hyperexcitability is further discussed in 4.4.3.

4.4 SFAP recording

In the second part of my thesis, I established SFAP and mixed AP recording in the skin-nerve preparation of NGRs. Initially, the long waiting time between euthanization and the start of the dissection likely affected the overall viability of the skin-nerve preparation. With the shortening of this time and improved dissection practice, its viability was increased and allowed for stable SFAP

recording (3.5.1-3.5.3). The responses were electrically identified as originating from Aδ- or C-fibers via latency testing and NCV determination (3.5.3). Importantly, since I demonstrated the development of PSN in T2D NGRs (Singh et al., 2018), I examined electrophysiological parameters such as activity-dependent latency changes, SFAP amplitude, NCV and electrical plus mechanical Von Frey thresholds of mechanosensitive fibers (3.5.4).

4.4.1 Establishment of the skin-nerve preparation

Initially, I attempted to map the extension of RFs. However, this desensitized or damaged the nerve fibers resulting in reduced viability, as discussed previously (Iggo, 1960). For example, it has been suggested that prolonged nerve stimulation extends the hyperpolarization phase due to increase in $Na^{+/}K^{+}$-ATPase pump activity resulting in diminished or no excitability (Bostock and Grafe, 1985; Krishnan et al., 2009). Therefore, due to the limited number of available NGRs, I focused on analyzing mechanically-evoked SFAP responses only from a single RF point and then proceeded directly to electrical stimulation. This approach increased the probability to identify SFAPs and characterize them electrically for a considerable number of Aδ- or C-fibers for > 24 h (Figs. 3-9).

4.4.2 Characterization of nerve fibers by electrical stimulation

Following the identification of SFAPs or mixed AP responses via rod stimulation, I evoked identical responses with electrical stimulation (Fig. 3-10) and recorded their activation thresholds. In line with previous studies, I could distinguish between Aδ- and C-fibers based on activity-dependent latency changes and NCV determination. However, I could not record from Aβ-fibers. Two explanations for this could be that either the RF points became desensitized or they represent large-diameter Aβ-fibers (NCV >16 m/s). The SFAP responses from Aβ-fibers were likely lost in

the initial stimulus artifact that sometimes lasted for ~5 ms and therefore could not be recorded. Previous studies, however, have demonstrated the characterization of Aβ-fibers is possible, e.g. by increasing the distance between the stimulation and recording sites (Reeh, 1986; Koltzenburg et al., 1997; Zimmermann et al., 2009).

Next, I could not subclassify the recorded Aδ- and C-fibers fibers due to the absence in my recording setup of a Peltier device, which controls heat and cold application to the RF point (Zimmermann et al., 2009; Hoffmann et al., 2017). With the Peltier device, mouse Aδ- and C-fibers can be further classified as mechano-heat, mechano-cold, cold, warm, heat, and polymodal responsive (Zimmermann et al., 2009). Once the NGR sensory fibers will be subclassified in future studies, their functional properties could also be further studied by the application of pharmacological compounds such as capsaicin (a TRPV1-agonist), mustard oil (a TRPM8-agonist) and icilin or menthol (the latter being TRPM8-agonists) (Reeh, 1988; Lennertz et al., 2010; Zimmermann et al., 2009). These compounds can be applied to the RF point that can be isolated from the rest of the chamber using a microperfusion ring that creates a diffusion barrier. For example, an RF point can be stimulated with menthol and a burst of SFAP response would indicate that the respective fiber is cold-responsive (TRPM8-positive) (Zimmermann et al., 2009). Similarly, application of capsaicin would identify a noxious heat-responsive (TRPV1-positive) sensory fiber (Zimmermann et al., 2009). Moreover, TTXr versus TTXs Nav could be investigated by application of different TTX doses (Zimmermann et al., 2009; Kistner et al., 2010; Kornecook et al., 2017). The skin-nerve preparation was used previously to study the link of Nav1.7, Nav1.8 and Nav1.9 with cold pain, hyperalgesia, and mechanical allodynia in T2D-PSN (Bierhaus et al., 2012; Hoffmann et al., 2016, 2017).

4.4.3 NCV, SFAP amplitude, electrical and mechanical excitability in Aδ- and C-fibers

Previous studies in patients and T2D rodent models of PSN demonstrated motor and sensory NCV slowing suggesting nerve fiber impairment (Moore et al., 1980; Kalichman et al., 1998; Patel and Tomlinson., 1999; Brussee et al., 2008; Murakami et al., 2013; Zotova and Arezzo, 2013; Biessels et al., 2013; Perkins and Bril, 2014). Our publication showed T2D-NGRs also demonstrated a slowing of motor NCV (Singh et al., 2018) indicative of PSN. Thus, I hypothesized that sensory fibers also have a slower NCV in T2D NGRs. However, there was no difference in that regard neither for Aδ- nor C-fibers (Fig. 3-14C, D). One plausible explanation for this could be technically related. For instance, all sensory NCV data from T2D-PSN patients and animal models stem from *in-vivo* recordings where depending on the type of sensory nerve, stimulation occurred either orthodromically (i.e., distal stimulation and proximal sensory nerve SNAP recordings) or antidromically (stimulating the nerve proximally and recording the SNAP distally) (Mallik and Weir, 2005). The measurement of NCV, however, relies only on large-diameter sensory fibers as small-fibers that are typically affected in PSN remain inaccessible to record in an intact nerve (Mallik and Weir, 2005; Perkins and Bril, 2014). Specifically, the large-diameter fiber SNAPs appear firstly after the stimulus artifact due to their fast NCV and they generate the majority of SNAP component, whereas SNAPs generated by Aδ- and C-fibers are typically lost in the background noise during NCV recordings (Binnie et al., 1995; Mallik and Weir, 2005; Perkins and Bril, 2014). In T2D NGRs, it is possible that sensory NCV slowing was exhibited by large diameter Aβ-fibers which could not be recorded in my current study (3.5.3). It has also been demonstrated that sensory NCV slowing takes place during the initial phase of T2D-PSN, followed by motor NCV slowing at more advanced stages (Moore et al., 1980; Weis et al., 1995; Perkins and Bril, 2014). Therefore, it is possible that NCV slowing was altogether absent in these sensory fibers in

the advanced-stages of T2D-PSN in NGRs. My results demonstrated a decrease in SFAP amplitude of both Aδ- and C-fibers in T2D NGRs (Fig. 3-14A, B). As explanation, it might be possible that in T2D NGRs Aδ- and C-fibers, the population of sensory fibers with larger amplitude SFAPs is selectively lost or degenerated. This degeneration could be further validated by immunohistochemically analyzing the sensory nerve innervation in the dorsal skin of the hind foot. While I demonstrated functional cutaneous sensory Aδ- and C-fibers in the dermal skin of NGRs, one of the important aims of my study was to investigate whether their excitability changes associated with T2D-PSN. The decreased electrical Aδ- and C-fiber thresholds in T2D NGRs suggests that these fibers are hyperexcitable at the nerve terminal (Fig. 3-14E, F). In T2D-PSN, it has been demonstrated that altered nodal Nav distribution in myelinated axons results in hyperexcitability of sensory fibers (Feldman et al., 2017; Waxman et al., 1995). With the help of threshold tracking techniques, an increase in nodal Na^+ currents was demonstrated in the peripheral sensory axons of T2D-PSN patients indicative of Nav-associated hyperexcitability (Misawa et al., 2009). Further, it was studied that APs in T2D-PSN patients had a prolonged refractory period due to dysfunctional Nav, related to nerve degeneration and slow recovery from Nav inactivation resulting in sustained depolarization (Misawa et al., 2004). Therefore, analyzing refractory periods can elucidate the excitable properties of axons that might be affected by injury. Since T2D is a metabolic syndrome, various metabolic mechanisms may play central roles in modifying or disrupting the function and morphological properties of sensory nerve fibers (Callaghan et al., 2012; Lee-Kubli and Calcutt, 2014; DeFronzo et al., 2015; Feldman et al., 2017). For example, it has been hypothesized that C-fibers are more susceptible to T2D insults due to the absence of a protective myelin sheath (Feldman et al., 2017).

In T2D, methylglyoxal can post-translationally modify the function of Nav in the distal sensory terminalsresulting in hyperexcitability (Bierhaus et al., 2012; Lee-Kubli and Calcutt, 2014; Schreiber et al., 2015; Feldman et al., 2017) (4.4). Furthermore, a gain-of-function mutation in Nav1.7 and Nav1.9 mutant mice has also been linked to hyperexcitability, allodynia and hyperalgesia in T2D-PSN (Craner et al., 2002; Rogers et al., 2006; Dib-Hajj et al., 2010; Waxman et al., 2014; Feldman et al., 2017). My studies demonstrated hyperexcitability of distal sensory Aδ- and C-fibers fibers and upregulation of Nav expression at the DRG. It is also important to consider that excitability changes at the distal terminals might not be directly associated with changes at the DRG level.

While responses consecutively evoked by rod and electrical stimulation were identical, different fibers were activated in the same RF point by Von Frey stimulation (Fig. 3-15). One explanation for this discrepancy could be the inherent human error of manual Von Frey filaments testing as the use of electronically controlled filaments enables to record identical SFAPs (Reeh, 1986; Koltzenburg et al., 2007; Zimmermann et al., 200). Furthermore, the trajectory of the finest (0.02 g) Von Frey filament used was affected by the surface tension of the superfusate. This difficulty is in combination with the slippery skin surface that could cause a slight lateral movement, caused difficulty in stabilizing the Von Frey filament at the specific RF point. Despite these technical difficulties, my analysis revealed a decrease in mechanical thresholds in mechanosensitive fibers fromT2D NGRs indicative of hyperexcitability (Fig. 3-16).

In the skin-nerve preparation of T2D NGRs, both electrical and Von Frey stimulation revealed hypersensitivity of fibers (Fig. 3-14E, F) whereas the behavioral data indicated hyposensitivity

(hypoesthesia) at the plantar skin surface to tactile and heat stimuli (Fig. 3-2D, E). There are several possible explanations for this discrepancy: (i) in the *ex-vivo* skin-nerve preparation the peripheral nerve is isolated at the axon level distal to the DRGN somata, spinal cord, and cortical projection targets, therefore in *in-vivo*, the nerve terminals may also be hyperexcitable, but central inhibition may attenuate the signal, (ii) the footpad and dorsal foot skin are innervated by tibial and saphenous nerves, respectively. It is thus possible that T2D-PSN affects these nerves differently, (iii) T2D patients often present with both numbness and pain (Kästenbauer et al., 2004; Bastyr et al., 2005; Bansal, 2006; Kaur et al., 2011; Spallone et al., 2013; Bril et al., 2018). Therefore, it is feasible that my findings of hypoesthesia (behavioral data) and hyperexcitability, i.e., pain response (skin-nerve preparation) stand. Independent on this discrepancy, if the retracted IENFs are still viable, reinnervation at the epidermis level may be possible and provide a target for future efforts to treat numbness due to T2D-PSN. This may be ambiguous, however, as reinnervation of retracted IENFs could result in hyperalgesia.

4.5 Summary and conclusion

My thesis demonstrates that male T2D NGRs display hallmark features of PSN when fed a high-fat, low fiber diet and thus are a new experimental model to study this neurological disease (Fig. 4-1). In addition, this is the first time that the skin-nerve preparation for SFAP recordings has been adapted in NGRs to study electrophysiological properties of sensory Aδ- and C-fibers. The major findings on T2D NGRs are:

(i) Hallmark clinical T2D-PSN features are present such as footpad epidermal skin denervation and hyposensitivity to both touch and heat stimuli.

(ii) Motor NCV is slowed like in T2D-PSN patients.

(iii) DRG show activated satellite glial cells and macrophage infiltration as an indication of inflammation.

(iv) DRGNs display upregulated Nav1.7 and Nav1.9, but not Nav1.8 expression.

(v) In the skin-nerve preparation, Aδ- and C-fibers show decreased electrically-evoked SFAP thresholds and amplitudes as well as decreased mechanical threshold of Von Frey-stimulated unidentified mechanosensitive fibers.

As current T2D-PSN models rely on genetic and pharmacological manipulation to develop T2D and none of these models demonstrate hallmark clinical features of T2D-PSN, the pathological features listed above make NGRs an excellent model to study T2D-PSN and fulfill the requirement for this proposed by NEURODIAB. In addition, the slow-progression of T2D in NGRs mimics the development of T2D in humans and therefore provides a unique future opportunity to address the onset of PSN (i.e., preclinical T2D) for early and effective pharmacological interventions and preventing the permanent nerve damage.

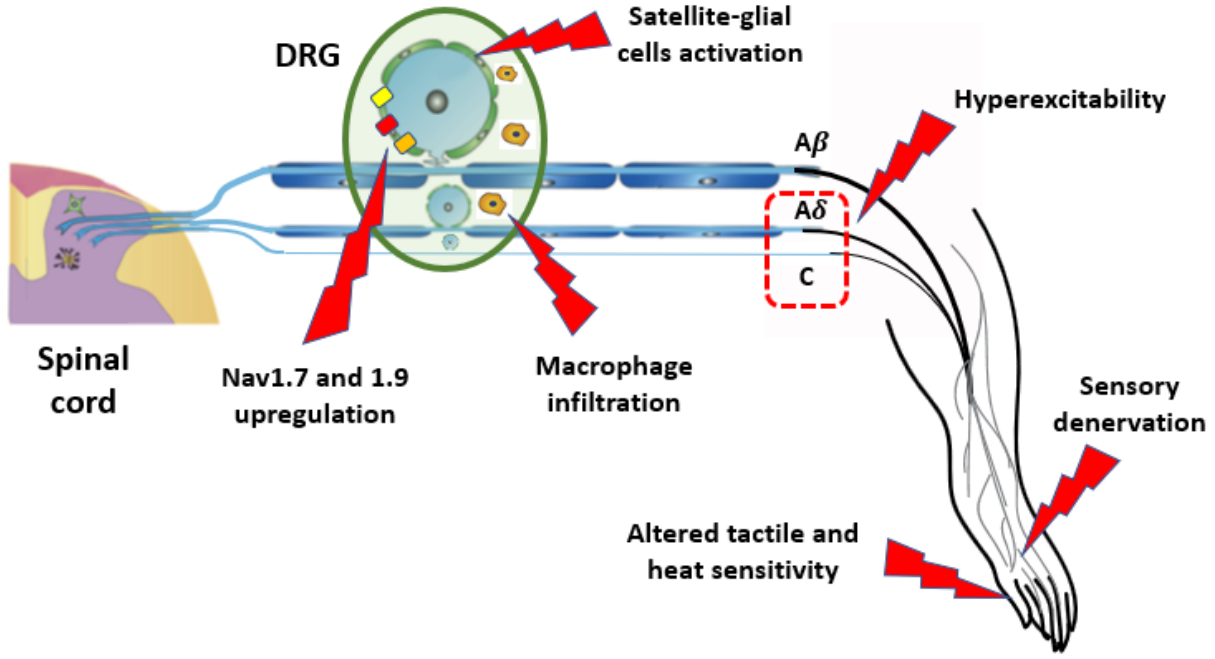

Fig. 4-1: Schema summarizing the pathology of T2D-PSN in NGRs at the distal sensory nerve fibers and their DRG.

4.6 Future directions

In line with previous studies (Noda et al., 2010; Yang et al., 2016), chow-fed NGRs used here demonstrated T2D based on hyperglycemia, increased body weight, and BMI. However, for more concise determination of their metabolic state, it would have been beneficial to measure their FBG, non-fasting blood glucose levels and fasting plasma insulin levels at various time points. To further confirm T2D outcome in NGRs, fasting and non-fasting plasma HbA1c levels, ketone bodies and urine values should also be measured at various time points. Here, some non-hyperglycemic NGRs were considered T2D based on comorbidities; however, to avoid this discrepancy in comparison among experimental groups and accurate analysis, it would be ideal in the future to study only hyperglycemic animals. Future studies can also focus on determining a normal physiological FBG range below which the T2D NGRs can be considered hypoglycemic which has previously not tested in these animals. The studies can then be extended to examine the pancreatic and hepatic health of T2D NGRs and to determine the cause of low FBG by measuring glucagon levels at different time points.

Here, I demonstrated NGRs with T2D had hallmark features of PSN; however, the studies could not be extended to identify the metabolic mechanisms related to peripheral sensory nerve fiber pathology. At elevated FBG, different metabolic cascades are involved in T2D-PSN-associated pathology and directly target and affect the peripheral nerves. Using skin autofluorescence techniques, accumulation of sorbitol, formed via the polyol pathway can be tested in the nerve terminals and their DRGN somata in T2D NGRs to demonstrate the activity of aldose reductase enzyme. The activity of the enzyme can be tested using biochemical enzymatic assays such as

enzyme-linked immunosorbent assays or protein estimation assays. Further, activation of another metabolic pathway, PKC, can be investigated in T2D NGRs. Pharmacologically, it will be interesting to investigate using potential aldose reductase- and PKC-inhibitors, if PSN-symptoms can be reversed or minimized in T2D NGRs, as previously demonstrated in other T2D rodent models (Drel et al., 2006; Obrosova, 2009; Yagihashi et al., 2011). These analyses will help in assessing the role of glycolytic end-products in T2D-PSN in NGRs and targeting the possible mechanisms for therapeutic interventions. Further, in T2D-NGRs it will interesting to investigate the presence of the metabolic end product AGE and use it as a marker to indicate the presence of oxidative stress in T2D-PSN.

The present study demonstrated epidermal denervation and behavioral hyposensitivity to tactile and thermal stimulation in T2D NGRs. As the epidermis is innervated by polymodal unmyelinated fibers, diminished sensitivity to heat may reflect selective loss of heat-sensitive fibers. Using skin biopsy in T2D NGRs, it can be studied if there is a reduced expression of heat-activated TRPV1 channels in these nerve terminals. Similarly, reduced mechanical sensitivity to Von Frey stimulation can be further explored in relation to large myelinated fibers and altered expression of myelin proteins as well as the distribution of mechanoreceptors in the skin can be assessed (see 4.2). Furthermore, the pathogenesis of slowing of motor NCV can be explored in more detail by using electrophysiological threshold tracking techniques to study abnormal Nav and K^+ conductance that may contribute to the slowing of motor NCV. Using morphometric analytical techniques that assess the extent of myelin in the sensory nerve fibers and their density in the nerve, signs of demyelination can be ruled out in T2D NGRs that will also reflect towards slowing of motor NCV in these animals.

As the major outcome of T2D is hyperglycemia-induced oxidative stress, it will also be interesting to investigate if there is any oxidative-injury to the DRGNs which may cause impaired mitochondrial function and Ca^{2+} homeostasis in these neurons and apoptosis, as previously studied (Huang et al., 2002; Schmeichel et al., 2003; Vincent et al., 2004; Rahman et al., 2016). For accurate analysis, T2D-mediated injury to DRGNs via apoptosis can also be assessed using a TUNEL assay. This assay identifies DNA degradation in the cells undergoing apoptosis. Additionally, using transmission electron microscopy, the metabolic dysfunction can be further assessed in the peripheral nerve fibers for any altered distribution of mitochondria or by immunocytochemistry using cytochrome oxidase staining in mitochondria of DRGNs in T2D NGRs (Schmeichel et al., 2003; Lennertz et al., 2011).

As CGRP was the only neuropeptide tested in the current study, there is room to investigate expression of other neuropeptides, channels and receptors such as substance P, neuropeptide Y, and neurokinin A, TRP channels (TRPV1, TRPA1, TRPM8), purinergic receptors like P2X3 in T2D NGRs and their role in PSN pathogenesis (Todorovic., 2015; Gram et al., 2017). In addition, expression of injury markers such as activating transcription factor (ATF-3) and the release of other inflammatory mediators such as IL-6, IL-8, IL-1β, TNFα, and pE_2 will be interesting to explore using immunohistochemical and molecular techniques as their presence may suggest inflammation and DRGN sensitization in T2D-PSN in NGRs (Hunt et al., 2012; Ramesh et al., 2013; Busui et al., 2016). Satellite glial cell activation and macrophage infiltration in DRG are inflammatory nerve-injury-mediated responses and may also get triggered directly in response to hyperglycemia-

mediated oxidative stress. Therefore, future studies could focus on investigating the expression of aldose reductase in satellite glial cells using immunohistochemical techniques.

Here, for the first time expression of Nav (Nav1.7, Nav1.9, and Nav1.8) has been determined in DRGNs of T2D NGRs; however at molecular level only. Using threshold tracking and whole-cell patch techniques in combination with molecular, biochemical and immunoprecipitation techniques in NGRs, altered function and distribution of Nav can be further explored in T2D NGRs.. These channels will serve as a potential focal point for future clinical targets to treat T2D-PSN.

During the establishment of the skin-nerve model in NGRs, several difficulties were experienced some of which were gradually solved. The primary important future aspect to perform SFAP recording in NGRs would be to proceed for dissections immediately after euthanasia. Future studies should also focus on subclassifying Aδ- and C-fibers and record from Aβ-fibers that could not be recorded here. Next, the adaptation properties of these nerve fibers during prolonged stimulation should be studied quantitatively and analyzed with examining the changes over prolonged periods. These properties could then be correlated with properties of cutaneous mechanoreceptor subtypes. This *ex-vivo* preparation also allows studying the effect of pharmacological compounds on cutaneous afferents. The properties of several ion channels and their distribution in sensory fibers can be further explored regarding pathological implications in T2D-PSN. Using the *ex-vivo* technique, the effect on cutaneous terminals of different metabolites that are elevated during hyperglycemia can be investigated and will provide a comprehensive profile on pathologies associated with T2D-PSN in NGRs. The subclassified individual nerve fibers can be studied for their excitability changes in T2D NGRs which could not be precisely explored in the current

studies. Next, it is important to adapt a more efficient mechanical stimulation method that allows a highly-controlled stimulus like the gravity-driven probes used by the Reeh group (Zimmermann et al., 2009; Hoffmann et al., 2017).

The thesis ends with a very specific technological aspect of the research on T2D NGRs, Contrary, a couple of sentences for a general Conclusion might be helpful referring to human T2D-PSN

REFERENCES

Abraira VE, Ginty DD (2013) The sensory neurons of touch. Neuron 79:618–639.

Al-Awar A, Kupai K, Veszelka M, Szűcs G, Attieh Z, Murlasits Z, Török S, Pósa A, Varga C (2016) Experimental Diabetes Mellitus in Different Animal Models. J Diabetes Res 2016.

Alam, Uazman, Omar Asghar, Shazli Azmi, and Rayaz A. Malik (2014) "General aspects of diabetes mellitus." In *Handbook of clinical neurology*, vol. 126, pp. 211-222. Elsevier.Alles SRA, Bandet M V., Eppler K, Noh M-C, Winship IR, Baker G, Ballanyi K, Smith PA (2017) Acute anti-allodynic action of gabapentin in dorsal horn and primary somatosensory cortex: Correlation of behavioural and physiological data. Neuropharmacology 113:576–590.

Amaya F, Wang H, Costigan M, Allchorne AJ, Hatcher JP, Egerton J, Stean T, Morisset V, Grose D, Gunthorpe MJ, Chessell IP, Tate S, Green PJ, Woolf CJ (2006) The Voltage-Gated Sodium Channel Nav1.9 Is an Effector of Peripheral Inflammatory Pain Hypersensitivity. J Neurosci 26:12852–12860.

Andersen H (2014). "Motor neuropathy." In *Handbook of clinical neurology*, vol. 126, pp. 81-95. Elsevier.

Akbarzadeh A, Norouzian D, Mehrabi MR, Jamshidi S, Farhangi A, Verdi AA, Mofidian SMA, Rad BL (2007) Induction of diabetes by Streptozotocin in rats. Indian J Clin Biochem 22:60–64.

Arezzo, J. C. (2013). Noninvasive Evaluation of Nerve Conduction in Small Diameter Fibers in the Rat. *Physiology journal*, *2013*.

Bansal V, Kalita J, Misra UK (2006) Diabetic neuropathy. Postgrad Med J 82:95–100.

Barbosa C, Cummins TR (2016) Unusual Voltage-Gated Sodium Currents as Targets for Pain. Curr Top Membr 78:599–638.

Barragán-Iglesias P, Oidor-Chan VH, Loeza-Alcocer E, Pineda-Farias JB, Velazquez-Lagunas I, Salinas-Abarca AB, Hong E, Sánchez-Mendoza A, Delgado-Lezama R, Price TJ, Granados-Soto V (2018) Evaluation of the neonatal streptozotocin model of diabetes in rats: Evidence for a model of neuropathic pain. Pharmacol Reports 70:294–303.

Barrière DA, Noll C, Roussy G, Lizotte F, Kessai A, Kirby K, Belleville K, Beaudet N, Longpré J-M, Carpentier AC, Geraldes P, Sarret P (2018) Combination of high-fat/high-fructose diet and low-dose streptozotocin to model long-term type-2 diabetes complications. Sci Rep 8:424.

Basbaum AI, Bautista DM, Scherrer G, Julius D (2009) Cellular and Molecular Mechanisms of Pain. Cell 139:267–284.

Bastyr EJ, Price KL, Bril V (2005) Development and validity testing of the neuropathy total symptom score-6: Questionnaire for the study of sensory symptoms of diabetic peripheral neuropathy. Clin Ther 27:1278–1294.

Beiswenger KK, Calcutt NA, Mizisin AP (2008) Epidermal nerve fiber quantification in the assessment of diabetic neuropathy. Acta Histochem 110:351–362.

Belanger S, Ma W, Chabot J-G, Quirion R (2002) Expression of calcitonin gene-related peptide, substance P and protein kinase C in cultured dorsal root ganglion neurons following chronic exposure to mu, delta and kappa opiates. Neuroscience 115:441–453.

Belkouch M, Dansereau MA, Tétreault P, Biet M, Beaudet N, Dumaine R, Chraibi A, Mélik-Parsadaniantz S, Sarret P (2014) Functional up-regulation of Nav1.8 sodium channel in Aβ afferent fibers subjected to chronic peripheral inflammation. J Neuroinflammation 11:1–17.

Bennett DLH, Woods CG (2014) Painful and painless channelopathies. Lancet Neurol 13:587–

599.

Bergman, Michael. "Pathophysiology of prediabetes and treatment implications for the prevention of type 2 diabetes mellitus." *Endocrine* 43, no. 3 (2013): 504-513. Bierhaus, Angelika, Thomas Fleming, Stoyan Stoyanov, Andreas Leffler, Alexandru Babes, Cristian Neacsu, Susanne K. Sauer et al. "Methylglyoxal modification of Na v 1.8 facilitates nociceptive neuron firing and causes hyperalgesia in diabetic neuropathy." *Nature medicine* 18, no. 6 (2012): 926. Biessels, G. J., V. Bril, N. A. Calcutt, N. E. Cameron, M. A. Cotter, R. Dobrowsky, E. L. Feldman et al. "Phenotyping animal models of diabetic neuropathy: a consensus statement of the diabetic neuropathy study group of the EASD (Neurodiab)." *Journal of the Peripheral Nervous System* 19, no. 2 (2014): 77-87. Binnie CD, Cooper R, Mauguiere F, Fowler CJ, Prior PF, Osselton JW. 'Clinical Neurophysiology : EMG, Nerve Conduction and Evoked Potentials.' Vol. 2. Elsevier, 1995.

Black JA, Frézel N, Dib-Hajj SD, Waxman SG (2012) Expression of Nav1.7 in DRG Neurons Extends from Peripheral Terminals in the Skin to Central Preterminal Branches and Terminals in the Dorsal Horn. Mol Pain 8:1744-8069-8–82.

Black JA, Waxman SG (2013) Perspective Noncanonical Roles of Voltage-Gated Sodium Channels. Neuron 80:280–291.

Blanchong JA, McElhinny TL, Mahoney MM, Smale L (1999) Nocturnal and Diurnal Rhythms in the Unstriped Nile Rat, *Arvicanthis niloticus*. J Biol Rhythms 14:364–377.

Blesneac I, Themistocleous AC, Fratter C, Conrad LJ, Ramirez JD, Cox JJ, Tesfaye S, Shillo PR, Rice ASC, Tucker SJ, Bennett DLH (2018) Rare Nav1.7 variants associated with painful diabetic peripheral neuropathy. Pain:159(3): 469.

Bolsinger, J., Landstrom, M., Pronczuk, A., Auerbach, A., & Hayes, K. C. (2017). Low glycemic

load diets protect against metabolic syndrome and Type 2 diabetes mellitus in the male Nile rat. *The Journal of nutritional biochemistry*, *42*, 134-148.

Bolsinger, J., Pronczuk, A., & Hayes, K. C. (2013). Dietary carbohydrate dictates development of type 2 diabetes in the Nile rat. *The Journal of nutritional biochemistry*, *24*(11), 1945-1952.

Bostock, H., Cikurel, K., & Burke, D. (1998). Threshold tracking techniques in the study of human peripheral nerve. *Muscle & Nerve: Official Journal of the American Association of Electrodiagnostic Medicine*, *21*(2), 137-158.

Boulton AJM (2014) 'Diabetic neuropathy and foot complications.' In *Handbook of clinical neurology*, vol. 126,, 97–107.

Bril, V., Breiner, A., Perkins, B. A., Zochodne, D., & Diabetes Canada Clinical Practice Guidelines Expert Committee. (2018). Neuropathy. *Canadian journal of diabetes*, *42*, S217-S221. Brownlee M (2001) Biochemistry and molecular cell biology of diabetic complications. Nature 414:813–820.

Brussee V, Guo G, Dong Y, Cheng C, Martinez JA, Smith D, Glazner GW, Fernyhough P, Zochodne DW (2008) Distal Degenerative Sensory Neuropathy in a Long-Term Type 2 Diabetes Rat Model. Diabetes 57:1664–1673.

Calcutt NA (2004) Modeling Diabetic Sensory Neuropathy in Rats. In: Pain Research, Humana Press. 55-65

Calcutt NA, Freshwater JD, Mizisin AP (2004) Prevention of sensory disorders in diabetic Sprague-Dawley rats by aldose reductase inhibition or treatment with ciliary neurotrophic factor. Diabetologia 47:718–724.

Calcutt NA, Jorge MC, Yaksh TL, Chaplan SR (1996) Tactile allodynia and formalin hyperalgesia in streptozotocin-diabetic rats: effects of insulin, aldose reductase inhibition and lidocaine.

Pain 68:293–299.

Caldwell JH (2009) Action Potential Initiation and Conduction in Axons. In: Encyclopedia of Neuroscience. Elsevier. 23-29.

Callaghan BC, Cheng HT, Stables CL, Smith AL, Feldman EL (2012) Diabetic neuropathy: clinical manifestations and current treatments. Lancet Neurol 11:521–534.

Campbell JN, Meyer RA (2006) Review Mechanisms of Neuropathic Pain. Neuron 52:77–92.

Chaabo F, Pronczuk A, Maslova E, Hayes K (2010) Nutritional correlates and dynamics of diabetes in the Nile rat (Arvicanthis niloticus): a novel model for diet-induced type 2 diabetes and the metabolic syndrome. Nutr Metab (Lond) 7:29.

Chao C-C, Tseng M-T, Lin Y-J, Yang W-S, Hsieh S-C, Lin Y-H, Chiu M-J, Chang Y-C, Hsieh S-T (2010) Pathophysiology of neuropathic pain in type 2 diabetes: skin denervation and contact heat-evoked potentials. Diabetes Care 33:2654–2659.

Chaplan SR, Bach FW, Pogrel JW, Chung JM, Yaksh TL (1994) Quantitative assessment of tactile allodynia in the rat paw. J Neurosci Methods 53:55–63.

Chattopadhyay M, Mata M, Fink DJ (2008) Continuous δ-Opioid Receptor Activation Reduces Neuronal Voltage-Gated Sodium Channel (Nav1.7) Levels through Activation of Protein Kinase C in Painful Diabetic Neuropathy. J Neurosci 28(26), 6652-6658.

Cheer K, Shearman C, Jude EB (2009) Managing complications of the diabetic foot. BMJ 339:b4905.

Chen YS, Chung SSM, Chung SK (2005) Noninvasive Monitoring of Diabetes-Induced Cutaneous Nerve Fiber Loss and Hypoalgesia in thy1-YFP Transgenic Mice. Diabetes 54(11), 3112-3118.

Cheng C, Singh V, Krishnan A, Kan M, Martinez JA, Zochodne DW (2013) Loss of Innervation

and Axon Plasticity Accompanies Impaired Diabetic Wound Healing Costigan M, ed. PLoS One 8:e75877.

Cheng HT, Dauch JR, Hayes JM, Hong Y, Feldman EL (2009) Nerve Growth Factor Mediates Mechanical Allodynia in a Mouse Model of Type 2 Diabetes. 68:1229–1243.

Coppey LJ, Davidson EP, Dunlap JA, Lund DD, Yorek MA (2000) Slowing of motor nerve conduction velocity in streptozotocin-induced diabetic rats is preceded by impaired vasodilation in arterioles that overlie the sciatic nerve. Int J Exp Diabetes Res 1:131–143.

Cortez M, Singleton JR, Smith AG (2014) "Glucose intolerance, metabolic syndrome, and neuropathy". In *Handbook of clinical neurology*, vol. 126:109–122.

Costa, F. A. L., & Moreira Neto, F. L. (2015). Satellite glial cells in sensory ganglia: its role in pain. *Revista brasileira de anestesiologia*, *65*(1), 73-81. Coutaux, A., Adam, F., Willer, J. C., & Le Bars, D. (2005). Hyperalgesia and allodynia: peripheral mechanisms. *Joint Bone Spine*, *72*(5), 359-371. Craner MJ, Klein JP, Renganathan M, Black JA, Waxman SG (2002) Changes of sodium channel expression in experimental painful diabetic neuropathy. Ann Neurol 52:786–792.

Cummins TR, Sheets PL, Waxman SG (2007) The roles of sodium channels in nociception: Implications for mechanisms of pain. Pain 131:243–257.

DeFronzo RA, Ferrannini E, Groop L, Henry RR, Herman WH, Holst JJ, Hu FB, Kahn CR, Raz I, Shulman GI, Simonson DC, Testa MA, Weiss R (2015) Type 2 diabetes mellitus. Nat Rev Dis Prim 1:15019.

Deuis JR, Dvorakova LS, Vetter I (2017) Methods Used to Evaluate Pain Behaviors in Rodents. Front Mol Neurosci 10:284.

Dib-Hajj SD, Black JA, Waxman SG (2015) Nav1.9: a sodium channel linked to human pain. Nat

Rev Neurosci 16:511–519.

Dib-Hajj SD, Cummins TR, Black JA, Waxman SG (2010) Sodium Channels in Normal and Pathological Pain. Annu Rev Neurosci 33:325–347.

Dib-Hajj SD, Yang Y, Black JA, Waxman SG (2012) The Nav1.7 sodium channel: from molecule to man. Nat Rev Neurosci 14:49–62.

Didangelos T, Doupis J, Veves A (2014) "Painful diabetic neuropathy: clinical aspects." In *Handbook of clinical neurology*, vol. 126:53–61.

Diemel LT, Brewster WJ, Fernyhough P, Tomlinson DR (1994) Expression of neuropeptides in experimental diabetes; effects of treatment with nerve growth factor or brain-derived neurotrophic factor. Brain Res Mol Brain Res 21:171–175.

Drel VR, Mashtalir N, Ilnytska O, Shin J, Li F, Lyzogubov V V, Obrosova IG (2006) The leptin-deficient (ob/ob) mouse: a new animal model of peripheral neuropathy of type 2 diabetes and obesity. Diabetes 55:3335–3343.

Drew, L. J., Rugiero, F., & Wood, J. N. (2007). Touch. In *Current topics in membranes* (Vol. 59, pp. 425-465). Academic Press. Dubin AE, Patapoutian A (2010) Nociceptors: The sensors of the pain pathway. J Clin Invest 120:3760–3772.

Dunnigan SK, Ebadi H, Breiner A, Katzberg HD, Lovblom LE, Perkins BA, Bril V (2013) Conduction slowing in diabetic sensorimotor polyneuropathy. Diabetes Care 36:3684–3690.

Ellis A, Bennett DLH (2013) Neuroinflammation and the generation of neuropathic pain. Br J Anaesth 111:26–37.

Emery EC, Luiz AP, Wood JN (2016) Nav1.7 and other voltage-gated sodium channels as drug targets for pain relief. Expert Opin Ther Targets 20:975–983.

Ellis A, Bennett DLH (2013) Neuroinflammation and the generation of neuropathic pain. Br J Anaesth 111:26–37.

Facer P, Casula MA, Smith GD, Benham CD, Chessell IP, Bountra C, Sinisi M, Birch R, Anand P (2007) Differential expression of the capsaicin receptor TRPV1 and related novel receptors TRPV3, TRPV4 and TRPM8 in normal human tissues and changes in traumatic and diabetic neuropathy. BMC Neurol 7:11.

Fang X, Djouhri L, Black J a, Dib-Hajj SD, Waxman SG, Lawson SN (2002) The presence and role of the tetrodotoxin-resistant sodium channel Nav1.9 (NaN) in nociceptive primary afferent neurons. J Neurosci 22:7425–7433.

Feldman EL, Nave KA, Jensen TS, Bennett DLH (2017) New Horizons in Diabetic Neuropathy: Mechanisms, Bioenergetics, and Pain. Neuron 93:1296–1313.

Fernyhough P (2015) Mitochondrial Dysfunction in Diabetic Neuropathy: a Series of Unfortunate Metabolic Events. Curr Diab Rep 15:89.

Fernyhough P, McGavock J (2014) "Mechanisms of disease: Mitochondrial dysfunction in sensory neuropathy and other complications in diabetes." In *Handbook of clinical neurology*, vol. 126353–377.

Field MJ, Bramwell S, Hughes J, Singh L (1999) Detection of static and dynamic components of mechanical allodynia in rat models of neuropathic pain: are they signalled by distinct primary sensory neurones? Pain 83:303–311.

Forbes JM, Cooper ME (2013) Mechanisms of diabetic complications. Physiol Rev 93:137–188.

Forde JJ, Ewelukwa O, Brar T, Cabrera R (2017) Intractable Fasting Hypoglycemia as a Manifestation of Hepatocellular Carcinoma. Case Reports Hepatol 2017:1–3.

Fraser, S. P., Ozerlat-Gunduz, I., Brackenbury, W. J., Fitzgerald, E. M., Campbell, T. M.,

Coombes, R. C., & Djamgoz, M. B. (2014). Regulation of voltage-gated sodium channel expression in cancer: hormones, growth factors and auto-regulation. *Philosophical Transactions of the Royal Society B: Biological Sciences*, *369*(1638), 20130105. Freeman R (2014) "Diabetic autonomic neuropathy." In *Handbook of clinical neurology*, vol. 126 :63–79.

Galloway C, Chattopadhyay M (2013) Increases in inflammatory mediators in DRG implicate in the pathogenesis of painful neuropathy in Type 2 diabetes. Cytokine 63:1–5.

Gao CF (2014) Animal Models of Diabetic Neuropathic Pain. Exp Clin Endocrinol Diabetes 122:100–106.

Garrison SR, Dietrich A, Stucky CL (2012) TRPC1 contributes to light-touch sensation and mechanical responses in low-threshold cutaneous sensory neurons. J Neurophysiol 107:913–922.

Gee MD, Lynn B, Cotsell B (1996) Activity-dependent slowing of conduction velocity provides a method for identifying different functional classes of C-fibre in the rat saphenous nerve. Neuroscience 73:667–675.

George A, Serra J, Navarro X, Bostock H (2007) Velocity recovery cycles of single C fibres innervating rat skin. J Physiol 578:213–232.

Gibbons CH, Freeman R (2012) Cutaneous Autonomic Innervation: Assessment by Skin Biopsy. Prim Auton Nerv Syst:413–417.

Gilron I, Watson CPN, Cahill CM, Moulin DE (2006) Neuropathic pain: a practical guide for the clinician. CMAJ 175:265–275.

Girard J (2017) Glucagon, a key factor in the pathophysiology of type 2 diabetes. Biochimie 143:33–36.

Gold MS, Gebhart GF (2010) Nociceptor sensitization in pain pathogenesis. Nat Med 16:1248–1257.

Gonçalves NP, Vægter CB, Andersen H, Østergaard L, Calcutt NA, Jensen TS (2017) Schwann cell interactions with axons and microvessels in diabetic neuropathy. Nat Rev Neurol 13:135–147.

Graham ML, Janecek JL, Kittredge JA, Hering BJ, Schuurman H-J (2011) The streptozotocin-induced diabetic nude mouse model: differences between animals from different sources. Comp Med 61:356–360.

Gram DX, Holst JJ, Szallasi A (2017) TRPV1: A Potential Therapeutic Target in Type 2 Diabetes and Comorbidities? Trends Mol Med 23:1002–1013.

Hædersdal S, Lund A, Knop FK, Vilsbøll T (2018) The Role of Glucagon in the Pathophysiology and Treatment of Type 2 Diabetes. Mayo Clin Proc 93:217–239.

Han C, Huang J, Waxman SG (2016) Sodium channel Nav1.8: Emerging links to human disease. Neurology 86:473–783.

Han WH, Gotzmann J, Kuny S, Huang H, Chan CB, Lemieux H, Sauvé Y (2017) Modifications in Retinal Mitochondrial Respiration Precede Type 2 Diabetes and Protracted Microvascular Retinopathy. Investig Opthalmology Vis Sci 58:3826.

Hanani M (2005) Satellite glial cells in sensory ganglia: from form to function. Brain Res Rev 48:457–476.

Hanani M, Blum E, Liu S, Peng L, Liang S (2014) Satellite glial cells in dorsal root ganglia are activated in streptozotocin-treated rodents. J Cell Mol Med 18:2367–2371.

Hargreaves K, Dubner R, Brown F, Flores C, Joris J (1988) A new and sensitive method for measuring thermal nociception in cutaneous hyperalgesia. Pain 32:77–88.

Heinricher MM (2004) Principles of Extracellular Single-Unit Recording Extracellular Recording: Neuronal Activity in a Functional Context, 8.

Herrmann DN, Griffin JW, Hauer P, Cornblath DR, McArthur JC (1999) Epidermal nerve fiber density and sural nerve morphometry in peripheral neuropathies. Neurology 53:1634–1640.

Hirade M, Yasuda H, Omatsu-Kanbe M, Kikkawa R, Kitasato H (1999) Tetrodotoxin-resistant sodium channels of dorsal root ganglion neurons are readily activated in diabetic rats. Neuroscience 90:933–939.

Ho C, O'Leary ME (2011) Single-cell analysis of sodium channel expression in dorsal root ganglion neurons. Mol Cell Neurosci 46:159–166.

Hoeijmakers JGJ, Faber CG, Merkies ISJ, Waxman SG (2014) Channelopathies, painful neuropathy, and diabetes: which way does the causal arrow point? Trends Mol Med 20:544–550.

Hoffmann T, De Col R, Messlinger K, Reeh PW, Weidner C (2015) Activation of mu-opioid receptors in the ventrolateral orbital cortex inhibits the GABAergic miniature inhibitory postsynaptic currents in rats. Neurosci Lett 592:12–16.

Hoffmann, T., Kistner, K., Carr, R. W., Nassar, M. A., Reeh, P. W., & Weidner, C. (2016). Reduced excitability and impaired nociception in peripheral unmyelinated fibers from Nav1. 9-null mice. *Pain*, *158*(1), 58-67. Hoffmann T, Kistner K, Nassar M, Reeh PW, Weidner C (2016) Use dependence of peripheral nociceptive conduction in the absence of tetrodotoxin-resistant sodium channel subtypes. J Physiol 594:5529–5541.

Hong S, Morrow TJ, Paulson PE, Isom LL, Wiley JW (2004) Early painful diabetic neuropathy is associated with differential changes in tetrodotoxin-sensitive and -resistant sodium

channels in dorsal root ganglion neurons in the rat. J Biol Chem 279:29341–29350.

Hong S, Wiley JW (2005) Early painful diabetic neuropathy is associated with differential changes in the expression and function of vanilloid receptor 1. J Biol Chem 280:618–627.

Hong S, Wiley JW (2006) Altered expression and function of sodium channels in large DRG neurons and myelinated A-fibers in early diabetic neuropathy in the rat. Biochem Biophys Res Commun 339:652–660.

Huang T-J, Sayers NM, Fernyhough P, Verkhratsky A (2002) Diabetes-induced alterations in calcium homeostasis in sensory neurones of streptozotocin-diabetic rats are restricted to lumbar ganglia and are prevented by neurotrophin-3. Diabetologia 45:560–570.

Huang Y, Zang Y, Zhou L, Gui W, Liu X, Zhong Y (2014) The role of TNF-alpha/NF-kappa B pathway on the up-regulation of voltage-gated sodium channel Nav1.7 in DRG neurons of rats with diabetic neuropathy. Neurochem Int 75:112–119.

Hübel N, Hosseini-Zare MS, Žiburkus J, Ullah G (2017) The role of glutamate in neuronal ion homeostasis: A case study of spreading depolarization Gutkin BS, ed. PLOS Comput Biol 13:e1005804.

Hudspeth, A. J., Jessell, T. M., Kandel, E. R., Schwartz, J. H., & Siegelbaum, S. A. (Eds.). (2013). *Principles of neural science*. McGraw-Hill, Health Professions Division.

Hunt D, Raivich G, Anderson PN (2012) Activating transcription factor 3 and the nervous system. Front Mol Neurosci 5:7.

Igarashi M, Wakasaki H, Takahara N, Ishii H, Jiang ZY, Yamauchi T, Kuboki K, Meier M, Rhodes CJ, King GL (1999) Glucose or diabetes activates p38 mitogen-activated protein kinase via different pathways. J Clin Invest 103:185–195.

Iglesias P, Díez JJ (2014) A clinical update on tumor-induced hypoglycemia. Eur J Endocrinol

170:147–157.

Ilfeld BM, Preciado J, Trescot AM (2016) Novel cryoneurolysis device for the treatment of sensory and motor peripheral nerves. Expert Rev Med Devices 13:713–725.

Immerman SC, Sener SF, Khandekar JD (1982) Causes and Evaluation of Tumor-Induced Hypoglycemia. Arch Surg 117:905.

International Diabetes Federation (2017) Idf Diabetes Atlas 8th edn. Brussels, Belgium.

Islam MS (2013) Animal models of diabetic neuropathy: Progress since 1960s. J Diabetes Res 2013.

Javed S, Petropoulos IN, Tavakoli M, Malik RA (2014) "Clinical and diagnostic features of small fiber damage in diabetic polyneuropathy:275–290.

Jenkins BA, Lumpkin EA (2017) Developing a sense of touch. Development 144:4078–4090.

Jiang Y, Calcutt NA, Rames KM, Mizisin AP (2006) Novel sites of aldose reductase immunolocalization in normal and streptozotocin-diabetic rats. J Peripher Nerv Syst 11:274–285.

Johansson, R. S. (1976). Skin mechanoreceptors in the human hand: receptive field characteristics. *Sensory functions of the skin in primates*, *27*. Kakrani AL, Gokhale VS, Vohra K V, Chaudhary N (2014) Clinical and Nerve Conduction Study Correlation in Patients of Diabetic Neuropathy. 62:24–27.

Kalichman MW, Dines KC, Bobik M, Mizisin AP (1998) Nerve conduction velocity, laser Doppler flow, and axonal caliber in galactose and streptozotocin diabetes. Brain Res 810:130–137.

Kästenbauer T, Irsigler P, Sauseng S, Grimm A, Prager R (2004) The prevalence of symptoms of sensorimotor and autonomic neuropathy in Type 1 and Type 2 diabetic subjects. J Diabetes Complications 18:27–31.

Katon JG, Reiber GE, Nelson KM (2013) Peripheral neuropathy defined by monofilament insensitivity and diabetes status: NHANES 1999-2004. Diabetes Care 36:1604–1606.

Kaur S, Pandhi P, Dutta P (2011) Painful diabetic neuropathy: an update. Ann Neurosci 18:168–175.

Kennedy WR, Wendelschafer-Crabb G (1993) The innervation of human epidermis. J Neurol Sci 115:184–190.

Kessler W, Kirchhoff C, Reeh PW, Handwerker HO (1992) Excitation of cutaneous afferent nerve endings in vitro by a combination of inflammatory mediators and conditioning effect of substance P. Exp Brain Res 91.

Khan GM, Chen SR, Pan HL (2002) Role of primary afferent nerves in allodynia caused by diabetic neuropathy in rats. Neuroscience 114:291–299.

Kistner, K., Zimmermann, K., Ehnert, C., Reeh, P. W., & Leffler, A. (2010). The tetrodotoxin-resistant Na+ channel Nav1. 8 reduces the potency of local anesthetics in blocking C-fiber nociceptors. *Pflügers Archiv-European Journal of Physiology*, *459*(5), 751-763. Koltzenburg M, Lewin GR (1997) Receptive Properties of Embryonic Chick Sensory Neurons Innervating Skin. J Neurophysiol 78:2560–2568.

Koltzenburg M, Stucky CL, Lewin GR (1997) Receptive Properties of Mouse Sensory Neurons Innervating Hairy Skin. J Neurophysiol 78:1841–1850.

Kornecook TJ et al. (2017) Pharmacologic Characterization of AMG8379, a Potent and Selective Small Molecule Sulfonamide Antagonist of the Voltage-Gated Sodium Channel Nav1.7. J Pharmacol Exp Ther 362:146–160.

Kou Z, Li C, Hu J, Yin J, Zhang D, Liao Y, Wu Z (2014) Alterations in the neural circuits from peripheral afferents to the spinal cord : possible implications for diabetic polyneuropathy

in streptozotocin-induced type 1 diabetic rats. *Frontiers in neural circuits*, *8*, 6.

Krishnan A V, Lin CSY, Park SB, Kiernan MC (2009) Axonal ion channels from bench to bedside: A translational neuroscience perspective. Prog Neurobiol 89:288–313.

Krishnan, A. V., & Kiernan, M. C. (2005). Altered nerve excitability properties in established diabetic neuropathy. *Brain*, *128*(5), 1178-1187. Lauria G, Ziegler D, Malik R, Merkies ISJ, Waxman SG, Faber CG and PROPANE Study group (2014) The Role of Sodium Channels in Painful Diabetic and Idiopathic Neuropathy. Curr Diab Rep 14(10):538.

Lawson SN (2002) Phenotype and function of somatic primary afferent nociceptive neurons with C-, Aδ- or Aα/β-fibres. Exp Physiol 87:239–244.

Le May C, Chu K, Hu M, Ortega CS, Simpson ER, Korach KS, Tsai M-J, Mauvais-Jarvis F (2006) Estrogens protect pancreatic beta-cells from apoptosis and prevent insulin-deficient diabetes mellitus in mice. Proc Natl Acad Sci USA 103:9232–9237.

Lee-Kubli CA, Calcutt NA (2014) "Painful neuropathy: Mechanisms." In *Handbook of clinical neurology*, vol. 126:533–557.

Lehto, S. G., Weyer, A. D., Youngblood, B. D., Zhang, M., Yin, R., Wang, W., ... & Geuns-Meyer, S. (2016). Selective antagonism of TRPA1 produces limited efficacy in models of inflammatory-and neuropathic-induced mechanical hypersensitivity in rats. *Molecular pain*, *12*, 1744806916677761. Lennertz RC, Medler KA, Bain JL, Wright DE, Stucky CL (2011) Impaired sensory nerve function and axon morphology in mice with diabetic neuropathy. J Neurophysiol 106:905–914.

Li T-P, Guo Z, Liu C-J, Sun T, Chen L, Zhao X (2017) Association of down-regulation of calcitonin gene-related peptide and substance P with increase of myocardial vulnerability in diabetic neuropathic rats. Peptides 96:1–7.

Lolignier S, Bonnet C, Gaudioso C, Noël J, Ruel J, Amsalem M, Ferrier J, Rodat-Despoix L, Bouvier V, Aissouni Y, Prival L, Chapuy E, Padilla F, Eschalier A, Delmas P, Busserolles J (2015) The Nav1.9 Channel Is a Key Determinant of Cold Pain Sensation and Cold Allodynia. Cell Rep 11:1067–1078.

Malik RA (2014) "Pathology of human diabetic neuropathy In *Handbook of clinical neurology*, vol. 126:249–259.

Mallik, A., & Weir, A. I. (2005). Nerve conduction studies: essentials and pitfalls in practice. *Journal of Neurology, Neurosurgery & Psychiatry*, *76*(suppl 2), ii23-ii31. Malon JT, Cao L (2016) Calcitonin gene-related peptide contributes to peripheral nerve injury-induced mechanical hypersensitivity through CCL5 and p38 pathways. J Neuroimmunol 297:68–75.

Manzano, G. M., Giuliano, L. M., & Nóbrega, J. A. (2008). A brief historical note on the classification of nerve fibers. *Arquivos de neuro-psiquiatria*, *66*(1), 117-119. McCarthy BG, Hsieh ST, Stocks A, Hauer P, Macko C, Cornblath DR, Griffin JW, McArthur JC (1995) Cutaneous innervation in sensory neuropathies: evaluation by skin biopsy. Neurology 45:1848–1855.

McMahon, S. B., Koltzenburg, M., Tracey, I., & Turk, D. C. (2013). *Wall & Melzack's Textbook of Pain, Expert Consult-Online and Print, 6: Wall & Melzack's Textbook of Pain*. Elsevier Health Sciences.

Meerwaldt R, Links TP, Graaff R, Hoogenberg K, Lefrandt JD, Baynes JW, Gans ROB, Smit AJ (2005) Increased accumulation of skin advanced glycation end-products precedes and correlates with clinical manifestation of diabetic neuropathy. Diabetologia 48:1637–1644.

Meyer, R. A. (2006). Peripheral mechanisms of cutaneous nociception. *Wall and Melzack's*

textbook of pain.Misawa S, Kuwabara S, Ogawara K, Kitano Y, Yagui K, Hattori T (2004) Hyperglycemia alters refractory periods in human diabetic neuropathy. Clin Neurophysiol 115:2525–2529.

Mizisin AP (2014) "Mechanisms of diabetic neuropathy: Schwann cells." In *Handbook of clinical neurology*, vol. 126: 401–428.

Mohseni S (2014) "Neurologic damage in hypoglycemia." In *Handbook of clinical neurology*, vol. 126:513–532.

Moore SA, Peterson RG, Felten DL, Cartwright TR, O'Connor BL (1980) Reduced sensory and motor conduction velocity in 25-week-old diabetic [C57BLKs (dbdb)] mice. Exp Neurol 70:548–555.

Murakami, T., Iwanaga, T., Ogawa, Y., Fujita, Y., Sato, E., Yoshitomi, H., ... & Nakamura, A. (2013). Development of sensory neuropathy in streptozotocin-induced diabetic mice. *Brain and behavior*, *3*(1), 35-41.

Myers, M. I., Peltier, A. C., & Li, J. (2013). Evaluating dermal myelinated nerve fibers in skin biopsy. *Muscle & nerve*, *47*(1), 1-11. Nascimento DSM, Castro-Lopes JM, Neto FLM (2014) Satellite Glial Cells Surrounding Primary Afferent Neurons Are Activated and Proliferate during Monoarthritis in Rats: Is There a Role for ATF3? Arai K, ed. PLoS One 9:e108152.

Nickel FT, Seifert F, Lanz S, Maihöfner C (2012) Mechanisms of neuropathic pain. Eur Neuropsychopharmacol 22:81–91.

Nieto FR, Cobos EJ, Tejada MÁ, Sánchez-Fernández C, González-Cano R, Cendán CM (2012) Tetrodotoxin (TTX) as a therapeutic agent for pain. Mar Drugs 10:281–305.

Noda K, Melhorn MI, Zandi S, Frimmel S, Tayyari F, Hisatomi T, Almulki L, Pronczuk A, Hayes

KC, Hafezi-Moghadam A (2010) An animal model of spontaneous metabolic syndrome: Nile grass rat. FASEB J 24:2443–2453.

Noda K, Nakao S, Zandi S, Sun D, Hayes KC, Hafezi-Moghadam A (2014) Retinopathy in a novel model of metabolic syndrome and type 2 diabetes: new insight on the inflammatory paradigm. FASEB J 28:2038–2046.

Oates P (2008) Aldose Reductase, Still a Compelling Target for Diabetic Neuropathy. Curr Drug Targets 9:14–36.

O'Brien, P. D., Sakowski, S. A., & Feldman, E. L. (2014). Mouse models of diabetic neuropathy. *ILAR journal*, *54*(3), 259-272.

Obrosova IG (2009) Diabetic painful and insensate neuropathy: Pathogenesis and potential treatments. Neurotherapeutics 6:638–647.

Ogden, C. L., Flegal, K. M., Carroll, M. D., & Johnson, C. L. (2002). Prevalence and trends in overweight among US children and adolescents, 1999-2000. *Jama*, *288*(14), 1728-1732.

Olokoba AB, Obateru OA, Olokoba LB (2012) Type 2 diabetes mellitus: a review of current trends. Oman Med J 27:269–273.

Pabbidi RM, Yu S-Q, Peng S, Khardori R, Pauza ME, Premkumar LS (2008) Influence of TRPV1 on diabetes-induced alterations in thermal pain sensitivity. Mol Pain 4:9.

Pasero, C. (2004). Pathophysiology of neuropathic pain. *Pain Management Nursing*, *5*, 3-8. Patel, J., & Tomlinson, D. R. (1999). Nerve conduction impairment in experimental diabetes—proximodistal gradient of severity. *Muscle & nerve*, *22*(10), 1403-1411.

Perkins B, Bril V (2014) " Electrophysiologic testing in diabetic neuropathy." In *Handbook of clinical neurology*, vol. 126:235–248.

Persson A-K, Kim I, Zhao P, Estacion M, Black JA, Waxman SG (2013) Sodium channels

contribute to degeneration of dorsal root ganglion neurites induced by mitochondrial dysfunction in an in vitro model of axonal injury. J Neurosci 33:19250–19261.

Pop-Busui R, Ang L, Holmes C, Gallagher K, Feldman EL (2016) Inflammation as a Therapeutic Target for Diabetic Neuropathies. Curr Diab Rep 16:29.

Price TJ, Flores CM (2007) Critical evaluation of the colocalization between calcitonin gene-related peptide, substance P, transient receptor potential vanilloid subfamily type 1 immunoreactivities, and isolectin B4 binding in primary afferent neurons of the rat and mouse. J Pain 8:263–272.

Price J (1985) An immunohistochemical and quantitative examination of dorsal root ganglion neuronal subpopulations. J Neurosci 5:2051–2059.

Purves, D., Augustine, G. J., Fitzpatrick, D., Hall, W. C., LaMantia, A. S., McNamara, J. O., & Williams, S. M. (2004). Neuroscience, Vol. Rahman MH, Jha MK, Kim J-H, Nam Y, Lee MG, Go Y, Harris RA, Park DH, Kook H, Lee I-K, Suk K (2016) Pyruvate Dehydrogenase Kinase-mediated Glycolytic Metabolic Shift in the Dorsal Root Ganglion Drives Painful Diabetic Neuropathy. J Biol Chem 291:6011–6025.

Ramesh, G., MacLean, A. G., & Philipp, M. T. (2013). Cytokines and chemokines at the crossroads of neuroinflammation, neurodegeneration, and neuropathic pain. *Mediators of inflammation*, *2013*. Reeh PW (1986) Sensory receptors in mammalian skin in an in vitro preparation. Neurosci Lett 66:141–146.

Reeh, P. W. (1988). Sensory receptors in a mammalian skin–nerve in vitro preparation. In *Progress in brain research* (Vol. 74, pp. 271-276). Elsevier. Refinetti, R. (2004). The Nile grass rat as a laboratory animal. *RESOURCE*, *33*(9).

Rogers, M., Tang, L., Madge, D. J., & Stevens, E. B. (2006, October). The role of sodium channels

in neuropathic pain. In *Seminars in cell & developmental biology* (Vol. 17, No. 5, pp. 571-581). Academic Press. Rosenbloom AL (2002) Increasing incidence of type 2 diabetes in children and adolescents: treatment considerations. Paediatr Drugs 4:209–221.

Rush AM, Waxman SG (2004) PGE2 increases the tetrodotoxin-resistant Nav1.9 sodium current in mouse DRG neurons via G-proteins. Brain Res 1023:264–271.

Russell FA, King R, Smillie S-J, Kodji X, Brain SD (2014) Calcitonin gene-related peptide: physiology and pathophysiology. Physiol Rev 94:1099–1142.

Said GR (2013) Diabetic neuropathy. Peripher Nerve Disord 115:579–589.

Sasaki T, Yasuda H, Maeda K, Kikkawa R (1998) Hyperalgesia and decreased neuronal nitric oxide synthase in diabetic rats. Neuroreport 9:243–247.

Schaible H-G (2007) Peripheral and central mechanisms of pain generation. Analgesia:3–28.

Schemmel, K. E., Padiyara, R. S., & D'Souza, J. J. (2010). Aldose reductase inhibitors in the treatment of diabetic peripheral neuropathy: a review. *Journal of Diabetes and its Complications*, *24*(5), 354-360.

Schmelz M, Forster C, Schmidt R, Ringkamp M, Handwerker HO, Torebjörk HE (1995) Delayed responses to electrical stimuli reflect C-fiber responsiveness in human microneurography. Exp Brain Res 104:331–336.

Schreiber AK, Nones CF, Reis RC, Chichorro JG, Cunha JM (2015) Diabetic neuropathic pain: Physiopathology and treatment. World J Diabetes 6:432–444.

Shin ES, Sorenson CM, Sheibani N (2014) Diabetes and retinal vascular dysfunction. J Ophthalmic Vis Res 9:362–373.

Shun, C. T., Chang, Y. C., Wu, H. P., Hsieh, S. C., Lin, W. M., Lin, Y. H., ... & Hsieh, S. T. (2004). Skin denervation in type 2 diabetes: correlations with diabetic duration and functional

impairments. *Brain*, *127*(7), 1593-1605.Sima AAF, Zhang W (2014) "Mechanisms of diabetic neuropathy: axon dysfunction." In *Handbook of clinical neurology*, vol. 126 :429–442.

Singh JN, Jain G, Sharma SS (2013) In vitro hyperglycemia enhances sodium currents in dorsal root ganglion neurons: An effect attenuated by carbamazepine. Neuroscience 232:64–73.

Singh, J., Yousuf, M. S., Jones, K. E., Shelemey, P. T., Joy, T., Macandili, H., ... & Webber, C. A. (2018). Characterization of the Nile Grass Rat as a Unique Model for Type 2 Diabetic Polyneuropathy. *Journal of Neuropathology & Experimental Neurology*, *77*(6), 469-478.

Sinnreich, M., Taylor, B. V., & Dyck, P. J. B. (2005). Diabetic neuropathies: classification, clinical features, and pathophysiological basis. *The neurologist*, *11*(2), 63-79.Sminkey L (2016) WHO | Global report on diabetes. Geneva, Switzerland.

Smith AK, O'Hara CL, Stucky CL (2013) Mechanical sensitization of cutaneous sensory fibers in the spared nerve injury mouse model. Mol Pain 9:61.

Spallone V, Greco C (2013) Painful and painless diabetic neuropathy: One disease or two? Curr Diab Rep 13:533–549.

Steck AJ, Stalder AK, Renaud S (2006) Anti-myelin-associated glycoprotein neuropathy. Curr Opin Neurol 19:458–463.

Steen, K. H., Reeh, P. W., Anton, F., & Handwerker, H. O. (1992). Protons selectively induce lasting excitation and sensitization to mechanical stimulation of nociceptors in rat skin, in vitro. *Journal of Neuroscience*, *12*(1), 86-95.

Steffens H, Dibaj P, Schomburg ED (2012) *In-vivo* Measurement of Conduction Velocities in Afferent and Efferent Nerve Fibre Groups in Mice. Physiol Res 61:203–214.

Subramaniam, A., Landstrom, M., Luu, A., & Hayes, K. C. (2018). The Nile Rat (Arvicanthis

niloticus) as a superior carbohydrate-sensitive model for type 2 diabetes mellitus (T2DM). *Nutrients*, *10*(2), 235.

Sugimoto K, Yasujima M, Yagihashi S (2008) Role of advanced glycation end products in diabetic neuropathy. Curr Pharm Des 14:953–961.

Suzuki Y, Sato J, Kawanishi M, Mizumura K (2002) Lowered response threshold and increased responsiveness to mechanical stimulation of cutaneous nociceptive fibers in streptozotocin-diabetic rat skin in vitro—correlates of mechanical allodynia and hyperalgesia observed in the early stage of diab. Neurosci Res 43:171–178.

Taguchi, T., Ota, H., Matsuda, T., Murase, S., & Mizumura, K. (2010). Cutaneous C-fiber nociceptor responses and nociceptive behaviors in aged Sprague–Dawley rats. *PAIN®*, *151*(3), 771-782.

Tellechea, A., Pradhan-Nabzdyk, L., LoGerfo, F. W., & Veves, A. (2018). Neuropeptides, Inflammation, and Diabetic Wound Healing: Lessons from Experimental Models and Human Subjects. In *The Diabetic Foot* (pp. 131-154). Humana Press, Cham.

Terenghi G, Chen S, Carrington AL, Polak JM, Tomlinson DR (1994) Changes in sensory neuropeptides in dorsal root ganglion and spinal cord of spontaneously diabetic BB rats. Acta Diabetol 31:198–204.

Tesfaye, S., Boulton, A. J., Dyck, P. J., Freeman, R., Horowitz, M., Kempler, P., ... & Bernardi, L. (2010). Diabetic neuropathies: update on definitions, diagnostic criteria, estimation of severity, and treatments. *Diabetes care*, *33*(10), 2285-2293.

Themistocleous AC, Ramirez JD, Serra J, Bennett DLH (2014) The clinical approach to small fibre neuropathy and painful channelopathy. Pract Neurol 14:368–379.

Thi Ton B-H, Chen Q, Gaina G, Tucureanu C, Georgescu A, Strungaru C, Flonta M-L, Sah D,

Ristoiu V (2013) Activation profile of dorsal root ganglia Iba-1 (+) macrophages varies with the type of lesion in rats. Acta Histochem 115:840–850.

Tigerholm J, Petersson ME, Obreja O, Eberhardt E, Namer B, Weidner C, Lampert A, Carr RW, Schmelz M, Franse E (2015) Article and Ion Channel Permeability. 108:1057–1071.

Tirabassi, R. S., Flanagan, J. F., Wu, T., Kislauskis, E. H., Birckbichler, P. J., & Guberski, D. L. (2004). The BBZDR/Wor rat model for investigating the complications of type 2 diabetes mellitus. *ILAR journal*, *45*(3), 292-302.

Todorovic SM (2015) Is Diabetic Nerve Pain Caused by Dysregulated Ion Channels in Sensory Neurons? Diabetes 64:3987–3989.

Togashi Y, Shirakawa J, Okuyama T, Yamazaki S, Kyohara M, Miyazawa A, Suzuki T, Hamada M, Terauchi Y (2016) Evaluation of the appropriateness of using glucometers for measuring the blood glucose levels in mice. Sci Rep 6:25465.

Ton B-HT, Chen Q, Gaina G, Tucureanu C, Georgescu A, Strungaru C, Flonta M-L, Sah D, Ristoiu V (2013) Activation profile of dorsal root ganglia Iba-1 (+) macrophages varies with the type of lesion in rats. Acta Histochem 115:840–850.

Tosaki T, Kamiya H, Yasuda Y, Naruse K, Kato K, Kozakae M, Nakamura N, Shibata T, Hamada Y, Nakashima E, Oiso Y, Nakamura J (2008) Reduced NGF secretion by Schwann cells under the high glucose condition decreases neurite outgrowth of DRG neurons. Exp Neurol 213:381–387.

Toth C, Rong LL, Yang C, Martinez J, Song F, Ramji N, Brussee V, Liu W, Durand J, Nguyen MD, Schmidt AM, Zochodne DW (2008) Receptor for Advanced Glycation End Products (RAGEs) and Experimental Diabetic Neuropathy. Diabetes 57:1002–1017.

Touska F, Turnquist B, Vlachova V, Reeh PW, Leffler A, Zimmermann K (2018) Heat-resistant

action potentials require TTX-resistant sodium channels Nav1.8 and Nav1.9. J Gen Physiol 150:1125–1144.

Tucker BA, Mearow KM (2008) Peripheral Sensory Axon Growth: From Receptor Binding to Cellular Signaling. Can J Neurol Sci 35:551–566.

Vallbo, A. B., Hagbarth, K. E., & Wallin, B. G. (2004). Microneurography: how the technique developed and its role in the investigation of the sympathetic nervous system. *Journal of Applied Physiology*, *96*(4), 1262-1269.

Vallbo AB, Johansson RS (1984) Properties of cutaneous mechanoreceptors in the human hand related to touch sensation. Hum Neurobiol 3:3–14.

Verge VMK, Andreassen CS, Arnason TG, Andersen H (2014) "Mechanisms of disease: role of neurotrophins in diabetes and diabetic neuropathy:443–460.

Veves A, Backonja M, Malik RA (2008) Painful Diabetic Neuropathy: Epidemiology, Natural History, Early Diagnosis, and Treatment Options. Pain Med 9:660–674.

Vincent AM, Edwards JL, McLean LL, Hong Y, Cerri F, Lopez I, Quattrini A, Feldman EL (2010) Mitochondrial biogenesis and fission in axons in cell culture and animal models of diabetic neuropathy. Acta Neuropathol 120:477–489.

Vouillarmet J, Maucort-Boulch D, Michon P, Thivolet C (2013) Advanced Glycation End Products Assessed by Skin Autofluorescence: A New Marker of Diabetic Foot Ulceration. Diabetes Technol Ther 15:601–605.

Wang, W., Gu, J., Li, Y. Q., & Tao, Y. X. (2011). Are voltage-gated sodium channels on the dorsal root ganglion involved in the development of neuropathic pain?. *Molecular pain*, *7*(1), 16. Warwick RA, Hanani M (2013) The contribution of satellite glial cells to chemotherapy-induced neuropathic pain. Eur J Pain 17:571–580.

Wattiez, A. S., Barrière, D., Dupuis, A., & Courteix, C. (2012). Rodent models of painful diabetic neuropathy: what can we learn from them. *Diabetes Metab S*, *5*.Waxman SG, Kocsis JD, Stys PK (1995) The axon : structure, function, and pathophysiology. Oxford University Press.Waxman SG, Zamponi GW (2014) Regulating excitability of peripheral afferents: Emerging ion channel targets. Nat Neurosci 17:153–163.

Webber CA, Salame J, Luu G-LS, Acharjee S, Ruangkittisakul A, Martinez JA, Jalali H, Watts R, Ballanyi K, Guo GF, Zochodne DW, Power C (2013) Nerve growth factor acts through the TrkA receptor to protect sensory neurons from the damaging effects of the HIV-1 viral protein, Vpr. Neuroscience 252:512–525.

Weir, G. C., & Bonner-Weir, S. (2004). Five stages of evolving beta-cell dysfunction during progression to diabetes. *Diabetes*, *53*(suppl 3), S16-S21. Weis, J., Schröder, J. M., & Dimpfel, W. (1995). Nerve conduction changes and fine structural alterations of extra-and intrafusal muscle and nerve fibers in streptozotocin diabetic rats. *Muscle & Nerve: Official Journal of the American Association of Electrodiagnostic Medicine*, *18*(2), 175-184.

Wilson NM, Wright DE (2014) "Experimental motor neuropathy in diabetes:461–467.

Won CK, Oh SJ, Jung SC, Choi YR, Kim YI, Leem JW, Shin HC (1997) Activity-dependent conduction velocity changes of Aδ-fibers in a rat model of neuropathy. Neuroreport 8:3201–3205.

Wood JN, Boorman JP, Okuse K, Baker MD (2004) Voltage-gated sodium channels and pain pathways. J Neurobiol 61:55–71.

Woolf CJ, Ma Q (2007) Nociceptors-Noxious Stimulus Detectors. Neuron 55:353–364.

Xiao, Y., Xia, Z., Wu, Y., & Zhao, B. (2016). Sodium channel Nav1. 7 expression is upregulated in the dorsal root ganglia in a rat model of paclitaxel-induced peripheral

neuropathy. *SpringerPlus*, *5*(1), 1738.

Wu D-F, Chandra D, McMahon T, Wang D, Dadgar J, Kharazia VN, Liang Y-J, Waxman SG, Dib-Hajj SD, Messing RO (2012) PKCε phosphorylation of the sodium channel Nav1.8 increases channel function and produces mechanical hyperalgesia in mice. J Clin Invest 122:1306–1315.

Yang K, Gotzmann J, Kuny S, Huang H, Sauvé Y, Chan CB (2016) Five stages of progressive β-cell dysfunction in the laboratory Nile rat model of type 2 diabetes. J Endocrinol 229:343–356.

Yang Q, Kaji R, Takagi T, Kohara N, Murase N, Yamada Y, Seino Y, Bostock H (2001) Abnormal axonal inward rectifier in streptozocin-induced experimental diabetic neuropathy. Brain 124:1149–1155.

Yorek MA (2016) Alternatives to the Streptozotocin-Diabetic Rodent. Int Rev Neurobiol 127:89–112.

Yousuf MS, Zubkow K, Tenorio G, Kerr B (2017) The chloride co-transporters, NKCC1 and KCC2, in experimental autoimmune encephalomyelitis (EAE). Neuroscience 344:178–186.

Ziegler D, Papanas N, Vinik AI, Shaw JE (2014) " Epidemiology of polyneuropathy in diabetes and prediabetes.":3–22.

Zimmerman, A., Bai, L., & Ginty, D. D. (2014). The gentle touch receptors of mammalian skin. *Science*, *346*(6212), 950-954. Zimmermann K, Hein A, Hager U, Kaczmarek JS, Turnquist BP, Clapham DE, Reeh PW (2009) Phenotyping sensory nerve endings in vitro in the mouse. Nat Protoc 4:174–196.

Zimmermann K, Leffler A, Babes A, Cendan CM, Carr RW, Kobayashi J, Nau C, Wood JN, Reeh PW (2007) Sensory neuron sodium channel Nav1.8 is essential for pain at low temperatures.

Nature 447:855-858.

Zochodne, D. W. (2007). Diabetes mellitus and the peripheral nervous system: manifestations and mechanisms. *Muscle & Nerve: Official Journal of the American Association of Electrodiagnostic Medicine*, *36*(2), 144-166.

Zochodne DW, Verge VMK, Cheng C, Sun H, Johnston J (2001) Does diabetes target ganglion neurones?: Progressive sensory neurone involvement in long-term experimental diabetes. Brain 124:2319–2334.

Zochodne, D. W. (2008). *Neurobiology of peripheral nerve regeneration*. Cambridge, UK: Cambridge University Press. Zochodne, D. W. (2014). Mechanisms of diabetic neuron damage: Molecular pathways. In *Handbook of clinical neurology* (Vol. 126, pp. 379-399). Elsevier.